Charles University
Second Faculty of Medicine

Doctoral study programme: Kinesiology and Rehabilitation

Mgr. Jan Svoboda

Permeability of blood brain barrier during cerebral ischemia

Prostupnost hematoencefalické bariéry při mozkové ischémii

Dissertation Thesis

Supervisor: prof. MUDr. Jakub Otáhal, Ph.D.

Prague, 2025

Statement

I declare that I have prepared my dissertation independently and that I have properly cited and referenced all sources and literature used. I also declare that the thesis has not been used to obtain another or the same degree.

I agree to the permanent storage of the electronic version of my thesis in the database of the inter-university project Theses.cz for the purpose of continuous checking of the similarity of qualifying theses.

In Prague 28.01.2025

Mgr. Jan Svoboda

……………………………………….

Signature

Permeability of blood brain barrier during cerebral ischemia

Abstract

Cerebral ischemia remains a leading cause of long-term disability and mortality worldwide, with blood-brain barrier (BBB) dysfunction playing a crucial role in its pathophysiology. This dissertation investigates the mechanisms of BBB permeability changes during ischemic stroke through both clinical and experimental approaches, providing new insights into stroke progression and potential therapeutic interventions. The clinical study involved MRI-based analysis of BBB disruption in ischemic stroke patients during the subacute phase (7–12 days post-stroke). By utilizing advanced imaging techniques, we assessed the localization and extent of BBB impairment in relation to ischemic lesion subregions. The findings indicate a strong correlation between lesion volume and BBB leakage, with significant gadolinium extravasation observed in FLAIR positive regions. The experimental study complemented these findings by employing a middle cerebral artery occlusion (MCAO) model in rodents, closely mimicking clinical stroke conditions and enabling a controlled investigation of BBB permeability changes. By comparing different rat strains, we identified significant variations in cerebrovascular responses, infarct size, and survival rates. Fluorescence spectrometry quantified BBB permeability by measuring Evans Blue (EB) extravasation, providing spaciotemporal evaluation of BBB disruption. Utilizing MRI, we assessed water diffusion abnormalities, offering insights into tissue integrity, edema formation, and the extent of ischemic damage. The combined clinical and experimental approach enhances our understanding of BBB disruption in ischemic stroke and its long-term consequences. The findings provide valuable markers for early detection of BBB dysfunction and contribute to the advancement of precision medicine in stroke care, emphasizing the importance of BBB integrity in optimizing patient outcomes and reducing post-stroke complications.

Keywords

blood-brain barrier, ischemic stroke, MRI, cerebral ischemia, vascular permeability, MCAO, neurovascular unit, post-stroke epilepsy, BBB disruption, experimental stroke model.

Prostupnost hematoencefalické bariéry při mozkové ischémii

Abstrakt

Mozková ischemie zůstává jednou z hlavních příčin dlouhodobé invalidity a mortality po celém světě, přičemž dysfunkce hematoencefalické bariéry (BBB) hraje klíčovou roli v její patofyziologii. Tato disertační práce zkoumá mechanismy změn permeability BBB během ischemické cévní mozkové příhody prostřednictvím klinických i experimentálních přístupů, čímž poskytuje nové poznatky o progresi cévní mozkové příhody a potenciálních terapeutických intervencích. Klinická studie zahrnovala analýzu narušení BBB u pacientů s ischemickou cévní mozkovou příhodou v subakutní fázi (7–12 dní po příhodě) pomocí magnetické rezonance (MRI). Využitím pokročilých zobrazovacích metod jsme hodnotili lokalizaci a rozsah poškození BBB v závislosti na subregionech ischemické léze. Výsledky ukázaly silnou korelaci mezi objemem léze a extravazací BBB, přičemž významná extravazace gadolinia byla pozorována ve FLAIR pozitivních oblastech. Experimentální studie tyto poznatky doplnila využitím modelu okluze střední mozkové arterie (MCAO) u hlodavců, který věrně napodobuje klinické podmínky cévní mozkové příhody a umožňuje kontrolované zkoumání změn permeability BBB. Porovnáním různých kmenů potkanů jsme identifikovali významné rozdíly v cerebrovaskulárních reakcích, velikosti infarktu a míře přežití. Fluorescenční spektrometrie kvantifikovala permeabilitu BBB měřením extravazace Evansovy modři (EB), což umožnilo prostorově-časové hodnocení narušení BBB. Pomocí MRI jsme analyzovali abnormality v difuzi vody, což poskytlo cenné informace o integritě tkáně, tvorbě edému a rozsahu ischemického poškození. Kombinovaný klinický a experimentální přístup rozšiřuje naše porozumění narušení BBB při ischemické cévní mozkové příhodě a jejím dlouhodobým důsledkům. Získané poznatky přispívají k rozvoji precizní medicíny v péči o pacienty po cévní mozkové příhodě, přičemž zdůrazňují důležitost integrity BBB pro optimalizaci výsledků léčby a snížení rizika komplikací po mozkové ischemii.

Klíčová slova

hematoencefalická bariéra, ischemická cévní mozková příhoda, MRI, mozková ischemie, cévní propustnost, MCAO, neurovaskulární jednotka, epilepsie po cévní mozkové příhodě, narušení BBB, experimentální model cévní mozkové příhody.

Acknowledgment

I would like to express my sincere gratitude to my supervisor, prof. MUDr. Jakub Otáhal, Ph.D., for his valuable guidance and support throughout this work.

I am also deeply thankful to my parents, friends, and colleagues from my research group at the Institute of Physiology CAS, and the Second Faculty of Medicine Charles University for their encouragement and for fostering a friendly and inspiring working atmosphere. In particular, I would like to acknowledge David Kala, Antonín Pošusta, Lukáš Michal, Jan Daněk and Peter Ergang for their moral support and collaboration.

The studies described in this thesis were supported by the grant project:

1) Czech Health Research Council NU21-02-00289.
2) NPO - no.LX22NPO5107 from the MEYS of the Czech Republic: Financed by EU – Next Generation EU

List of abbreviations

4VO – four vessel occlusion
ADC - apparent diffusion coefficient
AFF - Axonal Fiber Fraction
AJ – adherent junctions
AQP4 - aquaporin-4 channel
ATP - adenosine triphosphate
BBB – blood brain barrier
BCSFB - blood-cerebrospinal fluid barrier
CA – contrast agent
CBF – cerebral blood flow
CCA – common carotid artery
CNS - central nervous system
DALYs – disability-adjusted life years
DBSI - Diffusion Basis Spectrum Imaging
DEC - dynamic contrast-enhanced imaging
DKI - diffusion kurtosis imaging
DTI – diffusor tensor imaging
DWI - Diffusion-weighted imaging
EC - endothelial cell
ECA – external carotid artery
ECG – electrocorticography
ET-1 - endothelin-1
FLAIR - Fluid-Attenuated Inversion Recovery
fMRI - functional magnetic resonance imaging
HIDF – Hindered Isotropic Diffusion Fraction
ICA – internal carotid artery
IF - Isotropic Fraction
JAM – junctional adhesion molecules
LDF – laser Doppler flowmetry
MCA – middle cerebral artery
MCAO – middle cerebral artery occlusion
MMP - matrix metalloproteinases
MP – magnetic particle
MRI – magnetic resonance
NKCC1 Na^{+}-K^{+}-$2Cl^{-}$ cotransporter
NRIDF – Non-Restricted Isotropic Diffusion Fraction
NVU – neurovascular unit
PECAM-1 - endothelial cell adhesion molecule-1
rCBF – regional blood flow
pMCAO – permanent middle cerebral artery occlusion
RCF - relative centrifugal force
RIDF – Restricted Isotropic Diffusion Fraction
ROS – reactive oxygen species
SD – Sprague-Dawley
SHR – Spontaneously Hypertensive Rats
SIMPLE – stroke induced with magnetic particles
SNR – signal to noise ratio
SWI - Susceptibility weighted imaging

T – Tesla
TCA – trichloroacetic acid
TE – echo time
TJ – tight junction
tMCAO – transient middle cerebral artery occlusion
tPA - recombinant tissue plasminogen activator
TR – repetition time
VAMP – vascular access mini-port
VEGF - vascular endothelial growth factor
ZO – zonula occludens

Table of contents

1. Introduction

Stroke remains one of the most severe and pressing health challenges worldwide, despite the advancements in medical technologies. It is currently the second-leading cause of death and the third-leading cause of disability-adjusted life years (DALYs) globally. Every year, approximately 12 million new cases of stroke occur, leading to 6 million deaths, underscoring the immense personal, familial, and societal impact of this condition. In 2021, there were approximately 102 million stroke cases worldwide, with ischemic stroke accounting for 70 million of those cases (He et al., 2024). Furthermore, the incidence of ischemic stroke has been on a significant upward trajectory, rising from 4.07 million cases in 1990 to 7.86 million cases in 2021 (Li et al., 2024). Projections indicate that this number will continue to increase, with estimates suggesting nearly 9.62 million new ischemic stroke cases by 2030 (Pu et al., 2023).

Despite advancements in acute stroke interventions, ischemic stroke remains a leading cause of long-term disability, with survivors often facing lifelong consequences. The burden of stroke extends beyond the affected individuals, impacting families and communities, and placing a significant strain on healthcare systems and economies. While immediate post-stroke treatments, such as thrombolysis and thrombectomy, have improved acute outcomes, the chronic consequences of stroke remain underexplored, and long-term recovery is often incomplete.

This highlights the critical importance of high-quality, in-depth research that delves into the chronic effects of stroke, particularly in understanding the underlying pathophysiological processes that contribute to long-term disability. One such key area is the impairment of the blood-brain barrier (BBB), which plays a central role in ischemic stroke. BBB dysfunction is a hallmark of ischemic stroke, contributing to the progression of tissue damage, cerebral edema, and secondary neuroinflammation. Understanding the temporal and regional aspects of BBB impairment, especially during the subacute and chronic phases, is crucial for identifying therapeutic targets that could mitigate these long-lasting effects. As stroke incidence continues to rise, advancing our knowledge of BBB dysfunction will be pivotal in developing interventions aimed at improving outcomes, reducing chronic disability, and enhancing quality of life for stroke survivors.

2. Aims of thesis

The **primary objective** of this thesis is to investigate the permeability of the blood-brain barrier during cerebral ischemia, with a particular focus on the acute and subacute phases of stroke. The specific goals of the study are as follows:

- To characterize changes in BBB permeability in human patients following ischemic stroke, as assessed by MRI. This includes a detailed analysis of the temporal and spatial dynamics of BBB impairment in the subacute period (7-12 days after symptom onset), which is crucial for understanding the progression of ischemic damage and identifying potential therapeutic windows.

- To establish a clinically relevant experimental model of ischemic stroke with reperfusion, specifically targeting the middle cerebral artery occlusion (MCAO) model. This model is intended to replicate human ischemic stroke conditions and to study the detailed mechanisms of BBB dysfunction in vivo. By refining this model, we aim to facilitate future research on stroke pathophysiology and therapeutic interventions.

- To create a standardized methodology for evaluating BBB disruption in experimental models of ischemic stroke. This includes the use of advanced MRI techniques to quantify and map BBB permeability, offering a reliable tool for assessing the efficacy of potential therapeutic strategies targeting BBB repair or protection.

Through these aims, this thesis seeks to contribute to a better understanding of BBB impairment during ischemic stroke and to provide a foundation for future studies focused on mitigating the chronic effects of stroke and improving recovery outcomes for stroke survivors.

3. General background

3.1 The Blood–CSF Barrier

The protection and regulation of brain tissue primarily involves more independent structures. The foremost among them is the blood-brain barrier (BBB), which remains a major focus of this thesis. In this chapter I provide a short overview of another important existing structure, namely blood-cerebrospinal fluid barrier which should by distinguished from the BBB.

The blood-cerebrospinal fluid barrier (BCSFB) is a critical interface within the central nervous system (CNS), primarily formed by the epithelial cells of the choroid plexus. This barrier plays a vital role in maintaining the homeostasis of the cerebrospinal fluid (CSF) and regulating the exchange of substances between the blood and the CSF. The choroid plexus, which produces CSF, is composed of a highly vascularized structure that facilitates the selective transport of ions, nutrients, and waste products, thus contributing to the overall metabolic environment of the brain (Gião *et al.*, 2022; Solár *et al.*, 2020).

The anatomical structure of the BCSFB is characterized by a monolayer of epithelial cells that are interconnected by tight junctions. These tight junctions are crucial for maintaining the barrier's integrity, preventing the passive diffusion of large molecules and pathogens from the bloodstream into the CSF (Engelhardt and Sorokin, 2009). The epithelial cells of choroid plexus are also equipped with various transporters, such as glucose transporter GLUT1, which mediates the transport of glucose across the barrier (Singh Badhan *et al.*, 2014). This selective permeability is essential for ensuring that the brain receives an adequate energy supply while simultaneously protecting it from fluctuations in blood composition (Kincer *et al.*, 2022).

Functionally, the BCSFB is involved in several key processes, including the regulation of ion concentrations, the removal of metabolic waste, and the transport of signaling molecules. The barrier facilitates the active transport of ions such as sodium and potassium, which are critical for maintaining the electrochemical gradients necessary for neuronal function (Knox *et al.*, 2023). Additionally, the choroid plexus secretes various peptides and hormones into the CSF, contributing to the neuroendocrine signaling within the CNS (González-Marrero *et al.*, 2012; Hubert *et al.*, 2019). The dynamic nature of the BCSFB allows for rapid responses to changes in the internal environment, which is particularly important during pathological conditions such as infections or neuroinflammation (Boje *et al.*, 2003).

The BCSFB also interacts with the blood-brain barrier. While the BBB is primarily composed of endothelial cells forming tight junctions and BCSFB is formed by epithelial cells of the choroid plexus. Both barriers work together to maintain CNS homeostasis, but they exhibit distinct permeability characteristics and transport mechanisms (Morris *et al.*, 2017). The BCSFB allows for a higher turnover rate of CSF, facilitating the exchange of nutrients and the removal of waste products more efficiently compared to the BBB. This contrasts with the BBB, which is more selective and serves as a highly controlled gatekeeper, preventing the entry of many blood-borne molecules, including xenobiotics and large hydrophilic compounds (González-Marrero *et al.*, 2012; Morris *et al.*, 2017).

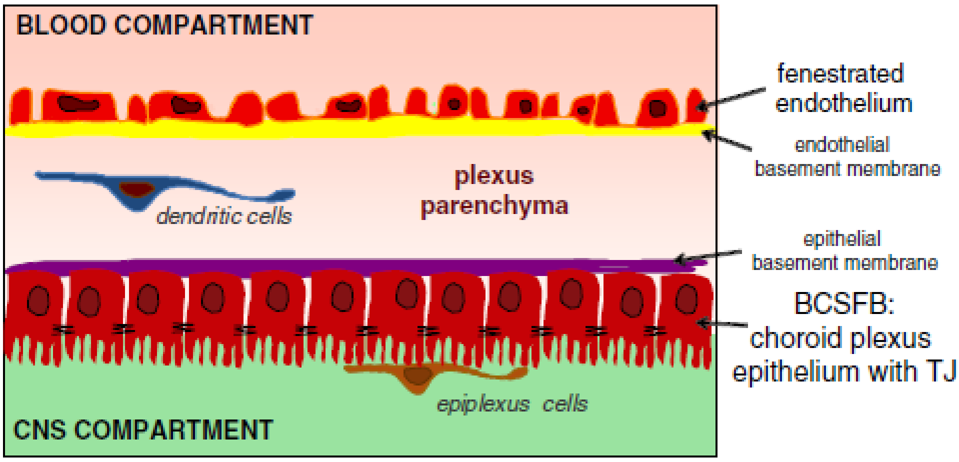

Figure 1 The BCSFB in the choroid plexus. Schematic drawing of the choroid plexus pointing out the fenestrated capillaries and the localization of the BCSFB at the level of choroid plexus epithelium (Engelhardt and Sorokin, 2009).

3.2 The Blood-Brain Barrier

Neurons require a continuous influx of oxygen and nutrients and are situated within a close proximity of 8–20 µm from capillaries. However, maintaining brain homeostasis is essential, as neurons are highly sensitive to various substances and even slight fluctuations in their concentrations. To address these needs, cerebral blood vessels undergo specialized modifications, giving rise to the blood-brain barrier. This structure serves as a selective interface between the bloodstream and neural tissue, preventing the entry of neurotoxic plasma components, blood cells, and pathogens while regulating the controlled exchange of essential molecules. (Barichello *et al.*, 2019; Kadry *et al.*, 2020; Tajes *et al.*, 2014).

3.2.1 Neurovascular unit

The NVU is a dynamic cellular assembly comprising endothelial cells, pericytes, astrocytes, microglia, neurons, and the extracellular matrix (Muoio *et al.*, 2014). It serves as a regulatory interface between the brain and the circulatory system, ensuring proper nutrient exchange and immune surveillance (McConnell *et al.*, 2017). The BBB is a structural component within the NVU, primarily formed by endothelial cells that line cerebral capillaries (Wu *et al.*, 2023). Pericytes, embedded in the basement membrane, regulate endothelial function and BBB integrity (Sá-Pereira *et al.*, 2012). Astrocytes provide metabolic and structural support, influencing BBB permeability through secreted factors such as vascular endothelial growth factor (VEGF) (Tajes *et al.*, 2014). Microglia, the resident immune cells of the CNS, contributes to BBB maintenance and inflammation regulation (Thurgur and Pinteaux, 2019). Neurons, through their synaptic activity, modulate vascular tone and endothelial cell function (Brandl and Reindl, 2023). While the NVU and BBB serve different primary functions, they are inherently interconnected. The NVU regulates BBB permeability through cellular interactions and biochemical signaling (Muoio *et al.*, 2014) (**Figure 2**).

3.2.2 Structure of BBB

3.2.2.1 Tight junctions

The BBB consists of a highly specialized monolayer of brain microvascular endothelial cells (EC), which are interconnected by tight junctions (TJ) that restrict paracellular permeability (Kadry *et al.*, 2020; Serlin *et al.*, 2015; Tajes *et al.*, 2014). These endothelial cells are unique compared to other vascular endothelial cells due to their lack of fenestrations, reduced pinocytotic activity, and presence of an intricate network of TJ (Sweeney *et al.*, 2019). The tight junction complex is composed of transmembrane proteins, including claudins, occludins, and junctional adhesion molecules (JAM), which are anchored to cytoplasmic scaffold proteins like zonula occludens (ZO-1, ZO-2, and ZO-3) (Barichello *et al.*, 2019; Zlokovic, 2008).

Claudins play a major role in maintaining the structural integrity of the BBB by forming a tight seal between adjacent endothelial cells. The most abundant and functionally significant claudin in the BBB is claudin-5, which is essential for size-selective permeability, preventing molecules larger than 800 Da from passing through (Kadry *et al.*, 2020; Shimizu *et al.*, 2012; Zlokovic, 2008). Claudin-5 also interacts with zonula occludens (ZO) proteins, particularly ZO-1, which helps anchor claudins to the actin cytoskeleton. This interaction stabilizes tight junction integrity, preventing unregulated solute transport (Kadry *et al.*, 2020). Studies have demonstrated that alterations in claudin-5 expression can lead to significant changes in BBB permeability, which can have profound implications for neurological health (McMillin *et al.*, 2015).

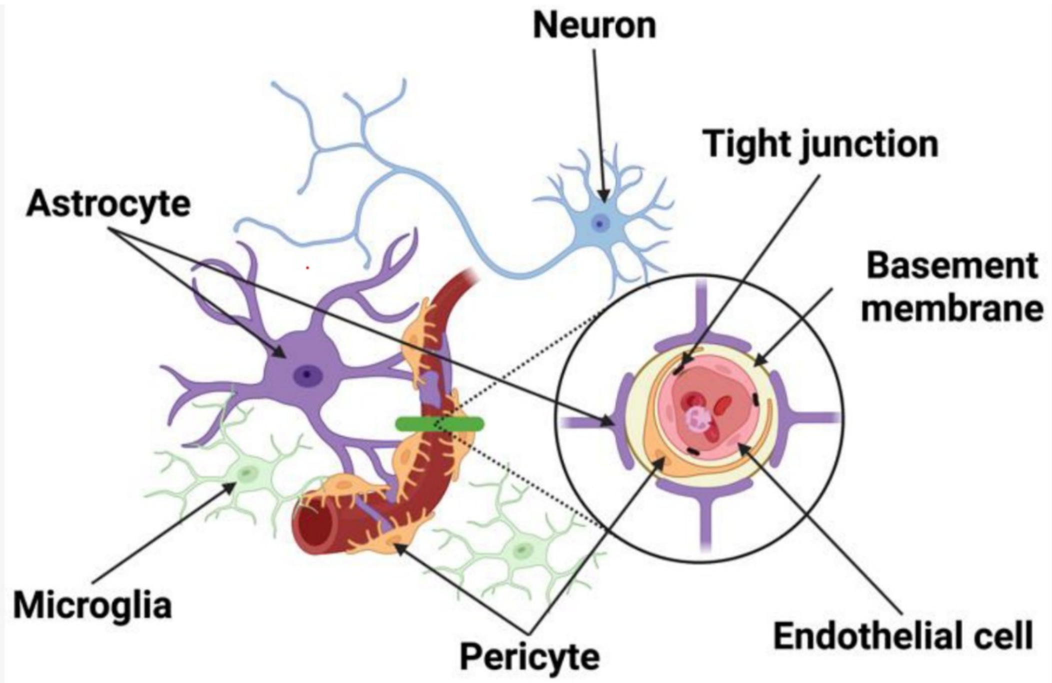

Figure 2 Neurovascular unit scheme

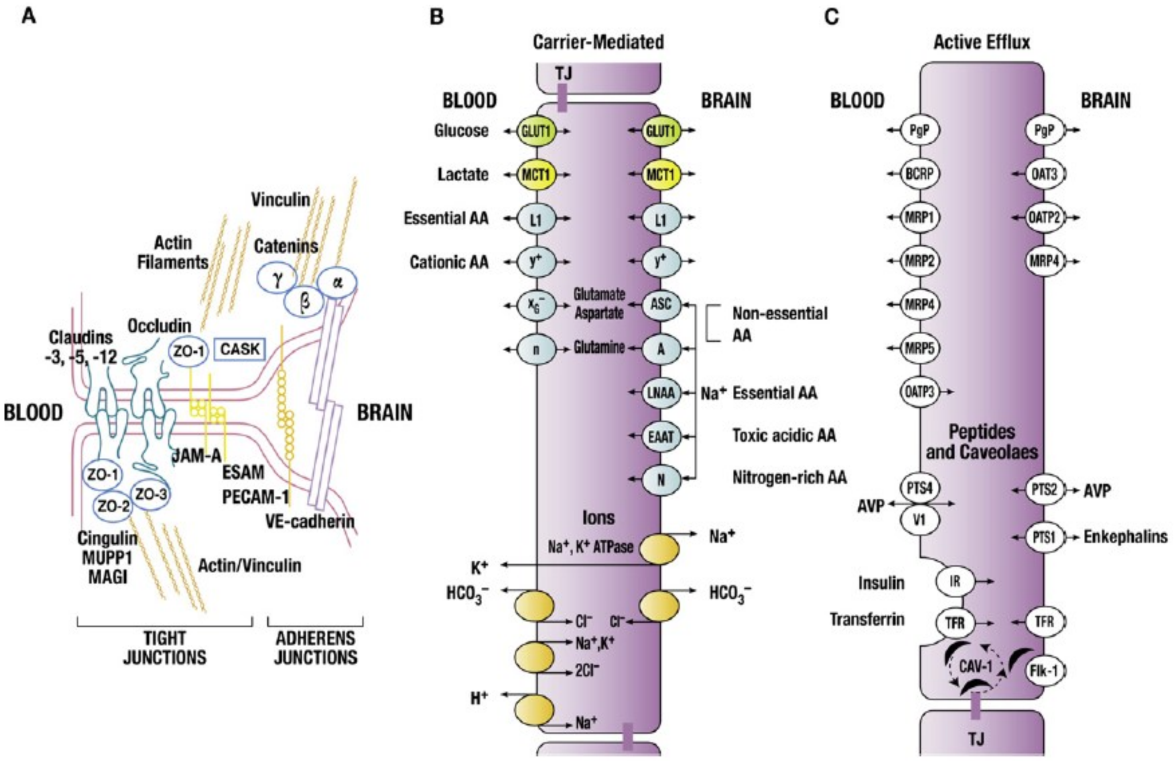

Figure 3 A Simplified Molecular Atlas of the BBB (Zlokovic, 2008)

(A) Tight junctions. Claudins (claudin-3, -5, and -12) and occludin have four transmembrane domains with two extracellular loops. The junctional adhesion molecule A (JAM-A) and the endothelial cell-selective adhesion molecule (ESMA) aremembers of the Ig superfamily. Zonula occludens proteins (ZO-1, ZO-2, and ZO-3) and the calcium-dependent serine protein kinase (CASK) are first-order cytoplasmic adaptor proteins that contain PDZ binding domains for the C terminus of the intramembrane proteins. Cingulin, multi-PDZ protein 1 (MUPP1), and the membrane-associated guanylate kinase with an inverted orientation of protein-protein interaction domain (MAGI) are examples of second-order adaptor molecules. The first- and second-order adaptor molecules together with signaling molecules control the interaction between the intramembrane proteins and actin/vinculin-based cytoskeleton. Adherens junctions. The vascular endothelial cadherin (VE-cadherin) is the key molecule. Platelet endothelial cell adhesion molecule 1 (PECAM-1) mediates homophilic adhesion. Catenins (a, b, c) link adhesion junctions to actin/vinculin-based cytoskeleton (Zlokovic, 2008).

(B) Carrier-mediated transporters. GLUT1, glucose transporter, and monocarboxylate transporter 1 (MCT1) for lactate exist at both the luminal and the abluminalmembranes. All essential amino acids (AA) are transported by the L1 and y+ systems on each membrane. Five Na+-dependent transport systems mediate eliminationof nonessential AA (ASC, A), essential AA (LNAA), the excitatory acidic AA (EAAT) (e.g., glutamate and aspartate), and nitrogen-rich AA (N) (e.g., glutamine)from the brain. Facilitative transporters xG and n on the luminal membrane mediate glutamate, aspartate, and glutamine efflux to blood. Ion transporters. Thesodium pump (Na+, K+-ATPase) on the abluminal membrane controls Na+ influx and K+ efflux. Sodium-hydrogen exchanger on the luminal membrane is a keyregulator of intracellular pH. Na+-K+-2Cl– cotransporter is on the luminal membrane. The chloride-bicarbonate exchanger exists on each membrane (Zlokovic, 2008).

(C) Active efflux transporters. Multidrug efflux transporters at the luminal membrane limit drug uptake into the brain. Transporters at the abluminal membrane could act in concert with luminal transporters to eliminate drugs from brain ISF. P-gp is expressed on each membrane. Breast cancer resistance protein (BCRP) is on the luminal membrane. Multidrug resistance-associated proteins (MRPs) are expressed mainly on the luminal membrane. Organic anion transporting polypeptide (OATP) 2 and 3 exist on the luminal and abluminal membranes, respectively. Organic anion transporter 3 (OAT3) is on the abluminal membrane.Peptide transporters and caveolae. Peptide transport system 1 (PTS-1) on the abluminal membrane mediates efflux of opioid peptides (e.g., enkephalins) from brain. PTS-2 mediates efflux of arginine-vasopressin (AVP). PTS-4 on the luminal membrane requires the vasopressinergic receptor 1 (V1) to transport AVP into the brain. Receptors for insulin (IR) and transferrin (TFR) are found in the caveolar membranes. Caveolin-1 (Cav-1) could be associated with receptors (e.g., TFR),tight junctions (TJ), or growth factor receptors, such as vascular endothelial growth factor receptor (Flk-1) (Zlokovic, 2008).

In models of inflammatory conditions, such as experimental autoimmune encephalomyelitis, the downregulation of claudin-5 has been associated with increased BBB permeability and subsequent neuroinflammation (Lanz *et al.*, 2013). Furthermore, mice lacking claudin-5 exhibit severe BBB leakage, leading to lethal neurological dysfunction shortly after birth (Nitta *et al.*, 2003).

While claudin-1 has been identified in various epithelial barriers, its presence in brain endothelial cells remains debated (Kadry *et al.*, 2020; Pfeiffer *et al.*, 2011; Zlokovic, 2008). In fact, some studies have reported a lack of claudin-1 expression in brain endothelial cells, particularly in the context of the BBB

Other claudins, such as claudin-3 and claudin-12, also contribute to barrier function, though their precise roles are still under investigation (Kadry *et al.*, 2020; Zlokovic, 2008). Sadowska et al. demonstrated that claudin-3 expression increases during the development of the ovine cerebral cortex, suggesting its involvement in the maturation of tight junctions in the vascular endothelium (Sadowska *et al.*, 2015). This finding aligns with the notion that claudin-3 contributes to the overall architecture of the BBB, promoting the sealing of paracellular pathways and thereby enhancing barrier function. Furthermore, claudin-3 has been implicated in the regulation of permeability, with studies indicating that its expression can influence the passage of ions and small molecules across the BBB (Brunner *et al.*, 2020; Koto *et al.*, 2007). In contrast, the role of claudin-12 in the BBB remains less clear. Research by Dias et al. indicated that claudin-12 is not essential for the maintenance of tight junction integrity in the BBB, suggesting that its presence may not significantly impact barrier function under normal physiological conditions (Castro Dias *et al.*, 2019). This finding raises questions about the specific functions of claudin-12, particularly in comparison to other claudins such as claudin-5, which is well-established as a critical component of the BBB (Nitta *et al.*, 2003).

The function of claudins in the BBB extends beyond passive restriction of molecular diffusion. They actively participate in maintaining ionic balance, a critical aspect of neural excitability and signaling. By working alongside transport systems, such as efflux pumps, claudins help regulate solute movement, ensuring that the brain environment remains stable and protected from fluctuations in the bloodstream (Sweeney *et al.*, 2019). Furthermore, claudins are integral to the NVU, where they interact with astrocytes, pericytes, and neurons.

These cellular interactions help regulate claudin expression and maintain the homeostatic functions of the BBB (Kadry *et al.*, 2020).

Occludin, a 65-kDa phosphoprotein, interacts with the cytoskeleton via its association with ZO-1 and ZO-2, providing additional stability to the tight junctions (Kadry *et al.*, 2020). Although occludin is essential for regulating BBB permeability, studies in occludin-deficient mice indicate that tight junctions can still form, suggesting that occludin is not indispensable for BBB integrity but plays a modulatory role (Zlokovic, 2008). Interestingly occludin is susceptible to attack by matrix metalloproteinases (MMP) (Resenberg and Yang, 2007). In rodent stroke models, reperfusion injury leads to a biphasic BBB opening: an early transient phase due to MMP-2 activation and a later, more severe phase involving MMP-9 and MMP-3 (Cheng *et al.*, 2006; Zlokovic, 2008).

Junctional adhesion molecules are immunoglobulin superfamily proteins. These molecules, including JAM-A, JAM-B, and JAM-C, are primarily located within endothelial tight junctions and contribute to maintaining BBB integrity by regulating paracellular permeability and leukocyte transmigration (Engelhardt and Sorokin, 2009). JAM interact with cytoplasmic scaffolding proteins like ZO-1, ZO-2, and cingulin, which link them to the actin cytoskeleton, reinforcing tight junction stability (Kadry *et al.*, 2020). However, their precise function in BBB regulation under physiological and pathological conditions remains an active area of research (Barichello *et al.*, 2019).

Zonula occludens proteins, including ZO-1, ZO-2, and ZO-3, are key cytoplasmic scaffold proteins that regulate the integrity of the BBB by linking tight junction proteins such as claudins and occludin to the actin cytoskeleton. These proteins belong to the membrane-associated guanylate kinase family (Kadry *et al.*, 2020). ZO-1, the most studied member, plays a crucial role in maintaining BBB permeability by stabilizing claudins and occludin within endothelial tight junctions (Barichello *et al.*, 2019). Loss or redistribution of ZO-1 has been linked to BBB breakdown in various neurological disorders, including stroke and neuroinflammation (Engelhardt and Sorokin, 2009). Additionally, ZO proteins contribute to the recruitment of signaling molecules that regulate endothelial cell polarity and barrier function (Zlokovic, 2008).

3.2.2.2 Adherent junctions

Adherent junctions (AJ) are crucial structural components of the BBB, playing a significant role in maintaining endothelial cell adhesion, vascular integrity, and paracellular permeability regulation (Zlokovic, 2008). These junctions function alongside tight junctions to create a highly restrictive barrier, controlling the passage of substances between the bloodstream and the brain parenchyma (Kadry *et al.*, 2020). AJ are comprised of transmembrane and cytoplasmic plaque proteins. Their function is to link endothelial cells to the actin cytoskeleton, with vascular endothelial (VE)-cadherin being the primary adhesive molecule. VE-cadherin forms homophilic interactions between adjacent endothelial cells and is stabilized by scaffolding proteins such as catenins (α, β, γ, and p120), and other regulatory proteins like platelet and endothelial cell adhesion molecule-1 (PECAM-1) and nectins (Wu *et al.*, 2023). Various pathological conditions, including neurodegenerative diseases such as Alzheimer's and multiple sclerosis, as well as ischemic stroke, neuroinflammation, and brain tumors, have been linked to AJ dysfunction, leading to increased BBB permeability and neurovascular damage (Wilhelm *et al.*, 2016).

3.2.3 Function and permeability regulation

The BBB tightly regulates the transport of molecules through several mechanisms. Small, lipophilic molecules such as oxygen and carbon dioxide can diffuse freely across the endothelial membrane (Sweeney *et al.*, 2019; Zlokovic, 2008). Essential nutrients like glucose and amino acids are transported via solute carrier transporters, ensuring adequate metabolic supply to the brain (Kadry *et al.*, 2020). Large biomolecules, including insulin and transferrin, cross the BBB through receptor-mediated transcytosis, facilitated by specific receptors (Kadry *et al.*, 2020). Active efflux pumps, such as P-glycoprotein and multidrug resistance proteins, prevent the accumulation of potentially harmful compounds in the CNS (Zlokovic, 2008). Overview of all transport mechanisms can be seen in **(Figure 3).**

It is worth also worth to mention the selective nature of the BBB also poses a significant challenge for drug delivery to the CNS. Many therapeutic agents, including antibiotics and chemotherapeutics, exhibit poor BBB permeability, limiting their efficacy in treating brain diseases(Kadry *et al.*, 2020). Emerging strategies to enhance BBB permeability include focused ultrasound-mediated disruption, nanoparticle-based drug carriers, and receptor-mediated transcytosis approaches(Sweeney *et al.*, 2019).

3.2.4 Disruption of blood brain barrier in brain ischemia

Stroke occurs when there is a sudden and significant reduction in regional cerebral blood flow, often due to arterial occlusion. This leads to an immediate shortage of oxygen and glucose, critically affecting neurons, astrocytes, and oligodendrocytes in the impacted area (Jolly *et al.*, 2018). As ATP production plummets, ATP-dependent ion transporters, chiefly the Na^+/K^+-ATPase fail, causing sodium (Na^+) to accumulate intracellularly (Mohr *et al.*, 2010). This ionic overload drives water into cells along osmotic gradients, culminating in rapid cytotoxic edema. Concomitantly, ischemia diminishes the function of glutamate transporters (notably on astrocytes) (Jiang *et al.*, 2014), leading to excessive glutamate accumulation in the synaptic cleft. Overstimulation of NMDA and AMPA receptors on neuronal membranes results in further Na^+ and $Ca2^+$ influx, compounding the intracellular ionic crisis and accelerating cell injury (Lin *et al.*, 2014; Sekiya *et al.*, 2012). Intracellular $Ca2^+$ overload triggers the activation of proteolytic enzymes such as calpains, caspases, and other degradative pathways, thereby damaging cytoskeletal proteins, mitochondria, and nuclear DNA (Ruiz *et al.*, 2014; Xue *et al.*, 2017).

In tandem with these excitotoxic processes, the abrupt drop in cerebral blood flow initiates an inflammatory microenvironment. Endothelial cells respond by upregulating adhesion molecules (e.g., P-selectin, E-selectin) that can later facilitate leukocyte rolling and adhesion (Secor *et al.*, 2010). Mitochondrial damage and enzymatic conversion of xanthine dehydrogenase to xanthine oxidase become relevant as soon as reperfusion occurs (though the stage is set in this hyperacute interval), priming the tissue for a burst of reactive oxygen species (ROS) (Loor *et al.*, 2011).

Even though major blood-brain barrier breakdown is not usually profound at this earliest stage of brain ischemia, subtle endothelial and astroglial changes start to take place. Minor tight junction protein alterations (including phosphorylation or partial proteolysis of occludin and claudin-5 (Mansour *et al.*, 2020; Obenaus and Badaut, 2022), begin to compromise the selective permeability of the blood-brain barrier (BBB). These early disruptions do not yet allow significant plasma protein leakage but create an environment where ionic dysregulation starts to unfold. As ischemia persists beyond the first few hours, endothelial dysfunction further impairs BBB integrity, leading to the leakage of Na^+, Cl^-, and other small ions into the extracellular space. This shift is primarily mediated by the upregulation of the Na^+-K^+-$2Cl^-$ cotransporter (NKCC1) on endothelial cells (Jayakumar *et* *al.*, 2011). Furthermore, astrocytes begin to swell due to excessive sodium uptake via NKCC1 and dysregulated aquaporin-4 (AQP4) channel activity (Rutkowsky *et al.*, 2011; Thrane *et al.*, 2011) which lead to impaired water clearance from the extracellular space, further contributing to edema formation (Hawkins *et al.*, 2013). This marks the transition from purely intracellular swelling cytotoxic edema to a state where extracellular ionic disturbances drive further water influx into both cells and the perivascular space (ionic edema). Importantly, at this stage, while the BBB is still relatively intact against large proteins, the loss of ion selectivity creates osmotic gradients that facilitate uncontrolled water accumulation, setting the stage for increased brain tissue pressure and further neuronal injury.

When clinicians restore blood flow via pharmacological thrombolysis (e.g., intravenous recombinant tissue plasminogen activator or mechanical thrombectomy), there is a dual-edged effect. On the one hand, salvaging the peri-ischemic tissue is critically important for reducing the overall infarct volume. On the other hand, the sudden influx of oxygen and blood components into metabolically compromised tissue can amplify injury, often termed "reperfusion injury" (Hrishikesh Bhagwat *et al.*, 2022; Su *et al.*, 2022).

At the microvascular level, a phenomenon known as "no-reflow" can occur (Wang *et al.*, 2020). Even though the large vessel has been re-opened, many micro vessels remain obstructed by platelet-leukocyte aggregates, fibrin clots, and endothelial swelling (Brunner *et al.*, 2017). This continued microvascular compromise keeps portions of the brain parenchyma hypoxic, perpetuating ATP depletion in local neurons and glia. Cells that have not undergone irreversible injury might still recover if perfusion is improved, but for those with severely damaged mitochondria, the reintroduction of oxygen can exacerbate oxidative stress (Xie *et al.*, 2014). Damaged mitochondria produce ROS more vigorously when oxygen suddenly becomes abundant, and endothelial NADPH oxidase contributes additional ROS. These free radicals injure lipid membranes (particularly those rich in polyunsaturated fatty acids), cause protein misfolding, and degrade DNA (Ospel *et al.*, 2024).

At the BBB level, an early reperfusion sets off a rapid upregulation of matrix metalloproteinases especially MMP-9 facilitated by cytokines (TNF-α, IL-1β, IL-6) and chemokine signals (Jin *et al.*, 2018). MMP-9 and MMP-2 degrade type IV collagen, laminin, and fibronectin within the basement membrane, while also cleaving tight junction proteins (claudin-5, occludin, ZO-1) (Jin *et al.*, 2018; Liu *et al.*, 2017). As these proteins deteriorate, the normally restrictive endothelial barrier becomes more permeable, and vasogenic edema starts to develop. Moreover, endothelial cells themselves may become “blebbed” or detached from the basement membrane in patches due to cytoskeletal damage and disrupted integrin signaling.

Another critical event in the early reperfusion phase is the influx of calcium into endothelial cells, largely through reperfusion-induced mechano-sensitive or oxidative-sensitive channels (Fukumoto *et al.*, 2012). This perturbs actin cytoskeleton integrity and can widen paracellular clefts between endothelial cells, amplifying the leak of plasma proteins into the extracellular space. Meanwhile, astrocytes in the perivascular end-feet region experience oxidative and metabolic stress, impairing their ability to regulate extracellular potassium homeostasis and glutamate clearance. This dysfunction is exacerbated by the dysregulation of AQP4 (Zeng *et al.*, 2012).

As the stroke lesion matures, immune infiltration and microglial activation become dominant features. Resident microglia, typically in a resting or surveillant state, transform into an activated phenotype, often referred to as “M1-like”, releasing pro-inflammatory cytokines and chemokines (Li, Wernersbach, *et al.*, 2022). Damaged neurons and necrotic tissue release “danger-associated molecular patterns” such as HMGB1, peroxiredoxins (Faridová *et al.*, 2023), and DNA fragments, all of which further stimulate microglia and attract peripheral immune cells (Gao *et al.*, 2011).

Endothelial cells that have been exposed to ischemic and reperfusion stress express increased amounts of intercellular adhesion molecule-1 (ICAM-1), vascular cell adhesion molecule-1 VCAM-1, and selectins (Nielsen et al., 2020). Neutrophils are among the earliest leukocytes to infiltrate, though their numbers typically peak around 24–72 hours. Activated neutrophils secrete myeloperoxidase and can form neutrophil extracellular traps (NETs) that damage the microvasculature and exacerbate BBB disruption. Simultaneously, macrophages and T-lymphocytes begin to extravasate, guided by chemokine gradients (CCL2, CXCL10), and accumulate in both the infarct core and border regions (Curry *et al.*, 2010).

These inflammatory cells secrete additional MMPs, produce abundant ROS (via NADPH oxidase and other pathways), and release proteolytic enzymes. MMP-9 activity often peaks within this subacute window, leading to extensive breakdown of the basement membrane and pericyte detachment. Pericytes, which are integral to maintaining capillary integrity, can undergo apoptosis or transform phenotypically under severe stress, further destabilizing the vascular architecture (Dibble *et al.*, 2023). As tight junctions degrade and the basement membrane becomes porous, more plasma proteins, including albumin and fibrinogen, leak into the interstitial space. This elevates extracellular oncotic pressure, drawing fluid out of capillaries and intensifying vasogenic edema.

The risk of hemorrhagic transformation is pronounced during this subacute interval. If large segments of the microvasculature are compromised and the basement membrane is heavily digested, the structural integrity of these vessels is minimal. The presence of reperfusion in combination with systemic fibrinolysis (if used) and local blood pressure can cause extravasation of red blood cells. This hemorrhage may be mild – petechial, or more severe, resulting in large intracerebral hematomas that dramatically worsen outcomes via increased intracranial pressure and mass effect. Macrophages eventually clear red blood cells, leading to the formation of hemosiderin-laden macrophages (or siderophages) (Obenaus and Badaut, 2022), which signify prior hemorrhage when observed on histopathological or imaging images, such as SWI.

Meanwhile, phagocytes (microglia, infiltrating monocyte-derived macrophages) also clear necrotic neuronal and myelin debris from the lesion site. Although essential for cleaning up cellular detritus, this process releases additional pro-inflammatory mediators and, if uncontrolled, can exacerbate tissue damage. Astrocytes, for their part, become reactive, enlarging their processes, upregulating intermediate filament proteins like glial fibrillary acidic protein (GFAP), and forming a partial "barrier" around the infarct zone (Hill *et al.*, 2019). While this astroglial response helps contain inflammation and fosters a boundary between healthy and necrotic tissue, it also contributes to a long-term glial scarring (Conforti *et al.*, 2022).

Over time, the nature of the inflammatory infiltrate and the fate of the BBB evolve. By approximately one to two weeks after stroke onset, the predominantly pro-inflammatory M1-like microglial and macrophage profile may shift, at least in part, to a more anti-inflammatory or reparative M2-like phenotype. These cells produce factors such as IL-10 and TGF-β that can encourage vascular remodeling and aid in the partial reconstitution of the BBB (Chen *et al.*, 2019). Furthermore, astrocytes begin synthesizing extracellular matrix components to form a glial scar, which may help to stabilize the region by blocking ongoing infiltration of peripheral immune cells. However, the glial scar also limits axonal regeneration and synaptic reconnection, creating a barrier to neuronal plasticity in the infarct boundary zone.

Persistent BBB disruption can remain in certain patients, particularly those with large infarcts, hemorrhagic transformations, or comorbidities (hypertension, diabetes, hypercholesterolemia). Chronically elevated levels of MMPs or sustained oxidative stress hamper efforts at restoring normal endothelial function. Some capillaries may undergo "pseudo-normalization" structurally yet retain functional deficits in tight junction arrangement and transendothelial electrical resistance (Di *et al.*, 2021). The newly formed basement membrane might differ qualitatively from the original, featuring fibrotic changes that increase stiffness and reduce normal vasoactive responses. Pericyte loss or dysfunction may persist for weeks, destabilizing the microvascular unit and rendering it susceptible to small, ongoing leaks or microbleeds (Rustenhoven *et al.*, 2018).

In the chronic stages, edema typically subsides as fluid is resorbed and the necrotic tissue is replaced by a glial scar or cystic cavity. Although the major threat of large-scale vasogenic edema and hemorrhage recedes, the lingering microvascular alterations may predispose survivors to secondary pathologies such as vascular cognitive impairment or repeated ischemic events (Ihle-Hansen *et al.*, 2012). Some patients develop leukoaraiosis-like (diffuse white matter abnormalities) changes around the infarct (Cho *et al.*, 2015), possibly due to ongoing low-level BBB dysfunction and compromised perivascular clearance of metabolic waste.

While it is convenient to categorize the evolution of ischemic stroke and recanalization-associated injury into discrete phases, in reality these processes overlap extensively. The abrupt arrest of blood flow triggers instantaneous energy failure and excitotoxic cascades. Early reperfusion can halt or reverse some of these damaging processes in peri-lesional tissue, but it also initiates a parallel set of insults driven by oxidative stress, MMP activation, and inflammatory cell infiltration. Over hours to days, immune mechanisms and proteolysis peak, severely compromising the BBB and promoting vasogenic edema. Eventually, subacute and chronic reparative pathways emerge, with microglia and macrophages phagocytosing debris, astrocytes forming glial scars, and partial reconstitution of the BBB taking place. Yet in severe cases, the damage to micro vessels and surrounding tissue persists long-term, underscoring the complexity of post-stroke pathology.

4. Investigating disruption of blood brain barrier in clinical practice

4.1 Overview of MRI sequences used in clinical practice

Magnetic resonance imaging (MRI) is a widely used, non-invasive method for examining brain tissue following events such as strokes and related phenomena, including edema, gliosis, hemorrhage, and disruptions to the blood-brain barrier. Different MRI sequences are tailored to capture specific tissue properties or abnormalities in the brain, such as ischemia, hemorrhage, vascular structures, or cerebrospinal fluid. By utilizing information from a variety of MRI sequences, clinicians can gain a more comprehensive understanding of the patient's condition and achieve a better diagnostic perspective (Hagmann *et al.*, 2006).

The two primary MRI sequences commonly utilized are T1-weighted and T2-weighted imaging, with image contrast and brightness being predominantly influenced by the properties of the T1 relaxation process. A key distinction between these sequences lies in their depiction of cerebrospinal fluid (CSF): it appears dark on T1-weighted images but bright on T2-weighted ones (Wintermark *et al.*, 2008). Another widely used sequence is Fluid-Attenuated Inversion Recovery (FLAIR), which is conceptually similar to T2-weighted imaging but incorporates significantly longer echo time (TE) and repetition time (TR). This adjustment ensures that abnormalities remain bright while CSF becomes dark, making FLAIR especially effective in differentiating pathological changes from normal CSF signals (Tedyanto *et al.*, 2022).

T1-weighted imaging is often enhanced with the administration of gadolinium, a non-toxic, paramagnetic contrast agent that reduces T1 relaxation time and alters signal intensity. On T1-weighted scans, gadolinium appears bright and provides critical insights into the vascular system and disruptions of the blood-brain barrier (Lin and Liebeskind, 2016).

Diffusion-weighted imaging (DWI) is specifically designed to capture the random motion of water molecules, primarily free-moving protons in the extracellular space, while highlighting their restricted movement within cells. In normal conditions, water flows more freely in extracellular regions, but during ischemia, the sodium-potassium pump fails, leading to sodium accumulation inside cells. This disruption creates an osmotic imbalance, driving water from the extracellular to the intracellular compartment. DWI is highly sensitive to these changes, showing intense signals where water movement is restricted within cells, making it an excellent tool for detecting acute ischemia (Lin and Liebeskind, 2016; Srinivasan *et al.*, 2006).

DWI together with the apparent diffusion coefficient (ADC), can identify and measure ischemic changes within minutes of vessel occlusion. On DWI, ischemic tissue is clearly different from healthy brain regions, with brighter signals representing limited water diffusion. ADC maps further refine the assessment and distinguish ischemic areas from others that may show clear signals due to vasogenic edema or other T2-based effects. By showing restricted diffusion as dark areas on ADC maps, these tools allow accurate differentiation between acute infarcts and other high-signal abnormalities, ensuring accurate diagnosis (Lin and Liebeskind, 2016; Srinivasan *et al.*, 2006; Tedyanto *et al.*, 2022).

4.2 Clinical study composition

Damage to the blood-brain barrier is a critical process in ischemic stroke, highlighting the need for regional characterization. To explore this, we conducted an MRI clinical study aimed at assessing vascular dysfunction during the acute and subacute phases of ischemic stroke. Patients with ischemic stroke may arrive at the hospital at different times following the onset of the event. Based on the timeline, a stroke can be divided into several phases: early hyper-acute, late hyper-acute, acute, subacute, and chronic. On standard MRI, a stroke displays specific characteristics that vary depending on the age of the infarct. The typical timeline classification includes the following phases: hyper-acute (0–6 hours), late hyper-acute (6–24 hours), acute (1–7 days), subacute (7–21 days), and chronic stroke (more than 21 days) (Kim *et al.*, 2014).Vascular dysfunction, characterized by increased BBB permeability, is a key pathological feature in the acute phase of ischemic stroke. Previous studies have shown that gadolinium-based MRI contrast agents leak in close spatial correlation with FLAIR-positive MRI lesions during this phase (Giraud *et al.*, 2015). However, the maturation of ischemic lesions in later stages is also marked by changes in T2-weighted and FLAIR images (Allen *et al.*, 2012; Neumann-Haefelin *et al.*, 2000), although the exact timeline of these alterations remains unclear. Experimental studies in animal models have examined the timeline of BBB impairment, revealing a peak in the subacute phase, followed by a gradual reduction (Jiang et al., 2018). While BBB leakage has been observed up to one month after stroke in both rodents (Moisan *et al.*, 2014) and human patients (Liu *et al.*, 2013), indicating prolonged dysfunction, data on longer intervals are limited or nonexistent.

Perilesional tissue surrounding the ischemic lesion forms a glial scar, but recent findings suggest that these scars do not fully seal the ischemic lesions, allowing neurotoxic factors and blood components to infiltrate perilesional brain tissue for months after the stroke (Zbesko *et al.*, 2018). This infiltration contributes to swelling, functional alterations, and delayed neurodegeneration in adjacent regions, as demonstrated in animal models.

Early restoration of blood flow remains the most common therapy for ischemic stroke, offering the potential for full recovery of impaired brain functions if administered within the treatment window(Prabhakaran *et al.*, 2015). Currently, the therapeutic window extends up to 4.5 hours for fibrinolytic treatment and 6 hours for the mechanical recanalization strategy after the onset of the first signs of stroke (Powers *et al.*, 2019). However, recent studies suggest that some patients may benefit from reperfusion even beyond this time window (Pang *et al.*, 2019). For example, two randomized controlled clinical trials (DAWN and DEFUSE 3) on endovascular mechanical thrombectomy found that selective delayed recanalization, enhanced patients 90-day outcomes, even when performed between 16 and 24 hours after symptom onset (Ragoschke-Schumm and Walter, 2018). These outcomes are also supported by experimental studies. McBride et al. demonstrated that delayed recanalization promoted functional recovery in rats following permanent MCA occlusion. Delayed recanalization restored cerebral blood flow, facilitated sensorimotor recovery, enhanced learning and memory, and reduced infarct volume(McBride *et al.*, 2018). Nevertheless, as of today, 4.5 and 6 hours remain the gold standard time windows for thrombolytic therapy in ischemic stroke.

Although reperfusion therapies have reduced hospitalization times for ischemic stroke patients, typical discharge rarely occurs before one week (Tate *et al.*, 2019). During this time, pathophysiological processes, including inflammation, continue to affect ischemic lesions (Dirnagl, 2012). This motivated us to perform a detailed spatial analysis of vascular dysfunction maturation within the ischemic lesion during the subacute phase, a period that coincides with typical patient discharge. We conducted a series of MRI scans, both with and without gadolinium contrast, during the second week of hospitalization (7-12 days) and analyzed the spatial relationships between BBB impairment regions and ischemic lesion subregions, defined by FLAIR or DWI alterations. We also investigated whether gadolinium contrast could be detected in the tissue surrounding the ischemic lesion. Given the recent link between blood component extravasation and the development of acquired epilepsy

(Löscher and Friedman, 2020), we assessed the risk of vascular epilepsy using the SeLECT score (Galovic *et al.*, 2018) and correlated it with the presence of vascular dysfunction in the subacute period following stroke.

*The **SeLECT** score is a useful score for the prediction of late seizures after stroke and includes the severity of stroke (Se), large artery atherosclerosis (L), early seizure (E), cortical involvement (C), and the territory of the middle cerebral artery (T). and correlated it with the presence of vascular dysfunction in the subacute period following stroke.*

4.3 Methods

We collaborated on this part of the thesis in tight cooperation with Ing. David Kala PhD who created the data analysis which was included in his in his doctoral thesis (Kala, 2022) .

Patients admitted to the hospital with acute ischemic stroke between October 2015 and March 2017 were screened and recruited for the study. The inclusion criteria were age over 18 years, MRI-confirmed supratentorial acute ischemic lesion, and signed informed consent. Informed consent was obtained from patients directly when possible, with the level of information provided tailored to their understanding. In cases where patients with large hemispheric infarctions were unable to consent, consent was provided by a legally authorized representative (e.g., spouse or guardian) or an independent physician, in accordance with Czech law. Exclusion criteria included a history of prior stroke and contraindications to gadolinium administration. The study was approved by the Ethics Committee of University Hospital Motol (Ref. number: EK-1091/14). All patients received treatment according to current acute stroke guidelines, with contrast MRI scans incorporated into the diagnostic process. Patients showing clinical signs of acute stroke (sudden onset of speech impairment, unilateral weakness) received appropriate treatment, including intravenous thrombolysis or mechanical thrombectomy, based on the decision of an on-call stroke specialist. Stroke severity was assessed using the ASPECTS and NIHSS scales, and the SeLECT score was calculated to evaluate the risk of vascular epilepsy.

*The **ASPECTS** (Alberta Stroke Program Early CT Score) is a quantitate score that measures the extent of early ischemic changes in anterior circulation hyperacute ischemic stroke*

*The **NIHSS** is a 15-item neurological examination stroke scale used to evaluate the effect of acute cerebral infarction on the levels of consciousness, language, neglect, visual-field loss, extraocular movement, motor strength, ataxia, dysarthria, and sensory loss.*

Subacute MRI scans were performed between 7 and 12 days after symptom onset, which is a typical time for patient discharge. Imaging was conducted on a Philips Ingenia 1.5T MRI scanner. The following sequences were used: 3D T2-weighted (T2w), FLAIR, DWI, SWI, 3D T1-weighted (T1w), DTI, and post-contrast 3D T1w with gadolinium. The total scan duration was between 25 and 30 minutes. Gadovist (Bayer Pharma AG) was injected intravenously approximately 5 minutes before post-contrast T1w imaging.

MRI data were evaluated by an experienced radiologist and neurologist, noting signal alterations, ischemic lesions, BBB impairment, and hemorrhagic transformation across FLAIR, T1w, DWI, and SWI images. These images were processed using SPM12 and FreeSurfer software for registration and segmentation. All brain structures were segmented into cortical gray matter and subcortical white matter. Lesions were identified based on hyperintensity in FLAIR and DWI sequences, with manual analysis confirming the lesion characteristics.

Lesions were segmented using semiautomatic algorithms in both FLAIR and DWI images. Regions with hyperintensity in FLAIR and DWI were classified as FLAIR+ and DWI+, respectively. Regions without hyperintensity were classified as FLAIR- and DWI-. Lesions were further divided into three subregions based on the overlap of FLAIR+ and DWI+ volumes (FLAIR+DWI+, FLAIR+DWI-, FLAIR-DWI+) as depicted on **Figure 4**.

BBB impairment was assessed using T1w imaging with and without gadolinium contrast. The algorithm from Chassidim et al. was used for voxel-based comparisons of pre- and post-contrast images. Voxels showing significant increases in intensity after gadolinium administration were considered indicative of BBB impairment.

Only regions connected to ischemic lesions were analyzed to focus on local BBB dysfunction. Intensity differences between pre- and post-contrast images were normalized to a 0-1 range for intersubject comparability, using vitreous body and large vessel samples for normalization.

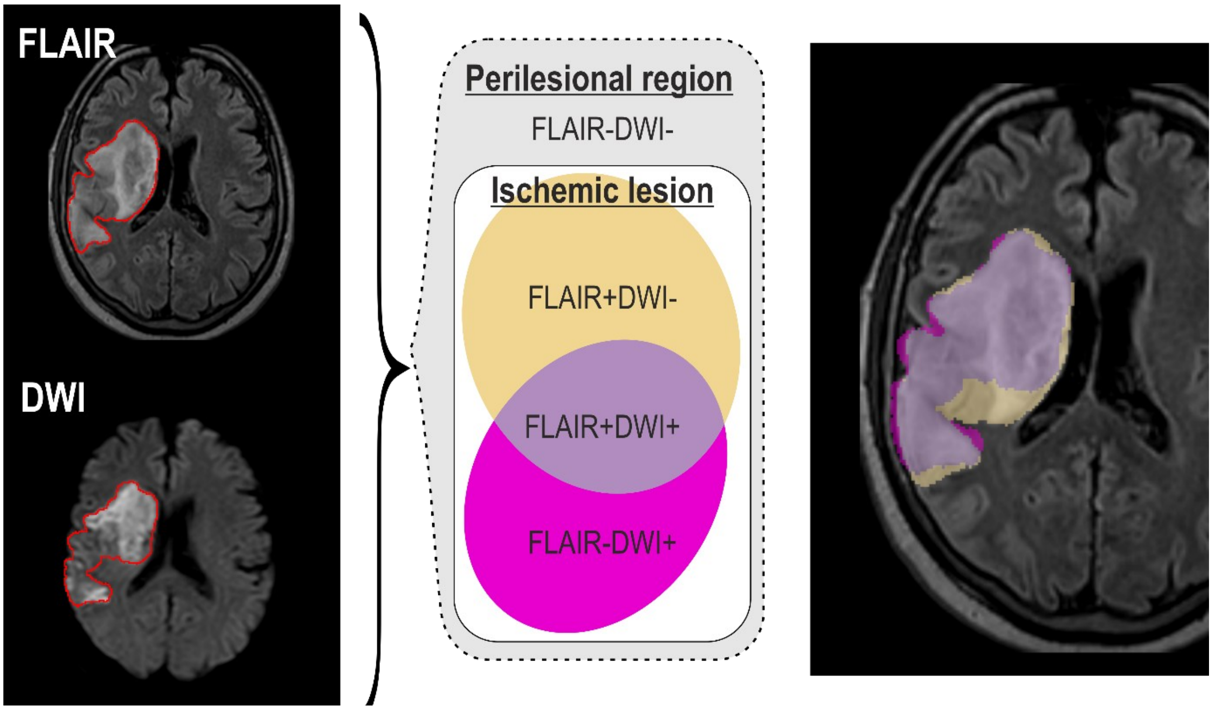

Figure 4 Lesion detection and definition of brain sub-regions. Four sub-regions were defined as a logical combination of FLAIR and DWI image positivity, i.e., FLAIR+DWI+, FLAIR-DWI+, and FLAIR+DWI- as ischemic sub-regions and FLAIR-DWI- as a perilesional region. The combination of FLAIR and DWI imaging techniques is commonly used to distinguish between individual types of cerebral edema and in the acute phase also between ischemic core and penumbra. FLAIR refers to altered water content in the extracellular space (vasogenic edema) and in later phases also to infiltration of inflammatory cells or gliosis. Hyperintesity in DWI refers to altered diffusion suggesting a shift of water content from extracellular to intracellular space of brain cells (cytotoxic edema) in acute or more pronounced T2 shine-through phenomenon in the subacute period. Because our data come from the later phase of lesion maturation, we intentionally avoided traditional pathophysiology-based terminology because it might be in this timepoint misleading. (Kala, 2022. fig.14, edited)

4.3.1 Statistical evaluation

Data were statistically compared using nonparametric statistical methods (the unpaired Wilcoxon rank-sum test and paired Wilcoxon signed-rank test where appropriate) while possessing a nonnormal distribution (tested by the Kolmogorov-Smirnov test). All data are expressed as the median and interquartile range (IQR, q75 – q25).

4.4 Results

Eighty-six patients met the inclusion criteria, but six were excluded due to severe MRI artifacts. The remaining 80 patients were included in the study, with 20 showing no evidence of BBB damage (no gadolinium leakage). Based on the presence of BBB disruption, patients were divided into two groups: those with leaking BBB and those with intact BBB. The clinical characteristics of both groups, shown in **Table 1**, were compared. Patients with intact BBB had a significantly lower ischemic lesion volume (4.6 mL vs 17 mL in the leaking BBB group), a higher ASPECTS (10 vs 10, but fewer lower scores in the intact BBB group), a lower SeLECT score (3 vs 3.5), and a lower incidence of hemorrhagic transformation (5% vs 36%) after ischemic insult. No other significant differences were found.

Table 1 Clinical characteristics of two groups of patients, with and without visible BBB disruption. Used abbreviations: ACA (anterior carotid artery), MCA: (middle cerebral artery), PCA (posterior cerebral artery), NIHSS (National Institute of Health Stroke Scale), ASPECTS (Alberta Stroke Program Early CT Score), IVT (intravenous thrombolysis), MT (mechanical thrombectomy)

	Group A With leaking BBB	Group B With intact BBB	p (-)
Number of patients	60	20	-
Gender (Man/Woman)	39/ 21	14/6	0.600
Age	68.5 (18)*	68 (18.5)*	0.63
Affected ACA territory	6%	15%	0.207
Affected MCA territory	79%	70%	0.421
Affected PCA territory	18%	10%	0.343
NIHSS on admission	5 (5)*	5 (5.5)*	0.493
NIHSS after 24h	4 (4)*	2 (3)*	0.085
NIHSS on discharge	2 (2)*	2 (2) *	0.326
ASPECTS	**10 (2)***	**10 (0)***	**0.004#**

SeLECT score	**3.5 (2)***	**3 (1)***	**0.025#**
Performed IVT or MT	41%	30%	0.386
Presence of hemorrhagic transformation	**36%**	**5%**	**0.007**
Volume of the ischemic lesion (mL)	**17.04(40.04)***	**4.59(7.99)***	**0.001**

*median (IQR)

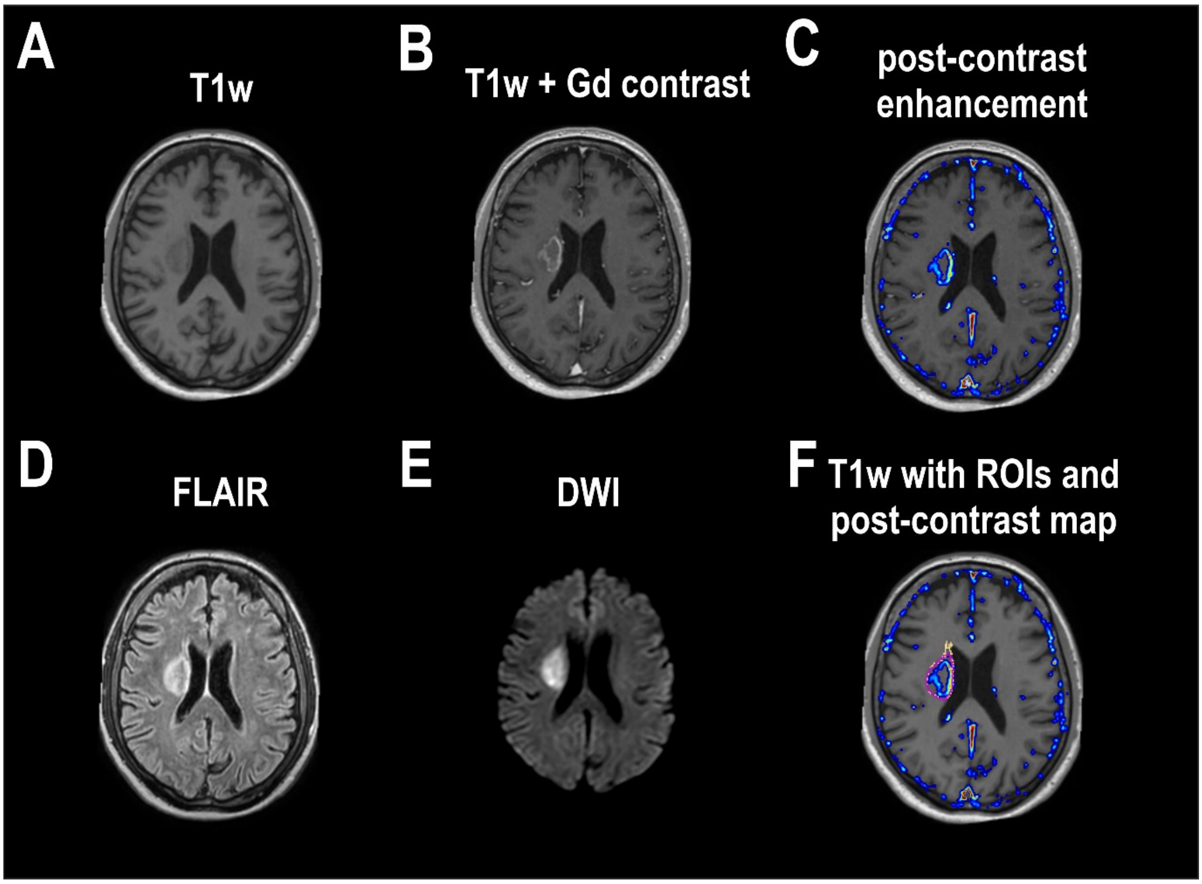

Figure 5 A typical patient dataset. Forty-seven years old man hospitalized with right-sided cerebral ischemia in MCA territory twelve days before MRI examination (NIHSS 5, SeLECT 3). Panels (A) and (B) show T1w images before and after contrast agent, respectively, and calculated postcontrast enhancement on panel (C) (blue=low, red=high). The ischemic lesion is visible in FLAIR (D) and DWI (E) MRI images. Panel (F) shows the result of the detection of FLAIR+ (yellow) and DWI+ (purple) regions outlined on the T1w image. In this patient, detections in FLAIR and DWI spatially correlate, and contrast agent extravasation is localized inside those regions.

Ischemic lesions were detected in both groups by FLAIR or DWI hyperintensities and divided into three sub-regions: FLAIR+DWI+, FLAIR+DWI-, and FLAIR-DWI+. The median ischemic lesion volume in the leaking BBB group was 17.04 mL (IQR 40.04 mL), while in the intact BBB group, it was significantly lower at 4.59 mL (IQR 10.42 mL, p=0.001). The composition of lesions also varied between groups: the FLAIR+DWI- sub-region was significantly larger in the leaking BBB group (57% vs 31% in the intact BBB group). The volume of BBB impairment strongly correlated with the ischemic lesion volume (Pearson coefficient 0.74, p<0.001;**Figure 6**).

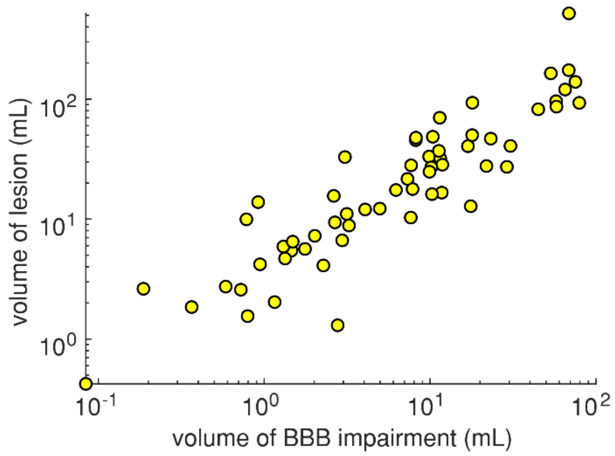

Figure 6 The volume of the ischemic lesion correlates with the volume of BBB impairment (Pearson coefficient 0.74, p<0.001) (Kala, 2022, fig .21)

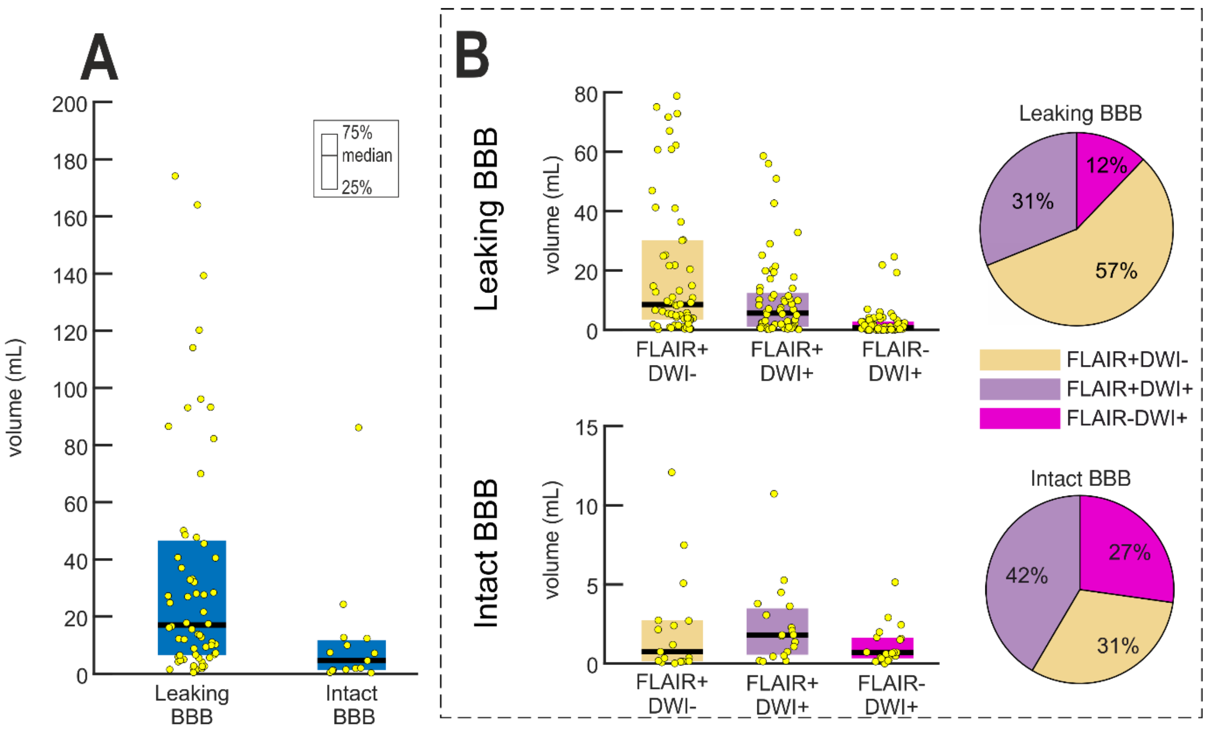

Figure 7 Characterization of the ischemic lesion. The volume of the ischemic lesion in patients with detected BBB leakage and with intact BBB (A). The proportion of lesion sub-regions according to FLAIR and DWI positivity in both groups (B)

To evaluate BBB integrity, T1w MRI with gadolinium contrast was measured 7-12 days post-stroke. In the leaking BBB group, the volume of gadolinium extravasation (7.76 mL, IQR 16.13 mL) was compared to the ischemic lesion volume (21.6 mL, IQR 25.3 mL), showing a strong positive correlation. The spatial distribution of extravasated gadolinium was analyzed in the leaking BBB group. Sixty-three percent (IQR 59.4%) of the extravasated gadolinium was located in the FLAIR+DWI- sub-region, 22% (IQR 44.3%) in FLAIR+DWI+, and less than 1% in FLAIR-DWI+. A total of 96% (IQR 8.1%) of the gadolinium was inside the lesion, with only a small amount (0.6 mL, IQR 2.2 mL) detected in the perilesional tissue. Extravasated gadolinium was significantly higher in gray matter (2%, IQR 6%) compared to white matter (0.5%, IQR 2.4%).

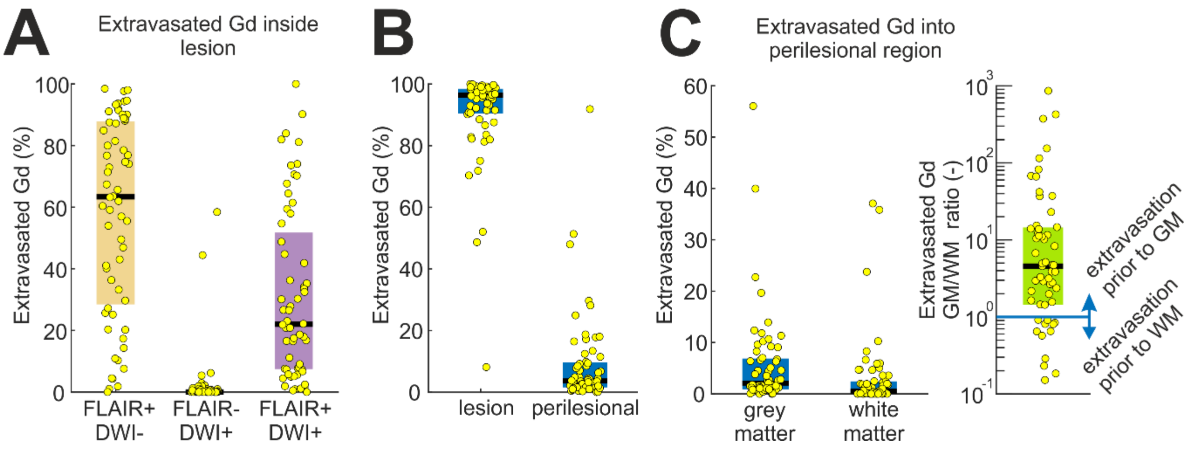

Figure 8 Localization of the BBB impairment in 60 patients with leaking BBB. Gadolinium is extravasated primarily into FLAIR positive sub-regions of the ischemic lesion (A). The majority of Gadolinium leakage was localized inside the ischemic lesion, however, a small part of extravasation was also detected inside surrounding perilesional brain tissue (B). Outside the ischemic lesion, gadolinium leaked preferentially into the gray matter (C) (Kala, 2022, fig.23, edited)

4.5 Discussion

In our clinical study, we thoroughly described the localization of the blood-brain barrier (BBB) impairment in relation to the ischemic lesion after a stroke at the time, when patients are typically discharged from the hospital. Patients recruited to the study were examined by MRI seven to twelve days after the ischemic insult. We have found that BBB is compromised inside the ischemic lesion in the majority of patients. However, BBB impairment is detected also outside the ischemic lesion in a non-negligible amount. Furthermore, our data suggest that vascular dysfunction significantly increases the risk of the development of vascular epilepsy.

In our data, the ischemic lesion was visible in FLAIR and DWI MRI with high contrast allowing to perform segmentation. ADC maps are corrected for the T2 component and represent a direct evaluation of water diffusion, however, in our datasets did not allow reliable segmentation of lesions. This likely corresponds with findings by Lansberg et al. (Lansberg *et al.*, 2001) where pseudonormalization (return to normal intensities) of ADC together with maximal intensity in DWI during the second week after ischemia was reported. Therefore, ADC wasn't used for lesion detection in this study. Because perilesional Gd enhancement has not been by its definition connected with changes in either FLAIR or DWI we were interested in whether exist sub-regions within ischemic lesion according to the presence of BBB leakage. Therefore, to describe the spatial localization of BBB impairment inside the ischemic lesion, we used positivity/negativity in FLAIR or DWI sequences.

Although both sequences utilize T2 relaxation, they manifest different pathophysiological processes. They are typically used in the acute assessment to distinguish ischemic core and penumbra (Perkins *et al.*, 2001), we intentionally avoided this terminology because our data come from the later phase of lesion maturation, and traditional acute terminology might be therefore misleading. Similarly, DWI signal later after the ischemia develops and usually possesses so-called T2 shine-through phenomenon where T2 component dominates over diffusion specific signal and thus it is not suitable for the evaluation of diffusion restriction without ADC. Therefore we have decided to define lesion as positivity in at least one of FLAIR or DWI signals and surrounding tissue as perilesional tissue. We further subdivided ischemic lesion into subregions according to the logical combination of FLAIR and DWI alterations as FLAIR+DWI+, FLAIR+DWI-, FLAIR-DWI+.

FLAIR refers to the water content in the tissue mostly in the extracellular space, which is due to vascular impairment and vasogenic edema (Lansberg *et al.*, 2001). Also, infiltration of inflammatory cells or gliosis, a process of maturation of ischemic lesion in later periods, is characterized by alterations of T2 weighted and FLAIR images (Chassidim *et al.*, 2013; Perkins *et al.*, 2001). To further elaborate on the source of DWI signal in our datasets we performed a manual analysis of signal profiles of DWI, ADC, FLAIR, pre-contrast T1w signal, and Extravasated Gd map in all recruited subjects. We confirmed our presumption that DWI+ is largely a T2 shine-through phenomenon and the FLAIR-DWI+ region is likely the result of imperfect spatial coregistration or segmentation of lesion. Therefore our definition of an ischemic lesion as positivity in either FLAIR or DWI represents a conservative approach to avoid false-positive results when assessing perilesional BBB leakage.

To assess blood-brain barrier integrity, we evaluated changes in intensity in T1w images that were due to extravasation of macrocyclic gadolinium contrast gadobutrol (Gadovist). We elaborated on the post-pre contrast method for the evaluation and pseudo-quantification of BBB leakage (Chassidim *et al.*, 2013; Kala *et al.*, 2017). Although dynamic contrast-enhanced imaging (DCE-MRI) is usually used in the quantitative assessment of vessel permeability (Thrippleton, 2019; Thrippleton *et al.*, 2019), it wasn't used in this study. The study aimed to spatially correlate a region with BBB leakage to an ischemic lesion and thus spatial resolution of T1w (which is similar to FLAIR) had priority over a quantitative assessment of BBB integrity with DCE-MRI and consequent pharmacokinetic analysis. Another important issue in stroke patients is the length and complexity of the imaging protocol. Recommended DCE-MRI routine anticipates 15-20 minute acquisition time and limited spatial resolution due to desired temporal resolution of less than 1 minute per scan (Thrippleton *et al.*, 2019). However, stroke patients 7-12 d after stroke are commonly hard to cooperate and data obtained from longer sequences frequently contain severe movement artifacts and negatively influences also scanning of other sequences in the scanning protocol (Thrippleton, 2019). The post-pre method allows reliable detection of regions with BBB leakage (although only qualitative) and good spatial correlation with altered regions detected in other scans throughout the brain (FLAIR and DWI) (Chassidim *et al.*, 2013; Kala *et al.*, 2017; Veksler *et al.*, 2020).

Disrupted BBB was detected in 60 patients (75%) out of 80 included in the study. Based on the presence of BBB disruption, patients were divided into two groups, with leaking BBB and with intact BBB. Patients with intact BBB have a significantly lower volume of the ischemic lesion, ASPECTS, SeLECT score, and presence of hemorrhagic transformation after ischemic insult. While the SeLECT score was designed and validated as an instrument to predict whether people are at high risk of developing post-stroke seizures (Galovic *et al.*, 2018) our data thus indirectly indicate that patients with disrupted BBB are at higher risk of developing vascular epilepsy. However, further analysis of the occurrence of spontaneous seizures in later periods after the ischemic stroke is desired to prove this assumption. On the other hand, it well corresponds to our finding of a strong correlation between the volume of the ischemic lesion (FLAIR or DWI positivity) and the volume of the region with compromised BBB. This relation has been also observed in experimental stroke animal models (Abo-Ramadan *et al.*, 2009).

We have spatially compared ischemic lesion with leaking BBB and found the majority of BBB disruption inside FLAIR positive sub-regions (either FLAIR+DWI+ or FLAIR+DWI-), while the only negligible overlap of BBB leakage and FLAIR negative sub-region (FLAIR-DWI+) was observed. This result also corresponds with previous findings (Lansberg *et al.*, 2015) that gadolinium-based MRI contrast agents leak is in tight spatial correlation with FLAIR positive MRI lesions and FLAIR negativity is likely due to imperfect spatial coregistration with DWI. The composition of ischemic lesions also varies between groups. In the group with leaking BBB, the FLAIR+DWI- sub-region extended over a significantly larger part of the ischemic lesion. A possible explanation is that while in patients with intact BBB FLAIR positivity is caused solely by gliosis as was reported for small vessel disease (Gouw *et al.*, 2011), in patients with leaking BBB FLAIR+ region manifests both gliosis and vasogenic edema in the tissue where BBB was compromised (Lansberg *et al.*, 2015).

Although, the majority (96%) of BBB leakage was observed inside the detected ischemic lesion extravasation of the gadolinium contrast agent was detected also in tissue without detectable FLAIR or DWI alterations. BBB impairment in peri-infarct regions with no structural histological alteration was previously reported in animal studies (Lapilover *et al.*, 2012; Nahirney *et al.*, 2016). One possible explanation for this finding is the presence of diffusion transport of the contrast agent from the lesion to its surroundings (Zhang *et al.*, 2020). However, in our setting, postcontrast MRI was performed approximately five minutes after contrast administration and because of this short period diffusion from the BBB region is not likely. Also, as the volume of perilesional BBB leakage detected in this study was rather low (0.6 mL) an effect of inaccuracies in image processing should be considered. The FLAIR sequence is based on spin-echo and DWI on gradient-echo MRI sequence (Symms *et al.*, 2004) and therefore there can be small morphometric differences between them leading to inaccuracies in image coregistration. Although the quality of image coregistration was visually controlled, subtle errors might be left unnoticed and affect the statistic result. However, we have performed a manual analysis of signal profiles to further elucidate the pattern of perilesional gadolinium enhancement. We have observed consistent three typical patterns of signal profiles – no Gd enhancement, Gd enhancement inside the lesion, and Gd enhancement inside and also outside the lesion. Although FLAIR+ and DWI+ regions spatially highly correlate likely due to T2 shine-through effect and peripheral region of the lesion (either DWI+ or FLAIR+ positive only) is likely due to precision of lesion segmentation on particular sequences, it is obvious that region which we termed "Perilesional" is distinct from the ischemic lesion. It should be noted that Gd enhancement outside lesion always coexists with inside lesion Gd detection in individual patients and as can be seen from **Figure 8B** although small in volume it is not negligible. Our findings support a recently published animal study that describes extensive alterations in perilesional brain tissue and a glial scar around liquefactive necrosis after stroke in mice (Zbesko *et al.*, 2018). The authors observed the presence of IgG, albumin, and even 10kDa Texas Red-labeled dextran within the glial scar after intravenous injection. Although it is likely due to a combination of both diffusion from an ischemic lesion and direct extravasation it clearly indicates the presence of perilesional tissue exposed to blood components. Furthermore, they observed significant swelling of neuronal cell bodies in the adjacent neural tissue and suggested it is indicative of cytotoxic edema. However, our analysis did not reveal any significant changes in diffusion parameters in perilesional tissue even in BBB leaking tissue.

To further evaluate regional differences, we have segmented brain images into gray and white matter, however, the segmentation process was successful only in perilesional tissue due to advanced decomposition and massive blurring of gray-white matter boundary inside the ischemic lesion in the subacute phase. Although higher susceptibility of white matter to BBB breakdown has been proposed (Bernier *et al.*, 2021), the analysis revealed higher extravasation of Gd in perilesional tissue in gray matter in comparison to white matter. Albeit the data possesses above mentioned methodological limitations the finding is in good agreement with current knowledge about regional differences in vascular densities. Gray matter is highly vascularized due to higher metabolic demand whereas vessels in white matter are less dense (Cavaglia M *et al.*, 2001; Hase *et al.*, 2019).

4.6 Conclusion

The study provides evidence that in the second week after ischemic insult the ischemic lesion still undergoes maturation, and the BBB is compromised in the majority of patients. Furthermore, our data suggest that vascular dysfunction significantly increases the risk of the development of vascular epilepsy.

5. Modelling cerebral ischemia in experimental practice

5.1 Introduction

Currently, the widespread availability of reperfusion therapies in developed countries has significantly improved survival rates for acute stroke patients, which, in turn, presents new challenges for preclinical research in neurology. While the improvements in survival are promising, stroke survivors often face severe long-term consequences, including conditions like vascular epilepsy, which can substantially reduce their quality of life. This highlights a critical gap in research: the need for reliable experimental models that not only replicate the acute effects of stroke but also capture the chronic consequences experienced by patients over time (Svoboda *et al.*, 2019).

Despite the critical need for experimental models that replicate both the acute and chronic consequences of stroke, a major limitation in preclinical research is the substantial variability in lesion size and location observed across animal models. This variability poses significant challenges in interpreting results and necessitates the use of large numbers of animals to achieve statistically meaningful conclusions. For example, in the embolic MCAO model, widely regarded as the gold standard for mimicking human ischemic stroke, infarct sizes vary significantly due to challenges in standardizing clot introduction and ensuring its stability (Ren *et al.*, 2012). This variability is further compounded by differences in stroke induction methods, anatomical characteristics, and biological responses across species, leading to inconsistencies in lesion size and functional outcomes (Karthikeyan *et al.*, 2019; Smith *et al.*, 2012; Svoboda *et al.*, 2019). While larger infarcts, often produced in animal models, are associated with severe impairments, they do not accurately reflect the typically smaller lesions observed in human strokes, which account for 4.5% to 14% of the ipsilesional hemisphere (Karthikeyan *et al.*, 2019). Furthermore, lesion size variability significantly impacts the study of long-term consequences, such as vascular epilepsy and cognitive deficits, which are key concerns for stroke survivors and represent a critical area of unmet need in stroke research(Svoboda *et al.*, 2019).

Additionally, the timing of therapeutic interventions, such as rehabilitation and neuroprotective treatments, introduces further variability, as these factors can interact with lesion characteristics to influence recovery trajectories (Lee *et al.*, 2022). Advanced imaging techniques, such as diffusion magnetic resonance imaging, have revealed that not just lesion size but also its heterogeneity is associated with functional outcomes, emphasizing the complexity of recovery processes (Henriques *et al.*, 2015).

Addressing these challenges is essential to improve the translational relevance of preclinical stroke research. Without standardized protocols and better characterization of lesion variability, the demand for large experimental groups will persist, increasing the ethical and logistical burdens of animal research while hindering progress in developing treatments for the chronic consequences of stroke (Li *et al.*, 2013; Svoboda *et al.*, 2019).

However, animal-based experimental models provide the only controlled experimental in vivo setting with manageable variables, such as age and sex, which enable a deeper understanding of clinical pathophysiology and disease mechanisms. They also facilitate the development and testing of potential therapies and the assessment of comorbidities. Animal models of cerebral ischemia offer the advantage of precisely controlled injury, allowing for the creation of well-defined and reproducible primary and secondary injuries, such as infarct size, neuroinflammation, and brain edema (Mcbride and Zhang, 2019). Most experimental studies on ischemic strokes are conducted using small animals, such as mice, rats, and rabbits. Advantages include lower costs and the higher ethical acceptability that often comes with working with smaller organisms. Among these animals, the rat is one of the most used species. One of the key factors contributing to the rat's frequent use in ischemic stroke research is the similarity between its cerebral vasculature and physiology and that of humans. Furthermore, rats exhibit relatively high strain homogeneity which is an important factor in ensuring consistent experimental outcomes. (Ström *et al.*, 2013). During past decades various techniques of occlusion of brain vessels were developed. Direct surgical occlusion of MCA (Tamura and Teasdale, 1981), endovascular occlusion with intraluminal filament (Longa *et al.*, 1989), photothrombic model (Brima, Mikulecká, *et al.*, 2013; Brima, Otáhal, *et al.*, 2013), four-vessel occlusion (4VO) model (Furlow, 1979) and several types of embolic occlusion using various embolizing elements as autologous blood clot, glass microspheres and magnetic nanoparticles (Fluri *et al.*, 2015).

Since ischemic stroke in humans is attributed to three primary causes, each with distinct mechanisms and implications for treatment an optimal experimental model should maximally mimic underlying processes. Large vessel atherosclerosis and the rupture of an atherosclerotic plaque account for approximately 50% of ischemic stroke cases.

Cardioembolism, which occurs when a blood clot from the heart travels to the brain, is responsible for around 20% of cases. The remaining 25% of cases result from small vessel disease, likely caused by the occlusion of deep perforating arteries, leading to the formation of lacunar infarcts. (Sommer, 2017). As for localization, the middle cerebral artery (MCA) and its branches are the cerebral vessels that are most often affected in human ischemic stroke, accounting for approximately 70% of infarcts. It is worth to mention that chronic complication such as vascular epilepsy is known to occur more frequently in patients after stroke affecting MCA territory (Galovic *et al.*, 2018; Janský *et al.*, 2020). Thus, techniques that occlude MCA are closest to human ischemic stroke (Fluri *et al.*, 2015).

5.2 Overview of Experimental Models of Ischemia

One of the widely utilized MCA occlusion techniques is **electrocoagulation**, which involves exposing the middle cerebral artery through craniotomy and coagulating it using electrodes to induce ischemia. Ligation or clipping can be also used to constrict targeted blood vessel (Braeuninger and Kleinschnitz, 2009). This approach reliably produces consistent, localized infarcts, primarily affecting cortical areas. It is particularly suitable for investigating cortical ischemia and its impact on neurobehavioral outcomes. However, the necessity of craniotomy introduces surgical variability, and the method is limited to permanent occlusion, making it less appropriate for studying thrombolytic therapies and reperfusion injury. Despite these drawbacks, the model is a valuable tool for research on cortical recovery and therapeutic strategies targeting specific brain regions affected by ischemia (Fluri *et al.*, 2015; Zeng *et al.*, 2023).

Another significant model is the **endothelin-1** (ET-1) induced occlusion, which employs ET-1, a potent vasoconstrictor, to create transient ischemia in specific MCA regions. This method enables precise targeting of cortical and subcortical areas, making it ideal for studies focused on neuroplasticity and recovery mechanisms (Fluri *et al.*, 2015). It has been shown that the ET-1 model disrupts the integrity of the BBB, leading to increased permeability and subsequent brain edema. Narushima et al. (2003) reported that repeated administration of ET-1 significantly enhances BBB permeability, which can result in the accumulation of fluid in the brain parenchyma (Narushima *et al.*, 2003). However, one of the primary issues with ET-1 induced occlusion is the variability in the onset and duration of ischemia. For instance, studies have shown that ET-1 can induce a gradual profile of ischemia over extended periods (12-16 hours), which complicates the establishment of a controlled ischemic window compared to more traditional methods like intraluminal middle cerebral artery (MCA) occlusion, which allows for tighter control over the timing of ischemia and reperfusion (Mecca *et al.*, 2011; Selvamani and Sohrabji, 2010). Furthermore, the outcomes can be influenced by factors such as the type of anesthetics used and systemic interactions with ET-1, which may complicate experimental consistency. Despite these challenges, this model has been instrumental in advancing our understanding of post-stroke recovery processes (Fluri *et al.*, 2015; Sommer, 2017).

The **photochemically induced thrombosis** model represents another interesting approach, utilizing photosensitive dyes activated by light to create thrombosis in the MCA territory. This technique is minimally invasive and allows precise localization of ischemic lesions, making it particularly advantageous for studying acute-phase interventions and pathophysiological changes in the ischemic cortex (Zeng *et al.*, 2023). However, the model lacks a penumbra, a key feature of human strokes, which limits its utility for neuroprotective therapies that target salvageable brain tissue. Additionally, the localized damage in this model does not replicate the widespread effects often seen in human ischemic strokes, reducing its translational applicability (Li and Zhang, 2021; Zeng *et al.*, 2023). Furthermore, the mechanism underlying photochemically induced thrombosis involves the generation of reactive oxygen species (ROS) upon light activation of the photosensitizer, which damages endothelial cells and promotes platelet aggregation (Labat-gest and Tomasi, 2013; Liu *et al.*, 2014). Once the thrombus forms, the restoration of blood flow—reperfusion—becomes problematic. Studies indicate that the thrombus formed via photochemical means is resistant to conventional thrombolytic therapies, such as tissue plasminogen activator (tPA), which is typically effective in other ischemic models (Gursoy-Ozdemir *et al.*, 2012; Lee *et al.*, 2017).

The **four-vessel occlusion** (4VO) model is a well-established method for inducing global cerebral ischemia in rats. This model involves the occlusion of both vertebral arteries and the temporary clipping of both common carotid arteries, leading to a reversible forebrain ischemia that closely mimics certain human ischemic conditions (Lu *et al.*, 2016). This model can be utilized to explore the mechanisms underlying ischemia-reperfusion injury, including the roles of inflammatory responses and oxidative stress, which are critical factors contributing to neuronal damage during reperfusion (Li *et al.*, 2012). Interestingly 4VO model has potential to produce behavioral seizures in a subset of animals following ischemic events. Research indicates that the incidence of seizures increases with the duration of ischemia, with significant behavioral seizures occurring in a notable percentage of animals subjected to longer occlusion times (Lei *et al.*, 2016). Nevertheless, one of the primary concerns regarding the 4VO model is the technical complexity involved in the surgical procedure. The occlusion of all four vessels requires a high level of surgical skill and precision, making it a technically demanding procedure. This complexity can lead to variability in the outcomes due to differences in surgical execution, which may affect the reproducibility of results across studies. Furthermore, the requirement for multiple surgeries can introduce additional stress and complications for the animals, potentially confounding the results (Sanderson and Wider, 2013). To address these limitations, a modified version of this model has been developed to improve reproducibility, reduce variability in outcomes, and enhance its utility in preclinical research. (Lu *et al.*, 2016). Additionally, protocols have also been established to standardize the procedure, ensuring consistent induction of ischemia and facilitating comparative studies across different laboratories (Kim *et al.*, 2023). The 4VO model has been instrumental in studying the pathophysiological mechanisms underlying global cerebral ischemia and evaluating potential therapeutic interventions (Lu *et al.*, 2016).

Thromboembolic models involve the introduction of autologous clots or artificial emboli into the MCA, closely mimicking the pathophysiology of human ischemic strokes (Fluri *et al.*, 2015). These models are especially valuable for investigating thrombolytic therapies and the dynamics of spontaneous reperfusion, a phenomenon frequently observed in human strokes (DiNapoli *et al.*, 2006; Pirzad Jahromi *et al.*, 2012; Zeng *et al.*, 2023). Their significance stems from their ability to closely replicate the natural progression of ischemic events, along with the associated immune and inflammatory responses that play a crucial role in stroke pathology (Dotson *et al.*, 2015; Hossmann, 2012). Ongoing improvements and advancements in thromboembolic stroke modeling have focused on developing techniques that enable the reproducible and controlled induction of ischemia. These advancements have contributed to lower mortality rates and reduced variability, enhancing the reliability of the models. (Ansar *et al.*, 2014; Dotson *et al.*, 2015). Additionally, the introduction of intra-arterial clot injection techniques has enhanced the fidelity of these models, allowing researchers to better simulate the clinical conditions of stroke (Ostrova *et al.*, 2021). The thromboembolic model is widely used for testing the application of thrombolytic agents, such as tissue plasminogen activator (tPA). Studies utilizing these models have provided critical insights into the timing and efficacy of thrombolytic therapy in restoring blood flow and minimizing brain damage (Howells *et al.*, 2010; Liu *et al.*, 2015; Zhang *et al.*, 2015). Moreover, these models have been instrumental in investigating clinically significant complications, such as hemorrhagic transformation, a critical risk associated with thrombolytic therapy (David *et al.*, 2010; Krueger *et al.*, 2013; Sun *et al.*, 2010; Ye *et al.*, 2022). Agents such as fingolimod have been evaluated for their potential to mitigate this risk, highlighting the significance of these models in translational research (Campos *et al.*, 2013). Additionally, the use of advanced imaging techniques in conjunction with thromboembolic models allows for real-time monitoring of cerebral blood flow and infarct progression, providing critical data for evaluating therapeutic efficacy (Canazza *et al.*, 2014).

However, despite their wide range of applications, the reproducibility of thromboembolic models remains limited due to variability in outcomes across different approaches. Research indicates that the induction of ischemia through methods such as autologous clot injection can lead to inconsistent results, particularly in terms of infarct size and neurological deficits (Ostrova *et al.*, 2021). This variability can stem from differences in the timing of embolization, the size and composition of the emboli, and the physiological state of the animal subjects (Braeuninger and Kleinschnitz, 2009). Additionally, the use of thrombolytic agents, such as tissue plasminogen activator (tPA), in these models can introduce complications that are not representative of human conditions. For instance, while tPA is a standard treatment for ischemic stroke, its administration can lead to increased blood-brain barrier (BBB) permeability and neurotoxicity in animal models, which may not occur to the same extent in human patients. This discrepancy can result in misleading conclusions regarding the safety and efficacy of thrombolytic therapies (Fanne *et al.*, 2010; Salas-Perdomo *et al.*, 2019). The further limitations of thromboembolic models extend to their ability to predict long-term outcomes following stroke. Many studies focus on acute responses to ischemia, neglecting the chronic effects and recovery processes that are critical for understanding stroke rehabilitation (Tuo *et al.*, 2022). Despite these limitations, thromboembolic models remain a critical tool for evaluating thrombolysis and other reperfusion therapies, contributing significantly to translational stroke research (Fluri *et al.*, 2015; Zeng *et al.*, 2023).

5.3 Innovative model of brain ischemia with magnetic nanoparticles

Two recent studies by Jia et al. (2016, 2018) have introduced and refined a novel technique, stroke induced with magnetic particles (SIMPLE), to address the challenges of studying ischemic perinatal stroke in small animal models.

The SIMPLE method utilizes magnetic nanoparticles (MP) to induce targeted occlusion in micro vessels or the distal middle cerebral artery (**Figure 9**). The occlusion is achieved by injecting superparamagnetic nanoparticles, coated with biocompatible materials such as polyethylene glycol (PEG-2000), into the bloodstream mice. These particles aggregate under the influence of external magnetic fields produced by cylindrical neodymium-iron-boron magnets. This approach enables researchers to control the site, size, and duration of ischemic events, as well as to reverse occlusions by removing the magnetic field (Jia *et al.*, 2016).

SIMPLE offers several significant advantages over traditional methods like photothrombosis or suture-mediated MCAO, making it a groundbreaking approach for ischemic stroke research. Notably, it is non-invasive, eliminating the need for procedures such as skull thinning or carotid artery surgery, which are particularly challenging in neonatal and perinatal mice due to their small size and fragility (Jia *et al.*, 2016, 2018). The technique also enables precise temporal control, allowing for the induction and reversal of occlusion by simply removing the magnet, which facilitates the study of reperfusion-related injuries in real-time (Jia *et al.*, 2018). Furthermore, SIMPLE is highly scalable, applicable across various developmental stages, from perinatal to adult mice, thereby enhancing its versatility for studying ischemic mechanisms throughout brain development (Jia *et al.*, 2016). Another critical advantage is its ability to target specific micro vessels through magnetic manipulation, providing researchers with unparalleled precision to investigate localized ischemia and its effects on the neurovascular unit (Jia *et al.*, 2018).

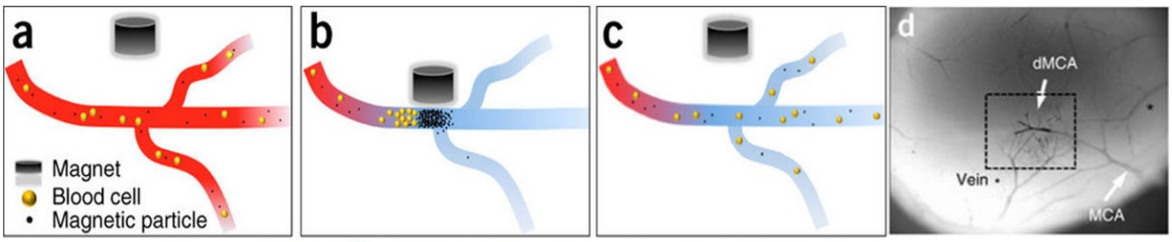

Figure 9 Scheme of SIMPLE (a, b, c). Particles forming a clot in distal middle cerebral artery (dMCA)(d).

Furthermore, Jia et al. (2018) expanded on this method, optimizing it for neonatal and perinatal mice (P0–P7). Traditional surgical methods for middle cerebral artery occlusion are challenging in such small animals due to the fragility and small diameter of their arteries. SIMPLE eliminates the need for invasive surgery, relying instead on the superficial temporal vein for magnetic particles delivery. This method allows the induction of both permanent and transient ischemic strokes and facilitates the examination of neurovascular unit disruption, neuronal death, and glial responses in vivo (Jia *et al.*, 2018).

5.3.1 Model evaluation in our laboratory

We evaluated the basic functionality of the SIMPLE model in our lab, and the results were published in a master's thesis by Zuzana Velentová wrote in 2020. First, we simulated clot formation using polyethylene tubing and a solution of MP in saline. Velentová (2020) then tested different doses of MP and found that a dose of 140 µg/g led to a significant reduction in cerebral blood flow and subsequent brain ischemia. However, little to no reperfusion occurred after magnet removal (**Figure 10**) (Valentová, 2020). Therefore, this model was deemed unsuitable for our future work on BBB opening, as we required a model with reliably achievable reperfusion.

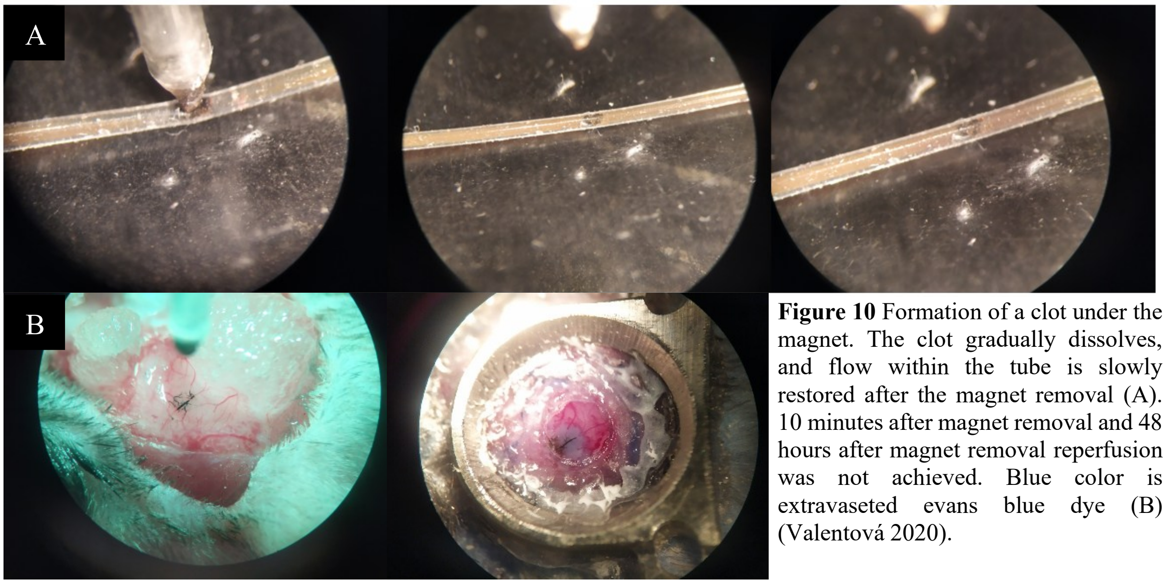

Figure 10 Formation of a clot under the magnet. The clot gradually dissolves, and flow within the tube is slowly restored after the magnet removal (A). 10 minutes after magnet removal and 48 hours after magnet removal reperfusion was not achieved. Blue color is extravaseted evans blue dye (B) (Valentová 2020).

6. Middle cerebral artery occlusion with intraluminal filament

MCAO is a significant stroke model due to its ability to replicate the pathophysiological conditions observed in human ischemic strokes, which predominantly affect the territory supplied by the middle cerebral artery (Alvi et al., 2020; Cao et al., 2022; Fluri et al., 2015; Li et al., 2022). Nowadays it is one of the most employed techniques for inducing focal cerebral ischemia in rodents. This method involves the insertion of a filament into the internal carotid artery, which occludes the MCA, leading to a reduction in blood flow to the affected brain region (Engel et al., 2011; Hu et al., 2023; Lee et al., 2014).

It can be classified into two main types: transient (tMCAO) and permanent (pMCAO), each serving distinct research purposes and offering unique insights into the ischemic process and subsequent recovery mechanisms (Alvi *et al.*, 2020; Gu *et al.*, 2023; Mcbride and Zhang, 2017). The ability to control the duration of occlusion makes this model particularly useful for studying both acute and chronic phases of ischemic injury, as well as the effects of reperfusion, mimicking the therapeutic procedure of mechanical thrombectomy (Engel *et al.*, 2011; Trotman-Lucas *et al.*, 2019). This is especially useful as the number of patients undergoing vessel recanalization continues to rise. Reducing injury and promoting healing after reperfusion are essential to improving outcomes following recanalization (Mcbride and Zhang, 2019). An important advantage of this method is that it does not require a craniectomy, thereby minimizing direct mechanical damage to the underlying brain structures (Lopez and Vemuganti, 2018). The reproducibility and stability of the MCAO model have been validated across numerous studies, making it a cornerstone in preclinical stroke research (Wu *et al.*, 2020; Zeng *et al.*, 2023).

Infarction after MCAO follows an almost stereotypical progression from early ischemia in the striatum to delayed infarction in the cortex overlying the striatum (Unekawa *et al.*, 2024). The MCA branches supplying the striatum are end arteries, which – in contrast to the cortical branches – do not form collaterals with the adjacent vascular territories. In MCAO with reperfusion, the striatum remains densely ischemic, but the overlying cortex returns to control blood flow values. Thus, in tMCAO striatal infarction is an ischemic core, and cortical infarction is a region of delayed, progressive neuronal death, or an ischemic penumbra (Carmichael, 2005).

To ensure precision and minimize experimental variability, tools like electrocorticography (ECG), laser Doppler flowmetry (LDF), and magnetic resonance imaging can guide filament placement effectively. These technologies help minimize variations caused by insertion distance, facilitate accurate placement, and enable the immediate detection of subarachnoid hemorrhages and premature reperfusion (Li and Zhang, 2021). The choice of filament coating is also particularly important. For instance, silicone-coated filaments have been shown to facilitate smoother insertion into the vascular system, reducing the risk of vascular damage and improving the reliability of the occlusion (Berny-Lang *et al.*, 2011; Bouley *et al.*, 2007; Eidizadeh *et al.*, 2015; Krey *et al.*, 2015). The coating can also influence the adhesion of the filament to the vessel wall, which is critical for maintaining occlusion during the ischemic period. Studies have indicated that filaments with poly-L-lysine coatings enhance adhesion and reduce variability in infarct size, leading to more consistent experimental results (Chen *et al.*, 2014; Eady *et al.*, 2014). In contrast, uncoated or poorly coated filaments may result in incomplete occlusion or premature reperfusion, which can skew results and complicate the interpretation of therapeutic interventions (Guan *et al.*, 2012). The size of the filament is another critical factor. The diameter and length of the filament must be appropriately matched to the size of the target artery to ensure effective occlusion. Filament that is too large may cause excessive trauma to the vessel, while one that is too small may not occlude the artery effectively, leading to variable infarct sizes (Li *et al.*, 2023; Zhai and Feng, 2018). Research has demonstrated that optimizing filament size according to the weight and strain of the animal can also significantly enhance the reproducibility of the MCAO model

In addition to its applications in basic research, the intraluminal filament MCAO model has significant implications for preclinical testing of novel therapeutic strategies. Interestingly, some studies have demonstrated the effectiveness of tissue plasminogen activator (tPA) in reducing infarct size when administered during the occlusion phase in this model (Zhang *et al.*, 2002; Zhu *et al.*, 2014). MCAO technique has also potential for investigating the phenomenon of spontaneous recanalization. Studies have demonstrated that spontaneous recanalization occurs in a notable percentage of patients with MCAO, with rates reported at 21.4% within 24 hours and 52.7% after one week (Mao *et al.*, 2017). This phenomenon is associated with improved prognoses, suggesting that therapeutic strategies aimed at facilitating recanalization could enhance recovery following ischemic events. However, the benefits of spontaneous recanalization can be tempered by the risk of reocclusion, particularly in patients with underlying atherosclerotic disease, which may predispose them to recurrent thrombotic events (Lee *et al.*, 2024).

Despite its advantages, the MCAO model is not without limitations. Variability in infarct size and location can occur due to differences in surgical technique, animal strain, and environmental factors, which may affect the reproducibility of results (Friedrich *et al.*, 2022; McCullough and Liu, 2011; Yoshimura *et al.*, 2024). Furthermore, the model primarily reflects the pathophysiology of large vessel occlusion strokes, which may not fully encompass the complexities of other stroke types, such as lacunar strokes or those resulting from embolism (Fluri *et al.*, 2015; Mcbride and Zhang, 2017). Other drawbacks include limited visibility, potential risk of subarachnoid hemorrhage, and its unsuitability for thrombolytic research (Zeng *et al.*, 2023). Therefore, it is important to utilize complementary models and approaches to gain a comprehensive understanding of stroke mechanisms and therapeutic targets (Fluri *et al.*, 2015; Liddle *et al.*, 2022).

6.1 Overview of rat strains used for modeling brain ischemia

The selection of an appropriate rat strain is critical in experimental stroke research due to inherent strain-specific differences in cerebrovascular anatomy and physiological responses. This section focuses on the commonly used Wistar and Sprague-Dawley (SD) strains, along with other rat strains, emphasizing their distinct characteristics in ischemic models.

Variations in cerebrovascular anatomy among animal strains significantly influence ischemic outcomes. Differences in the structure of the Circle of Willis, collateral circulation, and vascular density can affect the extent of ischemic damage (Sommer, 2017; Trueman *et al.*, 2017). Wistar rats often have an incomplete Circle of Willis, reducing collateral blood flow and increasing their vulnerability to ischemic damage and consequently leading to higher mortality rates compared to SD rats (Ström *et al.*, 2013). Sommer (2017) has shown that Wistar strain also possesses thinner posterior communicating arteries in comparison to SD rats. Sprague-Dawley rats on the other hand have atypical branching of the MCA in nearly 20%. This partly explains the high variance of infarct sizes even in the same species or strain after the occlusion of an artery (Sommer, 2017). Ma et al. (2020) demonstrated that the collateral flow in SD rats is significantly better during occlusive conditions, such as MCAO, compared to Wistar rats. This enhanced collateral circulation is believed to mitigate the extent of ischemic damage, as collateral vessels can provide alternative pathways for blood flow when primary vessels are compromised. In a study utilizing laser speckle contrast imaging, it was shown that SD rats had improved blood flow through collateral connections during ischemic conditions, which was not as pronounced in Wistar rats (Ma *et al.*, 2020).

Moreover, the anatomical and physiological differences between these strains extend beyond just collateral circulation. SD strain tends to have a higher expression of certain vascular markers, which may contribute to their enhanced collateralization. For instance, the expression of P-glycoprotein, a protein involved in drug transport and vascular integrity, was found to be higher in SD rats compared to Wistar rats, suggesting a potential mechanism for their superior vascular responses (Madla *et al.*, 2022). In addition, the anatomical features of the blood-brain barrier in Wistar rats exhibit a different permeability profile compared to Sprague-Dawley rats, which can affect the transport of substances across the BBB (Oluwasegun *et al.*, 2019). Sprague-Dawley rats also exhibit a more robust recovery from functional deficits compared to Wistar rats (Trueman *et al.*, 2017).

Seul et al. (2008) reported that Wistar rats subjected to permanent bilateral occlusion of the common carotid arteries exhibited significant vacuolation and disarrangement of myelin fibers in the optic tract, indicating severe white matter damage. In contrast, SD rats showed relatively intact white matter under similar conditions. This suggests that Wistar rats may be more prone to white matter injury following chronic cerebral hypoperfusion (Seul *et al.*, 2008). The histopathological examination of brain tissue following ischemic events further supports the notion that SD rats exhibit less white matter injury compared to Wistar rats. Study by Su (2018) has shown that the white matter in SD rats remains relatively preserved, even in the face of significant ischemic challenges, whereas Wistar rats demonstrate more extensive lesions and demyelination (Su *et al.*, 2018). Furthermore, in SD rats, the inflammatory response following ischemic events appears to be modulated differently compared to Wistar rats, potentially contributing to the mentioned differences in white matter damage (Mukda *et al.*, 2019).

Long-Evans rats, known for their enhanced vascular perfusion, tend to exhibit smaller infarct sizes following MCAO when compared to Wistar and SD rats. This characteristic contributes to their reduced ischemic vulnerability and makes them a suitable choice for studies focusing on vascular protection and recovery (Svoboda *et al.*, 2019).

Spontaneously Hypertensive Rats (SHR), on the other hand, serve as a robust model for hypertension-induced stroke. These rats display a heightened susceptibility to ischemic damage, primarily due to chronic vascular remodeling and impaired autoregulation, which mimic the pathophysiological processes observed in hypertensive human patients (Coyle and Jokelainen, 1982). For example, SHR rats exhibit an early onset of hypertension, with a high percentage experiencing strokes between 9 and 13 months of age, mirroring certain human pathophysiological conditions (Coyle and Jokelainen, 1982; Gubskiy *et al.*, 2018).

Fischer 344 rats, though less commonly utilized in stroke research, are highly valued for their genetic stability and unique suitability in aging-related ischemia studies. Their longevity and inherent resistance to tumorigenesis make them an important model for exploring the interplay between aging and ischemic outcomes (Sommer, 2017).

Recognizing strain-specific responses is crucial for experimental design in preclinical research. Selecting an appropriate strain that mirrors the human condition under study enhances the translational potential of findings (Howells *et al.*, 2010). Moreover, understanding these differences aids in interpreting conflicting results across studies and in developing standardized protocols (Fluri *et al.*, 2015).

6.2 Detection and quantification of Blood Brain Barrier disruption in animals

Detection and quantification of BBB disruption following brain ischemia is a critical area of research, particularly in understanding the pathophysiology of stroke and developing therapeutic interventions. One of the most widely used methods for assessing BBB integrity is the Evans Blue (EB) dye extravasation assay. The use of Evans blue dye in assessing BBB integrity is well-documented. This dye binds to serum albumin, and its extravasation into brain tissue is indicative of BBB disruption. Studies have shown that under pathological conditions, such as ischemia, the permeability of the BBB can significantly increase, allowing Evans blue to penetrate brain tissue (Kadry *et al.*, 2020).

EB assessment is typically combined with spectrophotometric or spectrofluorometric techniques to quantify dye concentration in tissue homogenates. These methods allow for precise detection of BBB leakage by measuring the absorbance or fluorescence of Evans blue at specific wavelengths, usually 620 nm for absorbance and 680 nm for fluorescence. This approach has been refined with the use of solvents such as ethanol or trichloroacetic acid (TCA), which enhance fluorescence sensitivity and reduce interference from biological solutes. These improvements enable researchers to quantify EB in small samples with high accuracy, making it particularly useful in studies involving small laboratory animals (Wang and Lai, 2014).

The use of Evans blue in conjunction with fluorescence spectrometry also facilitates the visualization of BBB disruption in real-time. For example, near-infrared fluorescence (NIR) imaging has been employed to enhance sensitivity while minimizing dye dosage. This approach enables detailed mapping of BBB leakage without compromising the health of experimental subjects, which is particularly advantageous for studying the progression of neurological diseases and evaluating therapeutic interventions (Ryu *et al.*, 2018). Moreover, EB has been found to be particularly effective in detecting BBB permeability changes following exposure to neuroinflammatory or oxidative stress stimuli, which are often major contributors to BBB dysfunction (Goldim *et al.*, 2019).

In addition to its diagnostic utility, EB-based spectrometric analysis provides insights into the mechanisms driving BBB disruption. By quantifying the extent and location of EB extravasation, researchers can correlate BBB permeability changes with specific pathological events, such as neuroinflammation or oxidative stress. Interestingly, Goldim et al. (2019) highlighted that EB extravasation is not only a measure of vascular leakage but also reflects broader changes in endothelial function and tight junction integrity, making it a valuable tool for investigating BBB dynamics in health and disease (Goldim *et al.*, 2019).

The methodological flexibility of this technique further enhances its applicability. EB quantification using spectrometry can be conducted with minimal tissue volumes, which is particularly beneficial in studies involving small rodents or limited sample availability. Optimized protocols have demonstrated that even in regions with minimal EB extravasation, such as intact or mildly disrupted BBB areas, the dye can be effectively extracted and measured, enabling detailed investigations of both severe and subtle vascular changes (Wang and Lai, 2014). Additionally, EB is compatible with multiple evaluation methods, including macroscopical identification within brain tissue, fluorescence microscopy and spectrophotofluorometry, providing researchers with versatile options for assessing BBB integrity (Goldim *et al.*, 2019).

However, studies over the long period of Evans blue application unveil many drawbacks which limit its use. These limitations include a substantial amount of free dye being present in an animal following the amounts injected, extensive binding to albumin and species-specific binding to other plasma proteins, unstable in saline and other salt solution, different studies showed it binds to tissues, inaccurate quantitative assessment of BBB damage due to spectroscopic limitations, Evans blue show spectral shifts in protein-containing solutions, in vivo potential lethal toxicity (Saunders *et al.*, 2015).

6.2.1 Experimental MRI

Various MRI modalities, including structural imaging, functional MRI (fMRI), and magnetic resonance spectroscopy (MRS), have been adapted for use in small animals, particularly rodents, to investigate disease mechanisms and evaluate therapeutic interventions (Pirko *et al.*, 2005).

Animal MRI studies require specialized small-bore MRI systems with high field strengths, typically ranging from 4.7 Tesla (T) to 11.7T, compared to the 1.5T to 3T used in clinical human MRI. The smaller brain size of animals, particularly rodents, necessitates higher spatial resolution and stronger gradient systems to obtain precise imaging data (Denic *et al.*, 2011). To ensure high-quality imaging, animals are typically anesthetized using inhalational agents such as isoflurane, which allows for continuous monitoring and adjustment of anesthetic depth. Alternative injectable anesthetics are used in some cases, but they provide less flexibility. Physiological parameters such as heart rate, respiratory rate, oxygen saturation, and body temperature are monitored to minimize motion artifacts and ensure animal well-being during imaging (Pirko *et al.*, 2005).

Once anesthetized, the animal is positioned within a purpose-built holder that minimizes movement. The rectal temperature is maintained at approximately 37°C using heated airflow or water circulation. MRI signal acquisition is performed using specialized coils, such as surface or volume coils, optimized for small animals to maximize signal-to-noise ratio (SNR). Sequences used for imaging vary based on the study's objectives, including T1- and T2-weighted sequences for anatomical studies. Diffusion tensor imaging (DTI) and diffusion weighted imaging (DWI) which are used to assess tissue microstructure by measuring the movement of water molecules within the brain and resting state and activity mapping with functional MRI (fMRI) for functional connectivity analysis (Hoyer *et* *al.*, 2014; Pirko *et al.*, 2005). A more detailed description of the above-mentioned MRI sequences is in chapter (**4.1 Overview of MRI sequences used in** clinical practice**).**

MRI in animal research has several advantages. One of the most significant benefits is its non-invasive nature, allowing repeated measurements in the same animal over time. This feature enables longitudinal tracking of disease progression and therapeutic effects while reducing the number of animals needed for experiments (Hoyer *et al.*, 2014). Additionally, MRI offers high spatial and contrast resolution, especially when high-field-strength scanners are used, making it possible to visualize fine anatomical structures and detect subtle pathological changes (Denic *et al.*, 2011). Furthermore, multimodal imaging approaches, such as combining MRI with spectroscopy or functional imaging, allow researchers to obtain comprehensive data on both structure and function (Hoyer *et al.*, 2014). Finally, MRI supports the 3R principle (Reduction, Refinement, Replacement) by enabling multiple scans in the same subject, thereby reducing overall animal use (Frahm *et al.*, 2006).

Despite its advantages, animal MRI presents several challenges. The small size of animal brains requires extremely high resolution, which demands longer scan times and advanced imaging protocols (Hoyer *et al.*, 2014). The low signal-to-noise ratio (SNR) in small structures, combined with motion artifacts from respiration and cardiac activity, further complicates image acquisition, requiring specialized correction techniques (Hoyer *et al.*, 2014). Additionally, anesthesia, while necessary to prevent movement, can alter physiological parameters such as cerebral blood flow and metabolic activity, potentially affecting experimental outcomes. Prolonged anesthesia also increases the risk of hypothermia and other complications (Pirko *et al.*, 2005).

Another limitation is the high cost of small animal MRI facilities, which require expensive high-field magnets, typically ranging from $800,000 to $2 million, with additional costs for maintenance, cryogenic cooling, and specialized technical expertise (Pirko *et al.*, 2005)Finally, the vast amount of data generated during MRI studies necessitates sophisticated processing and analysis. Investigators must have expertise in MRI data interpretation, and specialized software is required for image reconstruction, segmentation, and statistical evaluation (Pirko *et al.*, 2005).

6.3 Methods

6.3.1 Animals

An adult male rat population (n = 34), each weighing between 280 and 320 grams, was utilized in this experiment. Three distinct outbred rat strains were included: Wistar and Long Evans (both locally bred based on the Charles River strain) and Sprague Dawley, obtained directly from Charles River. The experimental protocol was reviewed and approved by the Animal Care and Use Committee of the Institute of Physiology, Academy of Sciences of the Czech Republic, in compliance with the Czech Animal Protection Law. This law fully aligns with the European Community Council's Directive 86/609/EEC, which establishes standards for the protection of animals used for scientific purposes. Furthermore, the Institute holds a Statement of Compliance with Standards of Humane Care and Use of Laboratory Animals (A5228-01) from the National Institutes of Health (NIH). Every possible effort was made to minimize animal suffering and reduce the number of animals used in these studies.

6.3.2 Preparation of surgical field and aftercare

Animals were anesthetized in the inducing chamber using 3-4 % of Isoflurane delivered by the veterinary anesthesia evaporator MSSVAP02. Spontaneously breathing animals were weighted and transferred to a heating surgical pad. Anesthesia was sustained with 1-2% Isoflurane throughout the experiment. Rectal temperature was monitored continuously, with adjustments made as needed to maintain a stable temperature of 37.1±0.25 °C. The animal was then positioned in a prone position to facilitate the surgical procedure. To prevent drying and irritation, the eyes were treated with a protective ophthalmic solution and then covered with a sterile swab. Surgical field was always disinfected with 70% ethanol, followed by an application of Betadine to further reduce the risk of infection. A second application of 70% ethanol was then used to ensure maximum sterility of the surgical area before proceeding. Postsurgical period was covered with. nonsteroid antiphlogistic Meloxicam (2 mg/kg s.c.) and Nurofen (4ml/l) into drinking water for 4 days.

6.3.3 Long-term vascular access establishment with custom made Mini-Port

In selected animals (n=6) we used a slightly modified version of the vascular access mini-port (VAMP) introduced by Fiebig et al., (2013) as a cost-effective and metal-free solution to facilitate repeated injections, blood collection and artifact-free imaging in small animals.

The construction of the VAMP involved using a shortened intravenous cannula cone paired with a rubber membrane, allowing it to be both durable and suitable for high resolution imaging. The cannula, sourced from a standard 26-gauge intravenous device, was modified by removing the suture wings and trimming its length to 5 mm. To reduce the cannula's diameter for an ideal fit, it was stretched with a needle holder, ensuring a streamlined structure. A polyethylene catheter (Smiths Medical International Ltd.) was then slid over the shortened cannula, facilitating ease of vascular access. To create a secure seal, a rubber membrane was trimmed using a punch to form a tapered cylinder that could be tightly fitted into the cannula cone. This membrane was further stabilized by heating the edge of the cannula cone and bending it over the membrane, securing it in place. The assembled VAMP was sterilized at temperatures or with alcohol, making it ready for experimental use (**Figure 11**).

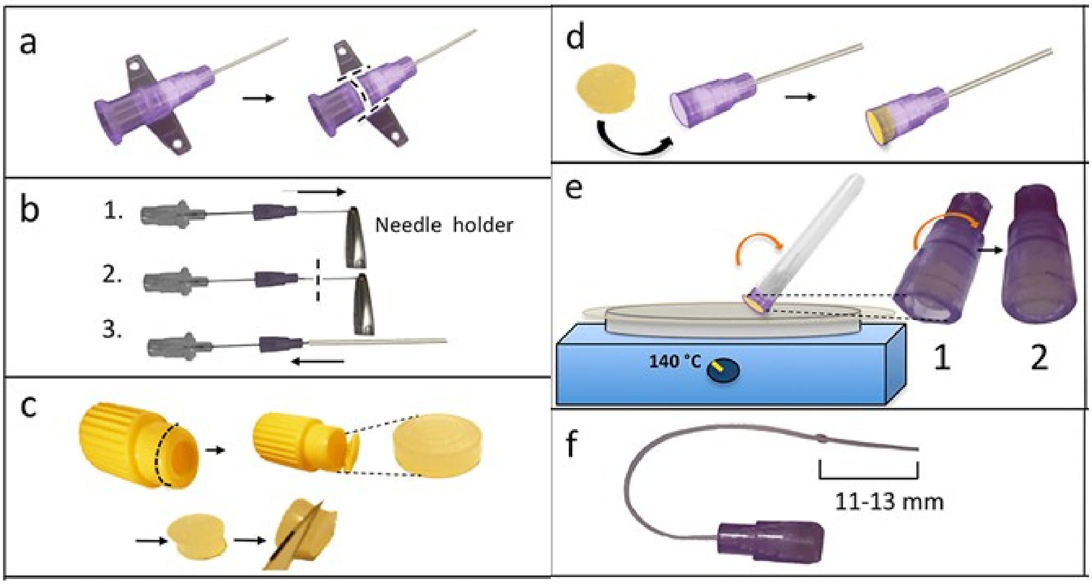

Figure 11 VAMP preparation scheme (Fiebig et al., 2013)

Implantation was performed according to slightly modified procedure originally described by Fiebig et al., (2013). Briefly after the animal was anesthetized the right jugular vein was then accessed through a small incision above the clavicle, the port system was inserted and secured to the place with two sutures. The VAMP and catheter were pre-flushed with heparinized saline (50 iu/ml) to prevent clotting, facilitating smooth vascular access once inserted. A subcutaneous tunnel was then created in the intra-scapular area. The cannula was moved to the area and fixed with sutures.

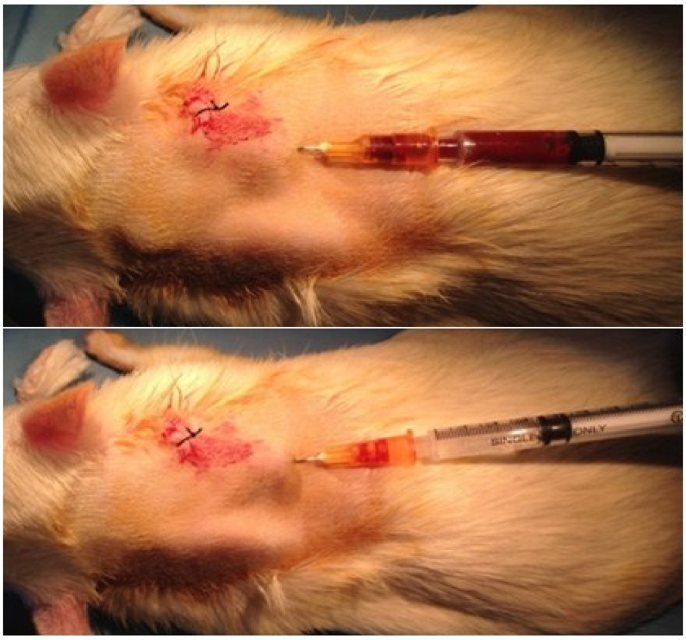

Figure 12 Blood collection and heparinization via VAMP

6.3.4 Monitoring of brain blood flow

To monitor the effect of middle cerebral occlusion on blood flow a laser Doppler flowmeter was used. Briefly the fur on the skull was carefully shaved using an electric shaver to ensure a clean area for the procedure. Clean skin overlying the skull was cut along the midline from the eyes level to the occipital bone and gently retracted to each side to fully expose the surgical area. To manage bleeding and maintain a clear surgical field, a long piece of sterile swab was carefully twisted and positioned between the retracted skin and the upper border of the temporal muscle. This swab served as both a hemostatic barrier to reduce minor bleeding and as a physical boundary to restrict accidental movement of retracted skin and better define the surgical field, ensuring optimal visibility and cleanliness throughout the procedure. The underlying connective tissue was carefully separated from the bone using the edge of the scalpel and then gently trimmed away with scissors.

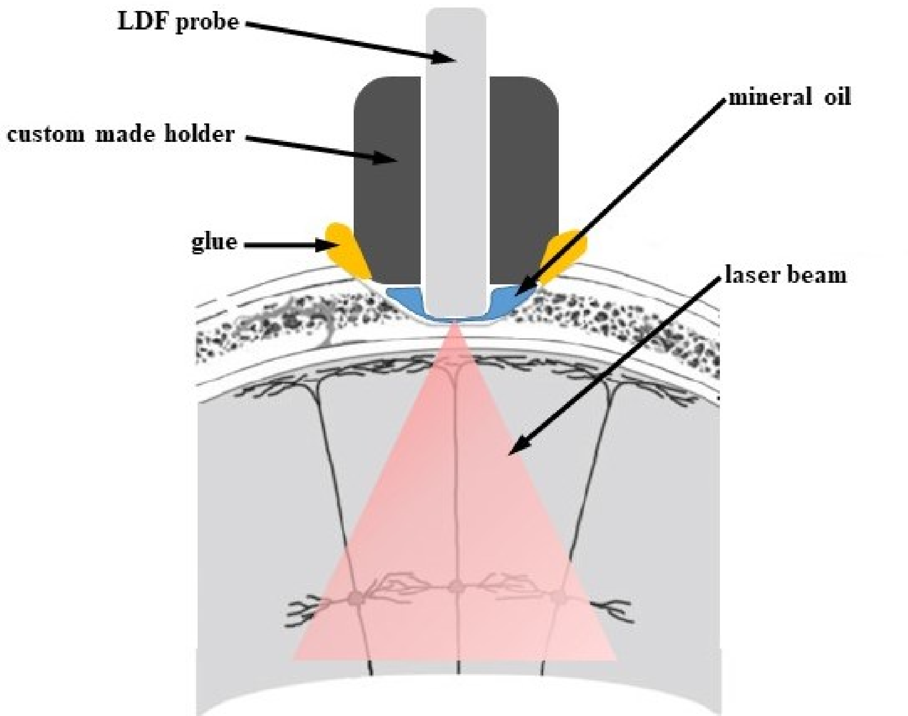

Figure 13 Laser Doppler flowmetry set-up scheme

To overcome the laser beam distortion caused by the substantial thickness of the parietal bone, we carefully removed the initial two layers of bone using a precision drilling technique. A bore polythene tubing (ID: 2mm; OD: 3mm; Smiths Medical International Ltd.) connected to an air pump was positioned over the exposed area to keep it dry and cool the bone during drilling. The upper compact and middle spongy portions of the parietal bone were carefully drilled away using an Omnidrill 35 hand drill, equipped with 1.5 mm round-oval Busch drill head. This modification in bone thickness proved essential for improving signal intensity and, consequently, the sensitivity of our LDF recordings. Drilling was performed in a controlled manner with short pauses for irrigation using sterile saline to further cool the bone. Drilling continued until the lower compact bone layer was reached. Through this thin layer, the operator could easily identify the terminal branch of the MCA and position the LDF holder directly over it.

The LDF holder was made from an aluminum piece with a hole drilled in the center, into which a polyethylene tubing (ID: 1 mm; OD: 2 mm; Smiths Medical International Ltd.) was inserted to securely hold the LDF probe in place. After positioning the holder, a small amount of cyanoacrylate glue (Loctite Power Flex) was applied to secure the holder in place and prevent any dislocation of the LDF probe during subsequent procedures. The cavity beneath the LDF holder was filled with mineral oil to further optimize the optical path of the laser beam. As a final step, the LDF probe was inserted into the holder, and the adhesive was tested by applying a slight lateral force to ensure it had cured properly.

Cerebral blood flow (CBF) was continuously monitored and recorded throughout the entire surgical procedure using a surface microprobe (Probe 407-1, Perimed; placement as described above) connected to a laser Doppler flowmeter (LDF, Periflow 5010, Perimed, Sweden). The analog LDF signal was transmitted to a 16-bit A/D converter (Power 1401) and recorded using Spike2 software (CED, Cambridge, United Kingdom). Data analysis was performed offline in Spike2, allowing for the assessment of the mean regional cerebral blood flow (rCBF) levels during the desired experimental periods.

6.3.5 Blood vessel occlusion

Animal was carefully positioned in the prone position, with its extremities secured using plaster to open and widen the surgical field. The position of the collarbone and carotid triangle was palpated and marked with a marker to minimize the incision size. A 1,5 cm sagittal neck incision was made with a scalpel, and the skin was gently retracted to the side. The underlying soft tissue and salivary glands were carefully cleared away using blunt dissection with anatomical tweezers and retracted to the side. A twisted sterile swab was inserted into the incision to serve as both a hemostatic barrier, reducing minor bleeding, and as a physical boundary to restrict accidental movement of the retracted tissues, providing a clearer surgical field.

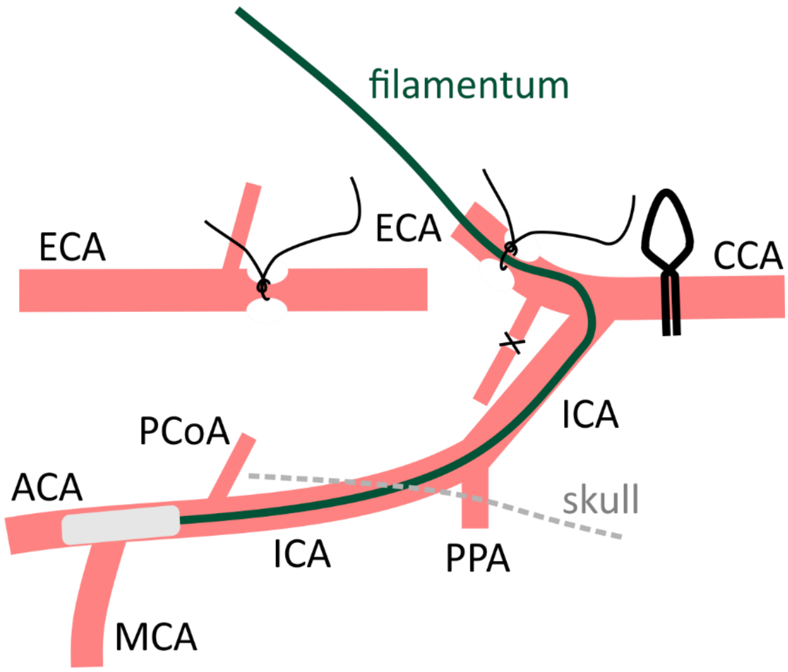

Figure 14 Middle cerebral artery occlusion scheme

Under surgical microscope the carotic triangle was identified and approached. The pretracheal muscles were retracted to the right, while the sternocleidomastoid muscle was gently diverted to the left. The right common carotid artery was then carefully isolated and dissected from surrounding structures using vascular tweezers with special caution to not traumatize the vagus nerve and its recurrent laryngeal branch. Then the bifurcation of common carotid artery (CCA) and outgoing trunks of internal (ICA) and external carotid (ECA) arteries with its branches were carefully exposed. A vascular microclip was placed over CCA and ICA. ECA was ligated over the origin of thyroid artery and occipital artery electro coagulated and cut to prevent retrograde blood flow. From small arteriotomy an appropriate nylon filament with silicon tip (Doccol, USA) was inserted into ECA and carefully advanced into an origin of ICA and after slight ligation and microclip removal further advanced into the ICA (**Figure 14**). The movement of the filament was visually inspected to prevent misplacement of the filament into a pterygopalatine artery. After small resistance was felt and simultaneous significant drop in CBF detected by LDF the filament was secured by tightening of the ligature.

Animals were left for the desired period of occlusion (60 min.) under mild anesthesia (0.5-1.5 % Isoflurane) and temperature control. Then, occluding filament was carefully withdrawn from the artery and arteriotomy closed with ligation to prevent further bleeding. Finally, microvascular clip was removed from CCA and surgical field closed with three to four sutures. Animals were routinely checked and weighed during postsurgical recovery to assess their overall status and motor deficit using Garcia score.

6.3.6 Noninvasive assessment of ischemic region

In 6 animals (Sprague-Dawley) series of scans on microPET/CT Albira (Bruker Biospin, Ettlingen, SRN) was performed to verify its suitability for noninvasive assessment of ischemic region in intraluminal MCAO. First series of µCT/PET were captured 24 h before and second 24 h after the MCAO procedure. The acquisition was performed according to the adapted protocol of (Balsara *et al.*, 2014). Briefly, animals were fasted overnight and 1 h before µCT/PET scan were intravenously injected with ~18 MBq of 18F-FDG diluted in saline to total volume 0.4 ml. The head of the animal was scanned in the for 30 min followed by CT scan in standard resolution. The data were analyzed offline in PMOD software (PMOD technologies LLC, Zurich, Switzerland) with use of Schiffers MRI rat brain atlas which implements the Paxinos coordinates allowing to assess FDG activity bilaterally in majority of brain regions (Schiffer *et al.*, 2006). 3D visualizations of the animal including brain with ischemic lesion were constructed from NIfTI data format of both µCT and PET utilizing 3D Slicer software (www.slicer.org, NIH, USA).

6.3.7 Tetrazolium staining

To evaluate the extent of the ischemic region, animals were sacrificed 24 hours to 7 days after MCAO, and their brains were rapidly removed from the skull. Fresh coronal brain slices were prepared using a 1 mm rat brain metal matrix and a razor blade. Tetrazolium staining (2,3,5-triphenyl-2H-tetrazolium chloride, Sigma Aldrich) was performed following a standard protocol (Liszczak *et al.*, 1984). Briefly, 1 mm thick fresh brain slices were incubated in a 2% tetrazolium solution at room temperature for 25-30 minutes. Images of the stained slices were then captured using a standard color camera and saved for subsequent quantitative analysis. Stained brain slices were stored in 4% paraformaldehyde for later use.

6.3.8 Fluorescence spectrometry

For this experiment, we used a modified protocol based on the study by Wang and Lai (2014). Brain tissue was obtained from 32 Wistar rats that underwent the MCAO procedure as described above in a timespan of three months. The animals were divided into five groups (1-5) according to the time elapsed since ischemia induction: 6 hours (n = 6), 24 hours (n = 6), 48 hours (n = 8), 72 hours (n = 7), and 7 days (n = 5). After the specified time post-ischemia induction, the animals were intravenously injected with a bolus of Evans blue dye (3 mg/kg of body weight), which was allowed to circulate for one hour. Following this, the animals were overdosed with urethane anesthesia. The brains were then removed and quickly sliced into 1 mm thick cortical sections. These slices were incubated in a 2% tetrazolium solution in saline for 30 minutes to assess the presence of ischemic lesions. After capturing images, the brain slices were stored in 4% formaldehyde for up to three months.

Once a sufficient amount of tissue was collected, the brains were removed from formaldehyde and briefly rinsed in saline. Then, 100 mg of tissue from the infarcted hemisphere was collected, along with 100 mg from the contralateral hemisphere as a control. The tissue samples were placed in 2 mL Eppendorf vials with 150 μL of saline and a specified number of ceramic beads (2.8 mm in diameter). The tissue was homogenized for 90 seconds at 4,500 rpm and then centrifuged for 60 seconds at 2,100 RCF. Following centrifugation and visual inspection of the homogenate quality, 150 μL of 100% trichloroacetic acid (TCA) was added to achieve a final concentration of 50% TCA, and the mixture was briefly vortexed. After 10 minutes, the samples were centrifuged for 25 minutes at 10,000 RCF. Next, 30 μL of the supernatant was pipetted into a clear 96-well tissue culture plate (96F, TPP, Switzerland), and 90 μL of isopropyl alcohol was added to enhance the signal. Evans blue fluorescence activity was measured using a Tecan Infinite 200 Pro plate reader (Tecan Austria GmbH, Austria), set to 620 nm for absorbance and 680 nm for fluorescence. The data acquired were analyzed using GraphPad Prism.

.

6.3.9 Experimental MRI

6.3.9.1 Animal preparation

For this study, we used Wistar rats (n=3) 48 hours after the induction of brain ischemia. The rats underwent the MCAO procedure as described above. Isoflurane anesthesia (1–3%) with air was used to maintain sedation during acquisition. For MRI acquisition, the animals were cannulated in the tail vein using a 26-gauge needle, and 50 cm polyethylene tubing (ID: 0.58 mm; OD: 0.96 mm; Smiths Medical International Ltd.) preloaded with contrast agent was connected to allow for contrast injection during data acquisition. The animals were then carefully transferred to the MRI holder, the MRI coil was securely fixed to the head, and the holder was positioned in the MRI scanner. The temperature was maintained at 36.8 ± 0.3 °C using a heating pad and was continuously monitored throughout the entire measurement.

Figure 15 Bruker Biospec MRI

6.3.9.2 Data acquisition

MRI scanning was performed using 7T MR spectrometer Bruker Biospec 70/30 (Bruker, Ettlingen, Germany, **Figure 15**) at Institute of Clinical and Experimental Medicine IKEM, Prague. The scanning protocol consists of T2 weighted (T2w) image, T1 weighted (T1w) image, T1 mapping performed by variable TR method, injection of contrast agent (CA), diffusion kurtosis imaging (DKI), followed by post-contrast repetition of T1mapping and T1w image. Acquisition parameters of sequences is summarized in **Table 2**. We have used gadolinium CA (Gadobutrol, 2mmol/kg of body weight). Post-contrast T1 mapping and T1w were scanned 10minutes, and 20 minutes after contrast injection, respectively.

Table 2 Detailed description of MRI data acquisition set up

Sequence	TR (ms)	TE (ms)	FA (deg)	Averaging	acquisition matrix (mm)	voxel size (mm)	Acceleration - factor	Duration (min:sec)
T2w	2500	33	180	1	35x35	0.137x0.137	1.00	1:20
T1w	200	4.5	60	2	35x35	0.137x0.137	1.33	1:16
T1mapping	variable*	8	180	1	25x25	0.260x0.260	1.00	9:07
Contrast application								
DKI**	3000	32	90	1	25x25	0.260x0.260	1.60	9:30
T1map	variable*	8	180	1	25x25	0.260x0.260	1.00	9:07
T1w	200	4.5	60	2	35x35	0.137x0.137	1.33	1:16

* Variable TR: 5500, 3000, 1500, 800, 400, 200

** b 1000, 3000, and 4000 s/mm^2 in 30 directions each + 5 b0 images

6.3.9.3 Diffusion MRI preprocessing and diffusion metrics calculation

To assess water distribution and tissue microstructure, we utilized Diffusion Basis Spectrum Imaging (DBSI) for post-processing of diffusion kurtosis imaging (DKI) datasets. DBSI is an advanced imaging technique that provides detailed insights into tissue microstructure by differentiating water diffusion properties within axonal fibers, inflammatory cells, and extracellular components such as edema. Unlike traditional diffusion tensor imaging (DTI), which averages diffusion across a voxel, DBSI employs a multi-tensor model for a more nuanced analysis of brain pathologies, including tumors, multiple sclerosis, and traumatic injuries (Chiang *et al.*, 2014; Wang *et al.*, 2019).

DBSI combines multiple anisotropic diffusion tensors, representing axonal diffusion, with isotropic tensors reflecting cellularity and extracellular components (Chiang *et al.*, 2014; Murphy *et al.*, 2016). This approach quantifies microstructural features such as axonal density and myelin integrity, aiding in the understanding of disease mechanisms and progression (Zhang *et al.*, 2022). For example, DBSI metrics like the restricted fraction correlate with tumor cellularity in glioblastoma, while axial and radial diffusivity provide insights into axonal injury and demyelination, respectively (Lin *et al.*, 2021; Ye *et al.*, n.d.).

DBSI has also been shown to differentiate tumor progression from treatment effects in high-grade gliomas, enhancing its utility in clinical settings (Han *et al.*, 2023). The integration of DBSI into existing imaging protocols with minimal modifications supports its feasibility for widespread clinical application. In this study, DBSI metrics were calculated using a MATLAB toolbox developed by Utt Kainen and William Spees (Washington University in St. Louis).

Table 3 Overview of diffusion metrics used in this study

Metric name	**Abbreviation**	**Model**	**Interpretation**
Axonal Fiber Fraction	**AFF**	DBSI	axonal density and integrity
Restricted Isotropic Diffusion Fraction	**RIDF**	DBSI	Cellular density
Hindered Isotropic Diffusion Fraction	**HIDF**	DBSI	Extra-axonal space density
Non-Restricted Isotropic Diffusion Fraction	**NRIDF**	DBSI	Free water density
Isotropic Fraction	**IF**	DBSI	Extracellular contribution

6.4 Statistical evaluation

Data were statistically analyzed using paired t-tests, repeated measures ANOVA, or ANOVA on ranks, as appropriate. Results are presented as mean ± SEM, and statistical significance was defined as $P < 0.05$ (*).

6.5 Results

The surgical procedure was consistent across the three rat strains included in the study, with no observable differences in the vascular anatomy of the neck vessels. Out of the 34 animals, only two (5.9%) died within four hours after the reperfusion period. Notably, both animals belonged to the Wistar rat strain. Postmortem inspection of the brain and skull suggested that subarachnoid hemorrhage was the likely cause of death. Additionally, a slight temperature increase (+0.3°C) was observed following MCA occlusion (data not shown). A modest weight reduction was recorded in all three strains within the first 24 hours post-MCAO; however, only Wistar rats exhibited a significant weight loss of 20.7 ± 4.6 g ($P<0.05$, **Figure 16**).

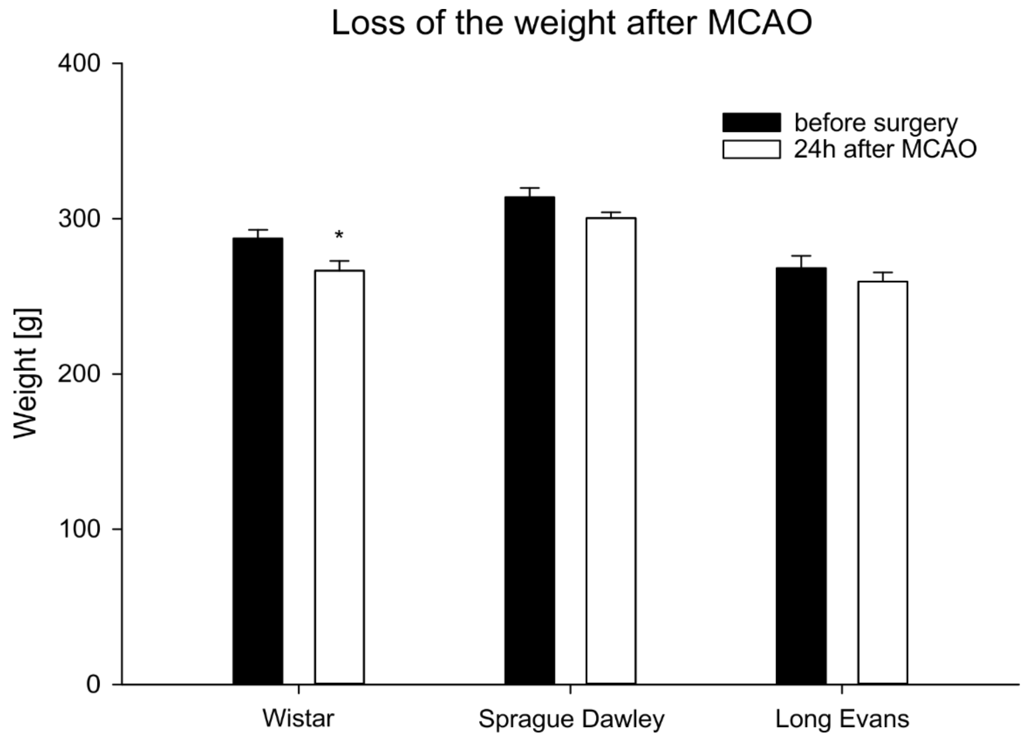

Figure 16 Surgical procedure and occlusion of middle cerebral artery led to decrease of weight of the animals.

All animals behave well after the MCAO and exhibit no or moderate neurological deficit (data not shown). Intraluminal occlusion of MCA origin resulted in ischemic injury to the affected hemisphere in all animals. Most extensive area of infarct, expressed as ratio of area of tetrazolium positive lesion to area of hemisphere, has been observed in Sprague-Dawley (50.2±10.3%) and Wistar rats (36.8±5.6%) while Long-Evans exhibited significantly smaller region of cerebral ischemia (18.8±3.5%, $P<0.05$). A similar pattern has been observed when rostro-caudal extension of the ischemic lesion has been compared

Figure 17. The affected areas differ between the rat strains. In Sprague-Dawley and Wistar animals where the infarcts were most extensive, the intraluminal occlusion of middle cerebral artery typically induced ischemic lesion affecting basal ganglia (caudoputamen), piriform and entorhinal cortices, primary somatosensory and marginally motor cortex. In contrast, only moderate infarcts of caudoputamen with delicate extension to surrounding sensorimotor cortex have been observed in Long-Evans animals 24h after the MCAO (**Figure 18**).

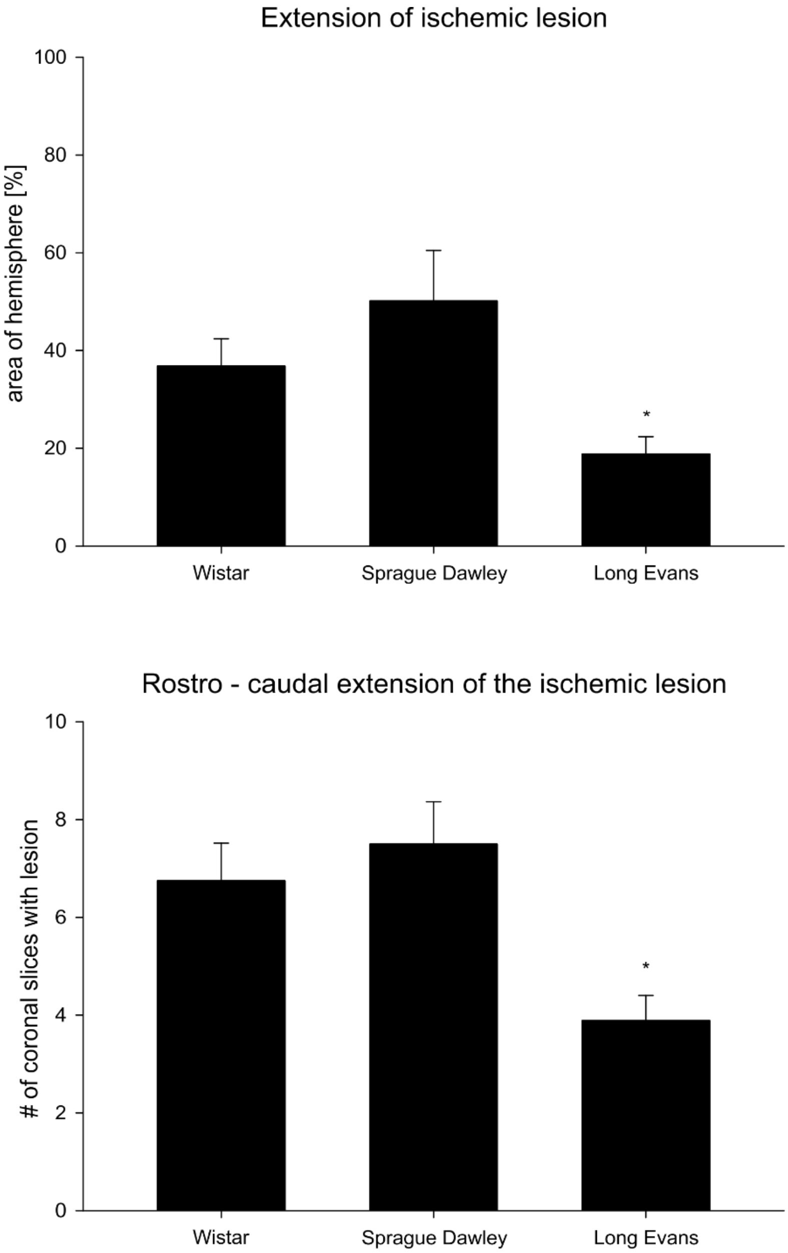

Figure 17 Extension of the ischemic lesion was significantly higher in Sprague-Dawley and Wistar rats in comparison to Long Evans rats.

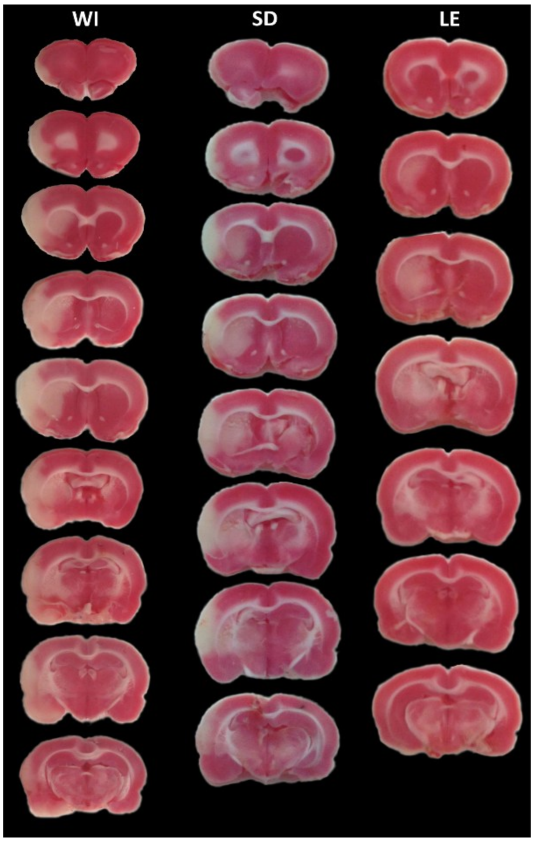

Figure 18 Tetrazolium staining revealed ischemic region of the brain (loss of pink color) in all three rat strains (WI – Wistar, SD – Sprague-Dawley, LE – Long Evans).

Regional cerebral blood flow tightly follows steps of the surgical procedure affecting cerebral blood inflow, which can be seen on typical LDF traces in **Figure 19A**. Basal regional cerebral blood flow did not significantly differ between strains and exhibited physiological oscillations arising from cardiac and ventilation activity. First significant drop in rCBF occurred with placement of microvascular clip on CCA. This value of rCBF was later used as reference resting level of the blood flow. Introduction of the filament tip into the MCA origin produced sudden decrease of rCBF in all rat strains namely to 48.0±6.2% in Wistar, to 37.5±6.0% in Sprague-Dawley and to 63.2±5.9 in Long-Evans rats. During period of occlusion (60 minutes) the rCBF had tendency to gradually but non-significantly increase. Withdrawal of the occluding filament from its position after the occluding period led to steep increase of the rCBF typically to values detected before pre-occlusion or even little higher (98.0±5.7% in Wistar, 112.2±19.9% in Sprague-Dawley and 97.2±8.4% in Long-Evans rats). The release of the clip from CCA caused additional increase to even higher levels (Wistar 131.1±13.0, Sprague-Dawley 143.2±26.0, Long-Evans 140.0±14.8%; **Figure 19B**).

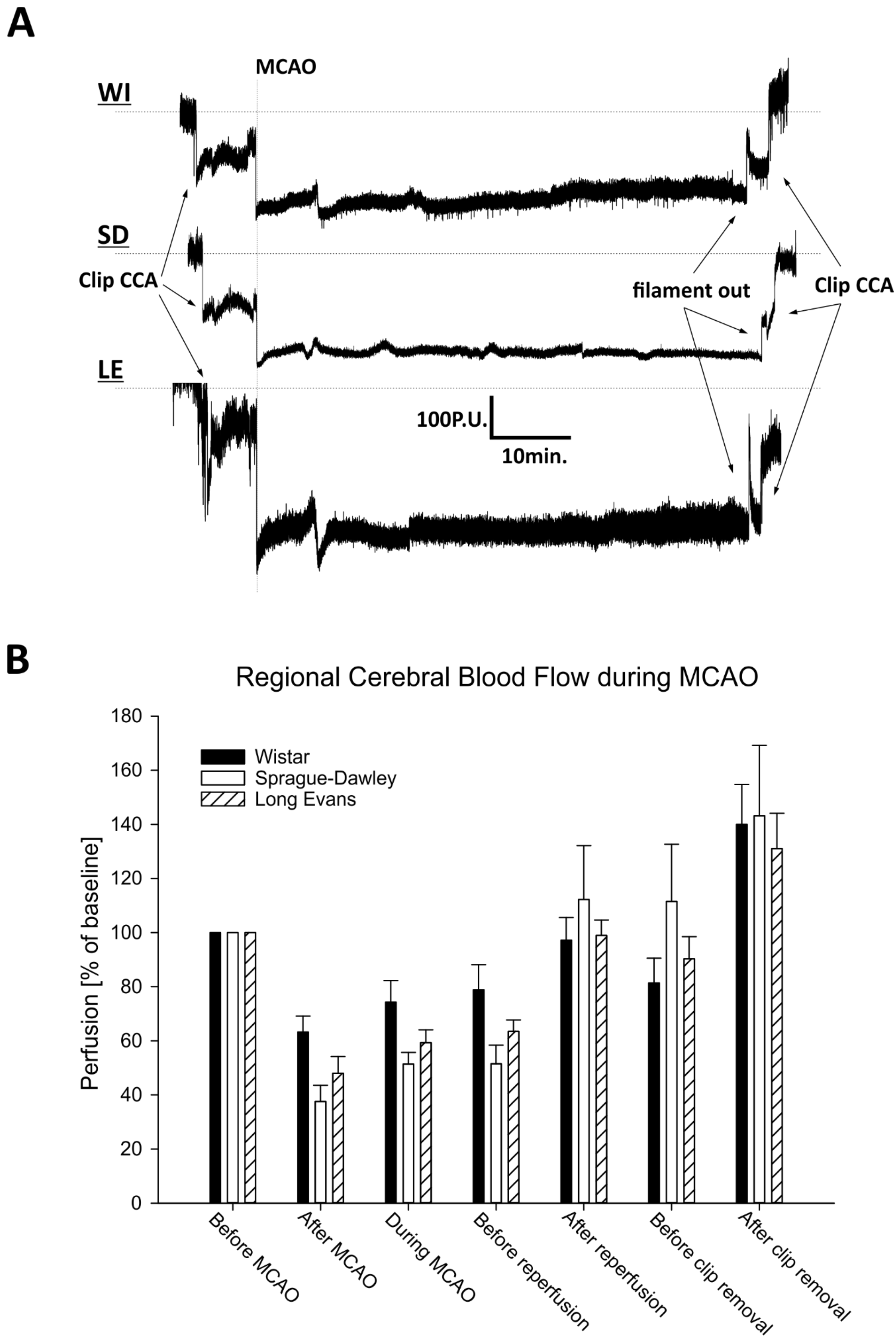

Figure 19 Regional cerebral blood flow was significantly reduced after the occlusion of middle cerebral artery (MCAO). After the removal of occluding filament and vascular microclip the cerebral blood flow returns to pre-occlusion level. **Panel A** shows representative measurement of CBF with LDF.

Cerebral ischemia produced significant reduction in focal brain metabolism as revealed by 18F-FDG PET scan. Representative PET images and 3D reconstruction are present in **Figure 20**. Cerebral ischemia was clearly visible as large hypometabolic region anatomically corresponding to ischemic region as revealed with tetrazolium staining of the same animal. Quantification of 18F-FDG activity in several brain regions were done using MRI atlas after space anatomical registration to PET and CT image series (for details see methods). Additionally, ratios between right and left side were calculated for individual neuroanatomical structures segmented by MRI atlas in both hemispheres (**Figure 21**).

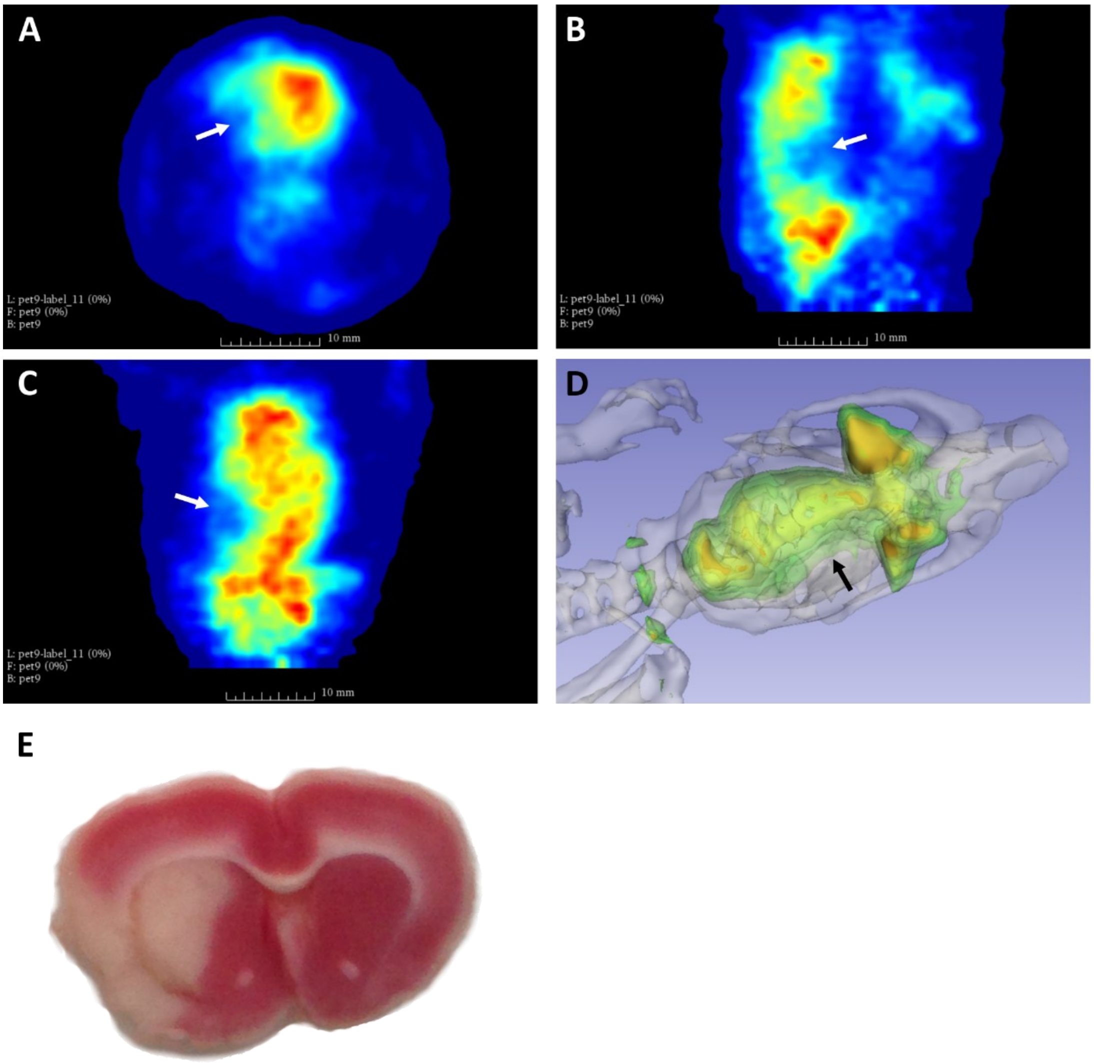

Figure 20 18F-fluorodeoxyglucose PET scans 24h after MCAO and reperfusion in Sprague-Dawley rats revealed extensive hypometabolic focus corresponding to ischemic region which has been visualized postmortem by tetrazolium staining.

A noticeable increase of the R/L index of the FDG activity was observed in all regions corresponding to the ischemic regions as revealed by tetrazolium staining (caudoputamen, amygdala, hypothalamus, diencephalon and several neocortical regions) while only cingulate exhibit statistically significant difference when comparing activities before and after MCAO. This was likely caused by small number of animals which underwent PET scan, however, obvious difference in signal from all other ischemic regions allowed us visually delineate ischemic region for every individual animal.

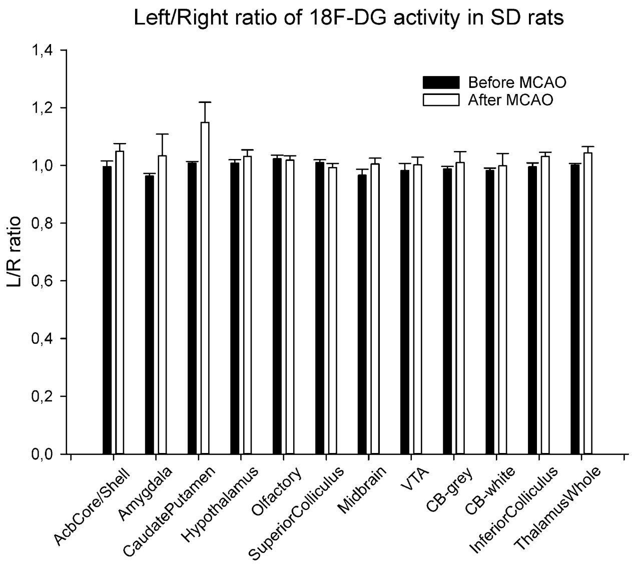

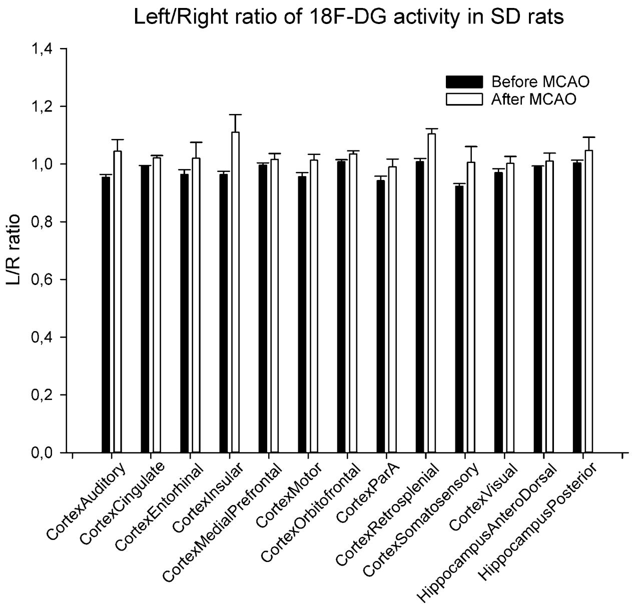

Figure 21 Statistical evaluation of 18F-fluorodeoxyglucose activity in selected brain regions expressed as ratio left/right hemisphere.

The spectrometry of Evans Blue (EB) revealed massive impairment of the blood-brain barrier (BBB) across all time points when compared to the contralateral side, confirming that BBB disruption is a consistent and prominent feature following ischemic injury (**Figure 22**). The results, expressed as fluorescence signal intensity (arbitrary units) ± SEM, clearly show that Evans Blue extravasation occurs in all experimental groups.

In Group 1 (6 hours post-reperfusion), the fluorescence intensity in the infarcted hemisphere was significantly higher at 885.5 ± 53.5, compared to 671.9 ± 26.9 in the control hemisphere. This group exhibited the most pronounced Evans Blue extravasation, indicating that BBB disruption is particularly severe in the acute phase following ischemia. This finding confirms that, at this early point, the BBB is extensively compromised.

In Group 2 (24 hours post-reperfusion), the signal intensity in the infarcted hemisphere was 512.8 ± 28.8, compared to 422.4 ± 24.6 in the control hemisphere. The overall fluorescence intensity was lower than that seen in Group 1, suggesting that while the BBB remains open, the extent of Evans Blue extravasation is reduced at this later time point. This indicates a partial recovery of BBB integrity, albeit still compromised compared to the contralateral control side.

In Group 3 (48 hours post-reperfusion), the fluorescence signal intensity in the infarcted hemisphere was 674 ± 34, compared to 558.18 in the control hemisphere. This again reflects significant Evans Blue leakage into the brain parenchyma, supporting the notion that the BBB remains impaired 48 hours after reperfusion. However, the signal intensity in this group is lower than that seen in Group 1, which may suggest a trend toward partial BBB recovery, although disruption persists.

In Group 4 (72 hours post-reperfusion), the fluorescence intensity in the infarcted hemisphere was 375.6 ± 44.3, compared to 298.6 ± 73.5 in the control hemisphere. This group exhibited the lowest fluorescence signal across all groups, indicating that the BBB disruption, though still present, is less pronounced at this later stage of reperfusion. The continued presence of Evans Blue extravasation suggests persistent, albeit reduced, BBB impairment.

Finally, in Group 5, the fluorescence intensity in the infarcted hemisphere was 617.3 ± 73.5, compared to 486 ± 40 in the control hemisphere, clearly indicating that BBB disruption persists even after 7 days, marking the beginning of the subacute phase of ischemia. This finding aligns with our clinical study results, where we investigated BBB impairment in ischemic stroke patients during the subacute phase (7–12 days post-stroke), further confirming the BBB opening is transitioning into this stage.

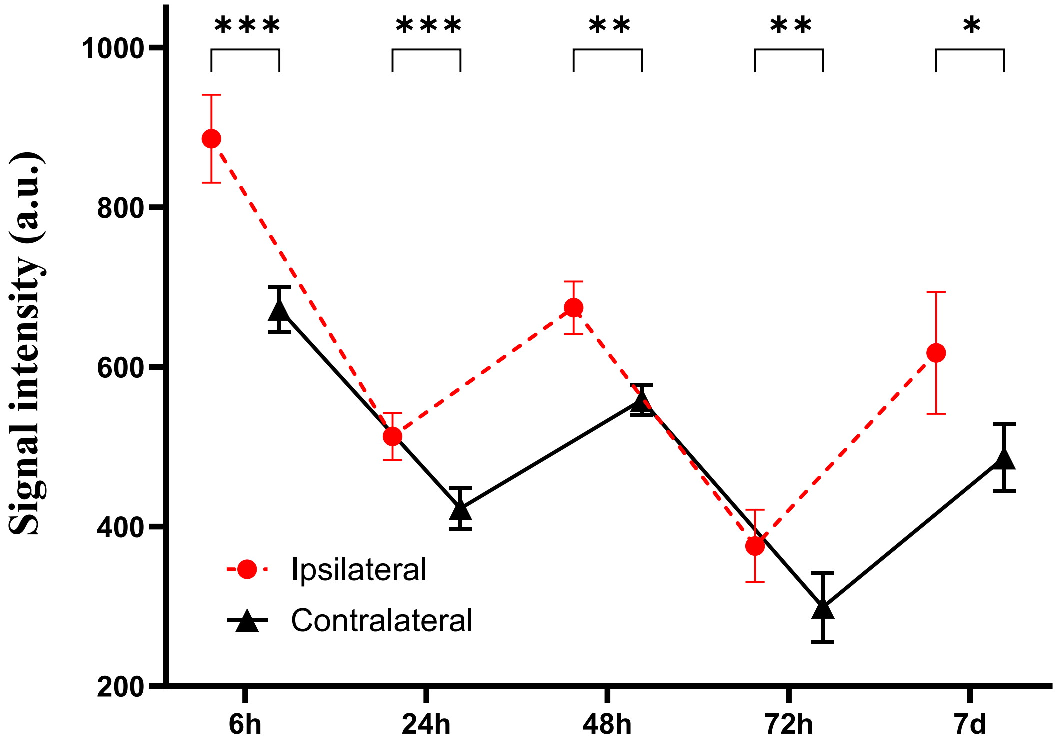

Figure 22 Evans Blue dye extravasation was present and statistically significant in all test groups at all time points (6h, 24h, 48h, 72h, 7d). Contralateral hemisphere was used as control. (*p< 0.05, **p< 0.01, ***p< 0.001)

It is important to note that we did not observe significant differences between the time points (**Figure 23**), which is likely a result of the experimental protocol used. The tissue was harvested one hour after the application of Evans Blue, which may have allowed equilibrium to be reached between the vascular compartment and the tissue extracellular space. This equilibrium likely provides a binary answer – BBB either "opened" or "closed" – but lacks the sensitivity to quantify the degree of permeability over time. Therefore, while the spectrometry data clearly confirms BBB disruption, it does not provide a detailed measure of permeability across the various stages of ischemic injury and recovery.

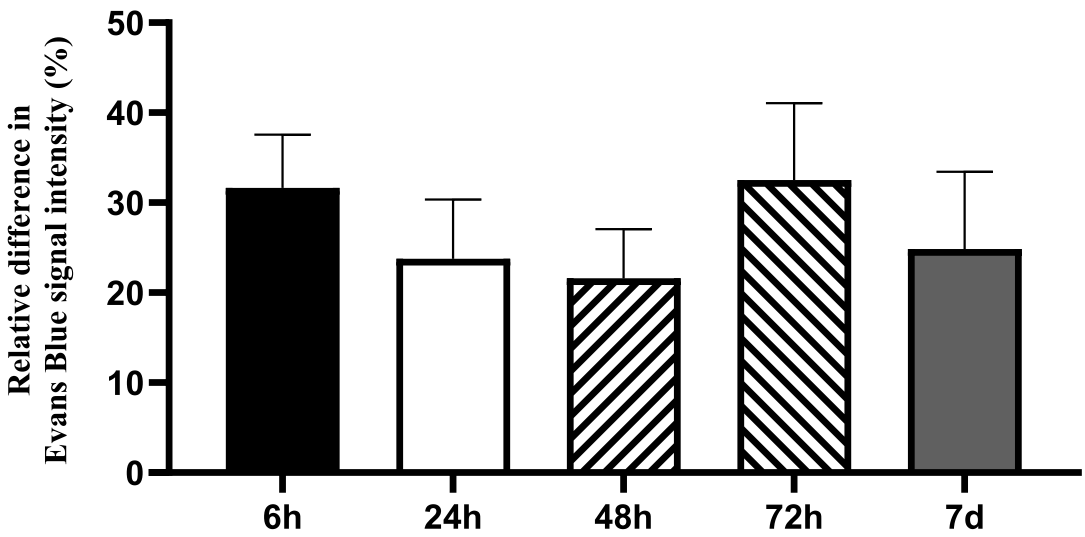

Figure 23 Relative difference in Evans Blue signal intensity between the ischemic and contralateral hemispheres showing no significant variation.

MRI scans obtained 48 hours after middle cerebral artery occlusion (MCAO) in the rat model provided detailed insights into the ischemic damage and associated pathophysiological changes (**Figure 24**).

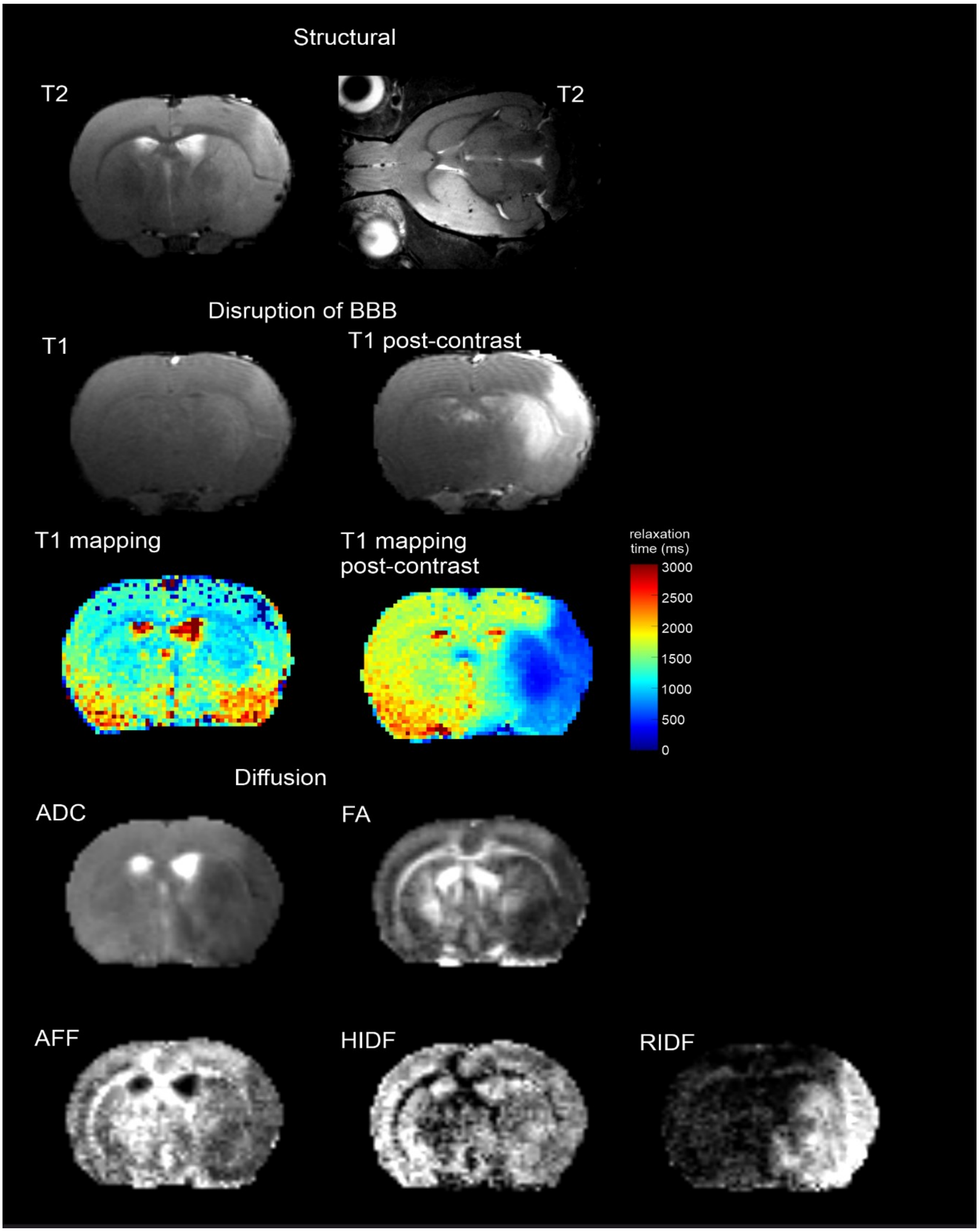

Figure 24 MRI scans from the experimental MCAO model in adult rat, acquired 48 hours after occlusion, are presented. Structural T2-weighted images clearly demonstrate a hyperintense ischemic region within the MCA territory, affecting the sensory cortex and caudoputamen. Post-contrast T1-weighted imaging and T1 mapping reveal contrast enhancement within the ischemic lesion, indicating a compromised blood-brain barrier (BBB). Altered diffusion is evident in both Gaussian diffusion metrics (ADC and FA) and compartmental analysis images. **ADC** - Apparent Diffusion Coefficient, **FA** - Fractional Anisotropy, **AFF** - Axonal Fiber Fraction, **HIDF** - Hindered Isotropic Diffusion Fraction , **RIDF** - Restricted Isotropic Diffusion Fraction

Structural T2-weighted images revealed a prominent hyperintense region within the middle cerebral artery (MCA) territory, specifically affecting the sensory cortex and caudoputamen. This hyperintensity is indicative of an ischemic lesion, likely caused by the accumulation of vasogenic edema, a hallmark of compromised blood-brain homeostasis (**Figure 25**). When compared to the corresponding healthy region on the contralateral side, the T2 signal was significantly elevated, supporting the presence of fluid extravasation and tissue swelling in the ischemic area.

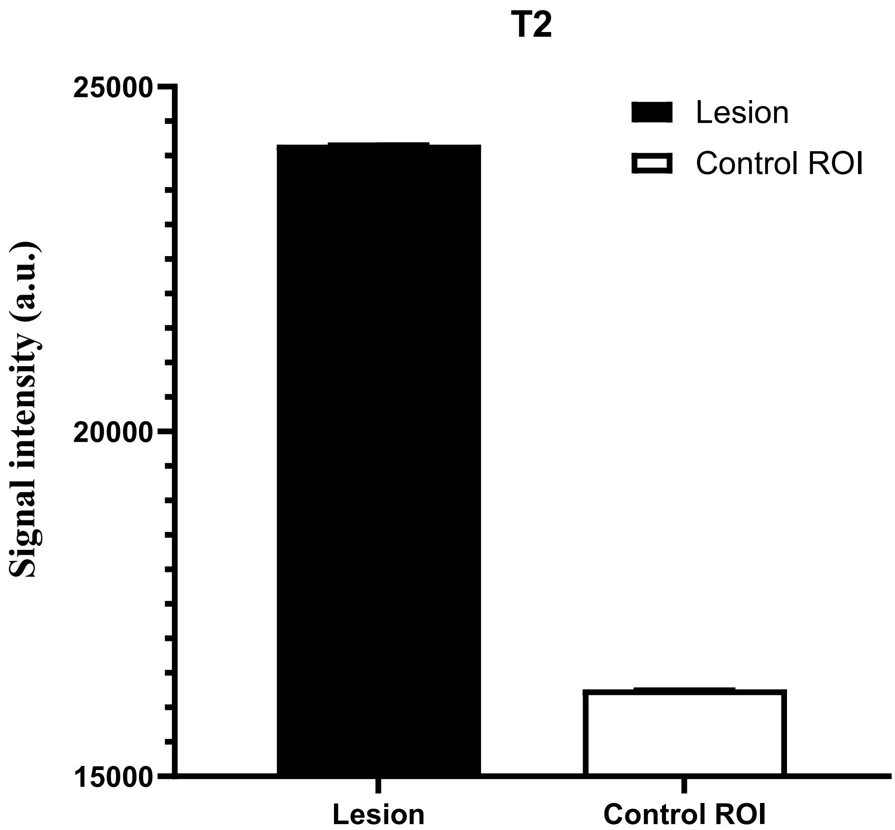

Figure 25 An increased T2 signal was observed within the ischemic lesion compared to the corresponding healthy region on the contralateral side, 48 hours after MCAO in the rat model.

Post-contrast T1-weighted imaging and T1 mapping (**Figure 26**) showed a marked increase in signal intensity within the ischemic lesion following gadolinium (Gd) contrast administration, further confirming blood-brain barrier (BBB) impairment. The contrast enhancement indicates a compromised BBB, allowing the leakage of Gd-based contrast agents into the extracellular space. This disruption is a key pathological feature of ischemic stroke and reflects the breakdown of vascular integrity within the affected area.

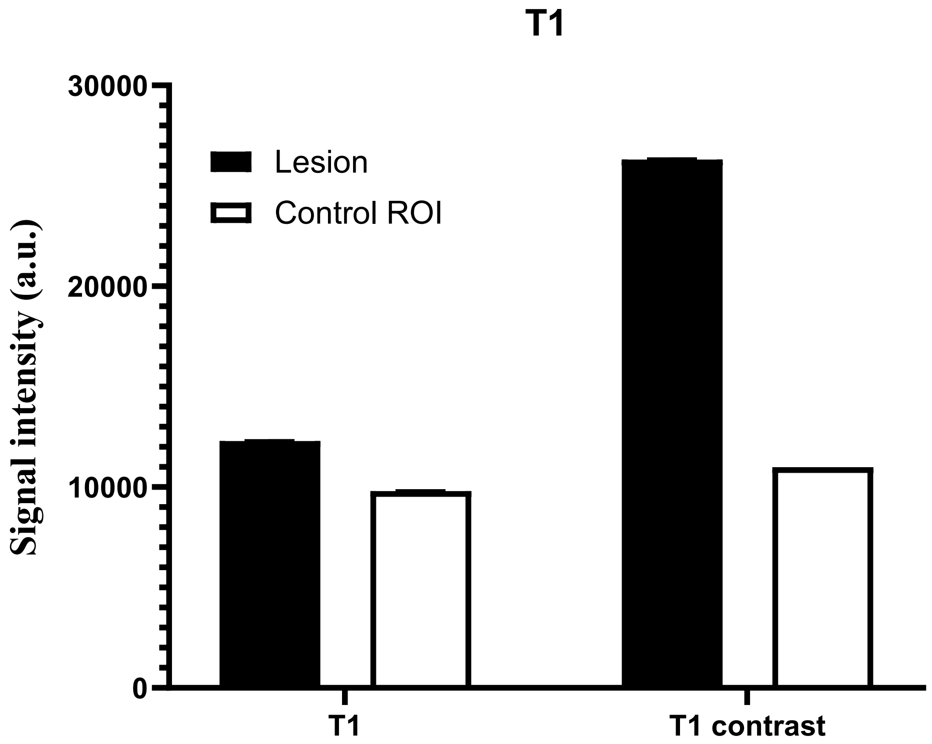

Figure 26 An increased T1 signal was observed within the ischemic lesion following the application of Gd contrast, compared to the corresponding healthy region on the contralateral side, 48 hours after MCAO in the rat model.

Alterations in diffusion metrics were also evident. Apparent diffusion coefficient (ADC) maps demonstrated a decreased signal within the ischemic lesion, consistent with restricted diffusion and the presence of cytotoxic edema (**Figure 27**). Cytotoxic edema results from cell swelling due to the failure of ionic pumps during ischemia, leading to water redistribution into cells and reduced extracellular space. Fractional anisotropy (FA) maps revealed a reduction in FA values within the lesion, suggesting early signs of tissue disorganization and loss of microstructural integrity. These findings align with the progression of ischemic damage, highlighting the interplay between cytotoxic and vasogenic edema.

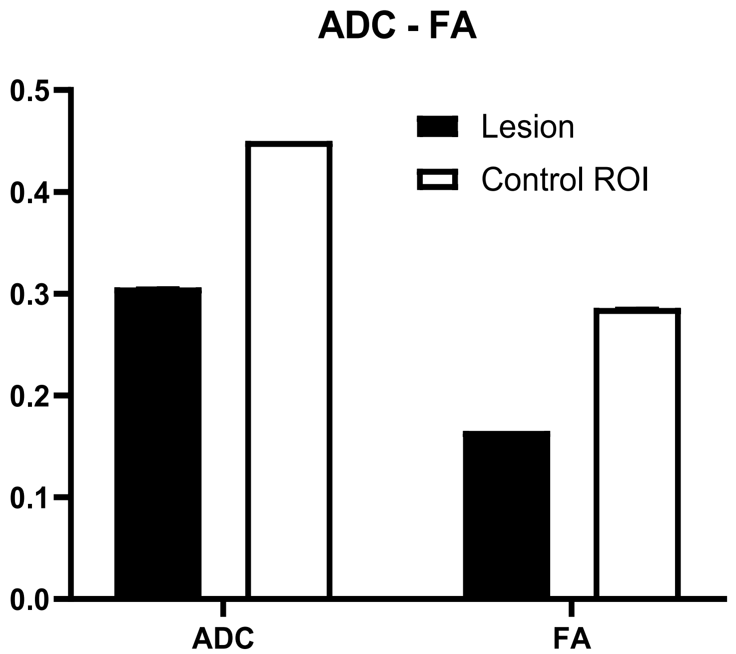

Figure 27 Restricted diffusion, indicated by a decreased ADC signal, and signs of tissue disorganization, reflected by a reduced FA signal, were observed.

.

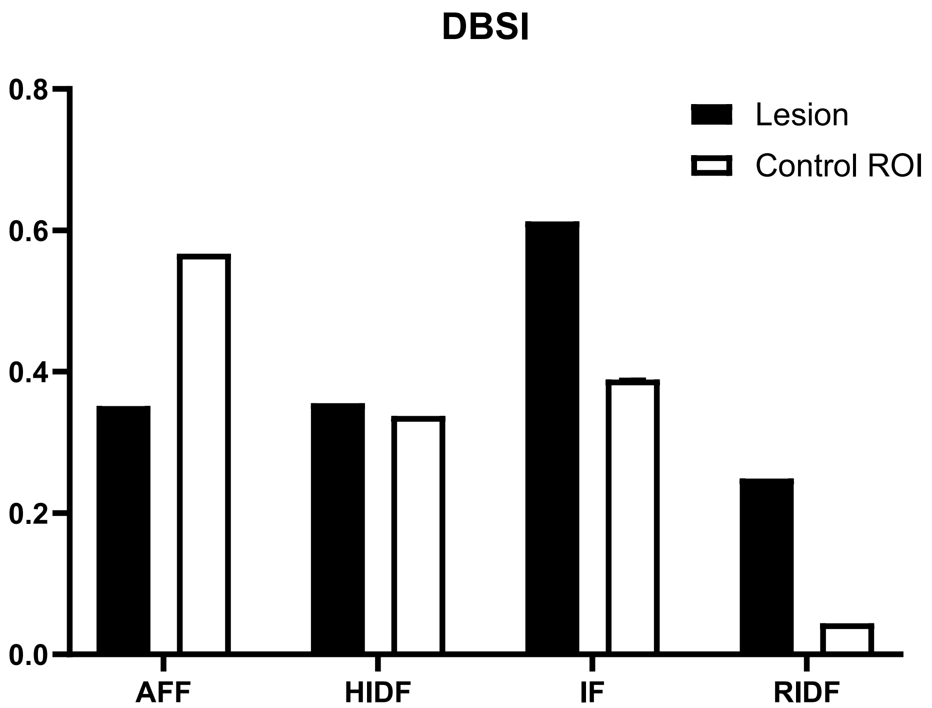

Figure 28 The compartmental model DBSI revealed an increased Axonal Fiber Fraction, along with decreased Restricted Isotropic Diffusion Fraction and Isotropic Fraction.

Advanced diffusion analysis using the compartmental model DBSI provided additional insights into tissue microstructure (**Figure 28**). The analysis revealed an increase in the Axonal Fiber Fraction, accompanied by decreases in the Restricted Isotropic Diffusion Fraction and Isotropic Fraction. These findings indicate a reduction in axonal density and integrity, which is likely reflective of axonal injury within the ischemic core. Additionally, the decreased isotropic fractions suggest alterations in cellular density and an increase in extracellular water contribution, consistent with the pathological processes observed in ischemic stroke. DBSI metrics provide a more nuanced understanding of tissue composition and highlight the extent of cellular damage and extracellular changes following ischemia.

6.6 Discussion

We have demonstrated that the extent of the ischemic region varies significantly between animal strains. We compared Wistar, Long-Evans, and Sprague-Dawley rat strains. Although the macroscopic structure of brain-supplying vessels does not differ between these strains, our findings on regional cerebral blood flow during occlusion suggest distinct meso- and microvascular characteristics. In Sprague-Dawley rats, cerebral blood flow dropped to one-third of pre-occlusion levels. In contrast, Wistar and Long-Evans rats exhibited a less severe decrease, with rCBF reducing to half in Wistar and to two-thirds in Long-Evans rats. While ischemic regions were reliably detected using tetrazolium staining in all three strains, the most consistent results were observed in Sprague-Dawley rats. The variation in rCBF decline following occlusion of the middle cerebral artery's origin is likely due to differences in the network of collateral anastomoses. It has been shown previously anatomy of terminal brain vessels significantly differs between rat strains and also between different vendors (Oliff *et al.*, 1997). In our conditions adult Sprague –Dawley outbred rats obtained from Charles River exhibited most reliable and consistent results.

Cerebral blood flow is typically monitored throughout the entire occlusion procedure, commonly using laser Doppler flowmetry (LDF). The sensing probe is affixed to the thinned skull, allowing for continuous monitoring of cerebral perfusion in the surrounding brain tissue. Due to the method's principles, the recorded values are expressed in arbitrary units (P.U. – perfusion units), which do not provide a quantitative measure of blood flow per unit of volume or weight of nervous tissue. This technique, therefore, enables comparative evaluation of blood flow, typically before and after occlusion. A critical step in the procedure is the correct placement and fixation of the LDF probe to prevent any movement. Continuous rCBF monitoring with LDF allowed us to detect a sudden reduction in rCBF during occlusion, followed by a rapid increase upon filament withdrawal. In two animals that died during or shortly after the surgical procedure, a gradual increase in rCBF following filament withdrawal was observed, suggesting subarachnoid hemorrhage (Woitzik and Schilling, 2002). This was subsequently confirmed by the presence of massive blood deposition at the skull base during autopsy. The fact that both animals which died during procedure were Wistar rats further limit usability of this strain in intraluminal MCAO. Reperfusion led to increase of the rCBF, which was even significantly higher in comparison to basal levels. This is likely caused by release of vasoactive substances e.g. nitric oxide which results in brain vasodilatation (Brožíčková and Otáhal, 2013; Iadecola and Nedergaard, 2007).

Occlusion of middle cerebral artery with intraluminal filament resulted in generation of extensive ischemic region as revealed by tetrazolium staining 24h after the reperfusion. We decided to test 60minutes occlusion interval because this time interval is on the lower edge of time window when reperfusion therapy might be appropriately provided to patients. Thus, it is likely that longer or permanent occlusion will lead to larger infarcts and presumably also to smaller differences between rat strains. Extension of ischemic lesion well correspond to levels of cerebral blood flow measured after the occlusion of MCA. Most extensive lesion was detected in Sprague-Dawley affecting almost half of the brain hemisphere including cerebral cortex and subcortical structures like basal ganglia. Contrary, Long-Evans rats developed less severe ischemia extending to fifth of the brain hemisphere dominantly affecting subcortical structures namely caudoputamen. The subcortical extension of ischemic lesion also explains less severe drop in cerebral blood flow, because cortical blood flow is mainly detected when surface LDF probe is used (Taninishi *et al.*, 2015). Obtained results in Sprague-Dawley and Wistar rats were comparable to those published elsewhere (Bardutzky *et al.*, 2005; Longa *et al.*, 1989).

The widespread implementation of reperfusion strategies in clinical practice, along with a substantial reduction in the time from stroke onset to reperfusion, now approaching the limits of healthcare efficiency—introduces new challenges for preclinical research. The growing number of stroke survivors could greatly benefit from secondary prevention strategies aimed at improving their quality of life. Rehabilitation and compensatory aids play a crucial role in helping patients regain motor function or compensate for motor deficits. However, stroke survivors are at risk of developing severe conditions that may negatively impact their post-stroke quality of life. Among these are epilepsy, depression, and anxiety, highlighting the need for long-term post-stroke studies to better understand the mechanisms underlying their development. To minimize the number of experimental animals while ensuring consistency, it is essential to select subjects with comparable lesion sizes immediately after stroke induction. Therefore, we investigated whether 18F-DG PET scanning, performed 24 hours after stroke induction, can reliably detect and assess the ischemic region. According to results obtained from tetrazolium staining we have selected Sprague-Dawley outbred rat strain for further testing. In agreement with Balsara (Balsara *et* *al.*, 2014) our results clearly indicates that PET can be used for outlining ischemic brain region 24h after reperfusion. Ischemic region has been detected as region with decreased 18F activity in comparison to remaining brain tissue. 18F-DG utilize same transport mechanisms as glucose and thus when intravenously injected it is distributed into metabolically active tissue according to activity of glucose transporters. When 18F-DG transported into cells it is converted with first enzyme of glucose metabolism and is not further capable to enter neither consequent steps of glycolysis nor leave the cell. 18F-DG thus accumulates in metabolically active cells. Observed hypometabolism thus represent decrease in cerebral glucose metabolism in affected tissue. We have utilized standard evaluation of 18F-DG activity based on left/right comparison and visual inspection. However, it has been shown recently that by employing more advanced mathematical analysis of the PET data, namely Statistical Parametric Mapping, it is possible to highly improve detection capabilities of the method (Nie *et al.*, 2014). Additionally, recent preclinical studies suggest that more specific radiotracers detecting neuroinflammation can be used after the stroke to predict the occurrence of spontaneous recurrent seizures later during life (Bertoglio *et al.*, 2017). Functional imaging by means of positron emission tomography seems to be promising method, which can elucidate processes leading to development of pathologies, which typically accompany stroke recovery such epilepsy or depression and help to discover strategies to prevent them.

Fluorescence spectrometry clearly indicated persistent BBB leakage throughout the acute ischemic phase, extending into the early subacute phase (7 days after reperfusion). Even though we detected a statistically significant difference between the ipsilateral and control hemisphere for all tested groups, we were still able to record high-intensity readings from the controls. This may be due to the absence of transcardial perfusion done by other authors (Ryu *et al.*, 2018; Strbian *et al.*, 2008; Wang and Lai, 2014). Instead, we washed the brain slices in tetrazolium/saline solution for 30 minutes, which may have allowed blood saturated with Evans Blue to remain trapped in the vasculature, potentially leading to false-positive signal readings. We also did not observe significant differences between the time points (6h, 24h, 48h, 72h, 7days), likely due to the nature of experimental protocol used. The tissue in our study was harvested one hour after the application of Evans Blue. In comparison, similar studies investigating BBB leakage with Evans Blue employed different circulation times, ranging from 25 minutes (Strbian *et al.*, 2008), two hours (Zhang *et al.*, 2019) up to 6 hours (Ryu *et al.*, 2018). Interestingly, all authors detected Evans Blue extravasated in the brain parenchyma. This suggests that the Evans Blue extravasation test lacks the sensitivity to accurately quantify changes in permeability over time. The limitations of EB as a marker for BBB permeability are further highlighted by Saunders (2015), who demonstrated that Evans Blue does not exclusively bind to blood albumin but also interacts with other blood proteins and tissues, with a portion remaining unbound in its free form. This variability in binding may affect its reliability in quantifying BBB leakage (Saunders *et al.*, 2015).

T2-weighted imaging has consistently demonstrated pronounced hyperintensity within ischemic lesions, particularly in the middle cerebral artery territory, which includes the sensory cortex and caudoputamen. This hyperintense signal is indicative of vasogenic edema, a hallmark of early ischemic injury, resulting from the breakdown of the blood-brain barrier (BBB) that allows plasma proteins and fluid to leak into the extracellular space (Koch *et al.*, 2019). This finding is corroborated by studies that report increased T2 signals as a marker of edema formation in rodent models of ischemia (Alfadeel, 2020).

Furthermore, the increased T1 signal observed following gadolinium (Gd) contrast administration further supports the notion of BBB disruption. The enhancement of contrast within the ischemic region confirms the leakage of Gd into the extracellular space, indicative of vascular permeability and structural damage to endothelial cells (Matos Diaz *et al.*, 2017). These observations align with previous reports that emphasize BBB impairment as a critical component of ischemic stroke pathology, contributing to secondary injury mechanisms, including inflammation and further edema formation (Kim *et al.*, 2021; Matos Diaz *et al.*, 2017). The coexistence of vasogenic and cytotoxic edema in ischemic lesions underscores the complexity of water distribution changes. Vasogenic edema primarily affects the extracellular space, while cytotoxic edema results from intracellular water accumulation due to ionic pump failure and energy depletion (Alfadeel, 2020). This dual mechanism highlights the dynamic progression of ischemic injury and emphasizes the necessity for imaging techniques capable of differentiating these processes.

Diffusion-weighted imaging (DWI) provides essential insights into microstructural changes within ischemic lesions. The decreased apparent diffusion coefficient (ADC) values observed reflect restricted diffusion, a hallmark of cytotoxic edema, which occurs due to the influx of water into cells following the failure of Na^+/K^+ ATPase pumps during ischemia (Alfadeel, 2020). The reduction in ADC values is consistent with findings from both preclinical and clinical studies that identify restricted diffusion as an early and reliable marker of ischemic damage (Gaddamanugu *et al.*, 2022).

In addition to ADC, the reduced fractional anisotropy (FA) values observed in the ischemic lesion indicate a loss of tissue organization and integrity. FA measures the degree of anisotropic diffusion, heavily influenced by the structural organization of white matter tracts. A decline in FA suggests disruption of axonal integrity and demyelination, known to occur in later stages of ischemic injury (Li *et al.*, 2019). These findings align with reports indicating that tissue disorganization begins as early as 24 hours post-ischemia and becomes more pronounced over time (Li *et al.*, 2019). The combination of decreased ADC and FA values underscores the interplay between cytotoxic edema and progressive structural disorganization.

DBSI offers a deeper understanding of tissue microstructure by distinguishing between various diffusion compartments within ischemic lesions. The increased Axonal Fiber Fraction observed may reflect relative preservation of axonal density in certain regions or an artifact of reduced isotropic diffusion contributions (Matos Diaz *et al.*, 2017). The decreased Restricted Isotropic Diffusion Fraction and Isotropic Fraction suggest reductions in cellularity and extracellular water, respectively, consistent with ongoing cellular damage and changes in water compartmentalization following ischemia (Kim *et al.*, 2021; Matos Diaz *et al.*, 2017).

The ability of DBSI to separate isotropic and anisotropic diffusion components provides significant advantages over traditional diffusion tensor imaging (DTI). Previous studies have shown that DBSI metrics correlate well with histological findings, providing reliable measures of axonal integrity, cellularity, and edema (Kim *et al.*, 2021; Matos Diaz *et al.*, 2017). In this context, the DBSI findings provide additional evidence of axonal damage and altered water distribution, reinforcing the role of DBSI as a valuable tool for studying ischemic pathology.

A limitation of our experimental MRI study is the small sample size, as this was our first trial using the Bruker 7T MRI. The machine was delivered to the Magnetic Resonance Research Group at IKEM in late 2023 and became fully operational for experiments by late 2024. This limited timeframe restricted our ability to acquire larger datasets for more in-depth analysis and statistical significance in this thesis.

6.7 Conclusion

The study demonstrated strain-dependent differences in ischemic lesion extent and cerebral blood flow after MCAO, with Sprague-Dawley rats showing the most extensive infarcts and reliable ischemic outcomes. PET imaging effectively identified hypometabolic regions, while fluorescence spectrometry confirmed persistent BBB leakage, though Evans Blue had limitations in quantifying permeability. MRI revealed vasogenic and cytotoxic edema, BBB disruption, and microstructural disorganization, with DBSI providing further insights into axonal damage and water redistribution. These findings highlight the importance of selecting suitable animal models and utilizing advanced imaging techniques for stroke research.

7. General conclusion

Clinical study

This study investigated blood-brain barrier (BBB) impairment in ischemic stroke patients during the subacute phase, particularly around hospital discharge. BBB disruption was observed in 75% of patients, predominantly within ischemic lesions, and was significantly associated with larger lesion volumes. Patients with intact BBB had smaller lesions, better ASPECTS scores, and a lower risk of hemorrhagic transformation, suggesting that BBB leakage correlates with more severe stroke outcomes and may increase the likelihood of vascular epilepsy. Ischemic lesions were identified using FLAIR and DWI MRI, with most BBB leakage occurring in FLAIR+ regions. Interestingly, Gd extravasation was also detected in perilesional gray matter, suggesting BBB dysfunction beyond the ischemic core.

Experimental study

In the experimental study, high variability between rat strains was observed in stroke induction using the intraluminal thread occlusion method. Sprague-Dawley rats proved to be the most reliable, whereas Wistar rats showed higher mortality, and Long-Evans rats developed significantly smaller infarcts. Positron emission tomography with 18F-fluorodeoxyglucose was validated as a suitable method for assessing ischemic lesion size. BBB disruption was evident at 6, 24, 48, 72 hours, and 7 days post-ischemia, with Evans Blue detection confirming BBB leakage. Finally, MRI revealed vasogenic and cytotoxic edema, BBB disruption, and microstructural disorganization, with DBSI providing further insights into axonal damage and water redistribution.

8. Summary

The primary objective of this thesis was to investigate the permeability of the blood-brain barrier (BBB) during cerebral ischemia, with particular focus on the acute and subacute phases. We aimed to characterize BBB dysfunction in ischemic stroke patients using clinical MRI data, and to establish an experimental model that could replicate human ischemic stroke conditions and provide deeper insights into BBB dynamics. Through these complementary approaches, the study sought to shed light on the role of BBB disruption in stroke progression, highlighting its potential as a target for therapeutic interventions to mitigate long-term consequences, such as neuroinflammation, ischemic damage, and vascular epilepsy.

Both clinical and experimental studies successfully addressed these goals. The clinical study demonstrated that BBB impairment is widespread and significant in ischemic stroke patients, with a marked correlation between BBB leakage and the volume of ischemic lesions. Specifically, patients with BBB disruption exhibited larger infarct volumes, higher ASPECTS scores, and a greater incidence of hemorrhagic transformation. These findings suggest that BBB leakage could serve as a biomarker for more severe stroke outcomes and may be linked to an increased risk of vascular epilepsy, as reflected by the SeLECT score. The MRI sequences employed—FLAIR, DWI, and post-contrast T1w—enabled reliable lesion segmentation, while also revealing that BBB disruption was predominantly localized in FLAIR-positive areas but also extended into the surrounding perilesional gray matter.

Furthermore, the experimental study validated the use of the middle cerebral artery occlusion (MCAO) model for studying BBB impairment, offering valuable insights into the temporal dynamics of BBB dysfunction. Our results from fluorescence spectrometry and Evans Blue extravasation indicated significant BBB disruption within the ischemic core, as well as some perilesional leakage, consistent with findings from clinical MRI. These results underscore the role of BBB dysfunction in ischemic injury, supporting the hypothesis that BBB breakdown contributes to the extension of ischemic damage and the persistence of neuronal injury. Moreover, the experimental model confirmed that BBB disruption occurs at multiple time points, including 6, 24, 48, 72 hours and 7 days post-reperfusion, with the highest levels of disruption occurring in the acute and subacute phases.

The combined clinical and experimental results highlight the significant, persistent nature of BBB impairment in ischemic stroke, even after reperfusion has occurred. Our data emphasizes the critical role that BBB disruption plays in stroke progression, particularly in the subacute phase when patients are typically discharged from the hospital. The observation that BBB leakage extends beyond the ischemic lesion into adjacent brain tissue, particularly in gray matter, suggests that the consequences of BBB breakdown are far-reaching and may contribute to additional neuronal damage in the perilesional regions.

From a clinical standpoint, these findings hold important implications for stroke management. The correlation between BBB disruption and vascular epilepsy highlights the need for further research into the potential role of BBB dysfunction in post-stroke epilepsy. The SeLECT score, which is used to predict the risk of post-stroke seizures, was found to be significantly higher in patients with BBB leakage, suggesting that BBB disruption could be a predictive factor for vascular epilepsy. The persistence of BBB dysfunction well beyond the acute phase suggests that therapeutic strategies targeting BBB repair or stabilization could be beneficial in preventing further neuronal damage and improving long-term recovery outcomes.

In conclusion, the results of this study contribute to a deeper understanding of BBB dysfunction in ischemic stroke, emphasizing its importance in stroke progression and its potential as a therapeutic target. The use of advanced imaging techniques, both in clinical settings and experimental models, has provided critical insights into the spatio-temporal dynamics of BBB impairment, highlighting the need for future research focused on developing interventions that can address the chronic consequences of stroke, including vascular epilepsy and neuronal degeneration. Potential interventions thus could focus on modulating the permeability of the BBB, either by protecting its integrity in the acute phase or promoting its repair in the subacute phase

9. Resumé

Hlavním cílem této práce bylo prozkoumat propustnost hematoencefalické bariéry (BBB) během mozkové ischemie se zvláštním zaměřením na akutní a subakutní fázi. Naším cílem bylo charakterizovat dysfunkci BBB u pacientů s ischemickou cévní mozkovou příhodou pomocí klinických dat z magnetické rezonance a vytvořit experimentální model, který by mohl replikovat podmínky lidské ischemické cévní mozkové příhody a poskytnout hlubší vhled do dynamiky BBB. Prostřednictvím těchto vzájemně se doplňujících přístupů se studie snažila objasnit roli narušení BBB v progresi cévní mozkové příhody a zdůraznit její potenciál jako cíle terapeutických zásahů ke zmírnění dlouhodobých následků, jako je zánět, ischemické poškození a vaskulární epilepsie.

Klinické i experimentální studie tyto cíle úspěšně splnily. Klinická studie prokázala, že poškození BBB je u pacientů s ischemickou cévní mozkovou příhodou rozsáhlé a významné, s výraznou korelací mezi únikem BBB a objemem ischemických lézí. Konkrétně pacienti s narušením BBB vykazovali větší objemy infarktů, vyšší skóre ASPECTS a vyšší výskyt hemoragické transformace. Tato zjištění naznačují, že únik BBB by mohl sloužit jako biomarker pro závažnější následky cévní mozkové příhody a může být spojen se zvýšeným rizikem vaskulární epilepsie, jak se odráží ve skóre SeLECT. Použité sekvence MRI – FLAIR, DWI a postkontrastní T1w – umožnily spolehlivou segmentaci lézí a zároveň odhalily, že narušení BBB bylo lokalizováno převážně v oblastech s pozitivním FLAIR, ale zasahovalo i do okolní perilesionální šedé hmoty.

Experimentální studie dále ověřila použití modelu okluze střední mozkové tepny (MCAO) pro studium poškození BBB a nabídla cenné poznatky o časové dynamice dysfunkce BBB. Naše výsledky fluorescenční spektrometrie a extravazace Evansovy modři naznačily významné narušení BBB v ischemickém jádru a také určitý perilesionální únik, což odpovídá nálezům z klinické MRI. Tyto výsledky podtrhují úlohu dysfunkce BBB při ischemickém poškození a podporují hypotézu, že porucha BBB přispívá k rozšíření ischemického poškození a přetrvávání neuronálního poškození. Experimentální model navíc potvrdil, že k narušení BBB dochází ve více časových bodech, včetně 6, 24, 48, 72 hodin a 7 dní po reperfuzi, přičemž k nejvyšší míře narušení dochází v akutní a subakutní fázi.

Kombinované klinické a experimentální výsledky poukazují na významnou a přetrvávající povahu poškození BBB u ischemické cévní mozkové příhody, a to i po reperfuzi. Naše údaje zdůrazňují kritickou roli, kterou narušení BBB hraje při progresi cévní mozkové příhody, zejména v subakutní fázi, kdy jsou pacienti obvykle propouštěni z nemocnice. Pozorování, že únik BBB přesahuje ischemickou lézi do přilehlé mozkové tkáně, zejména v šedé hmotě, naznačuje, že důsledky narušení BBB jsou dalekosáhlé a mohou přispívat k dalšímu poškození neuronů v perilesionálních oblastech.

Z klinického hlediska mají tato zjištění důležité důsledky pro léčbu mrtvice. Korelace mezi narušením BBB a vaskulární epilepsií zdůrazňuje potřebu dalšího výzkumu potenciální role dysfunkce BBB u epilepsie po cévní mozkové příhodě. Bylo zjištěno, že skóre SeLECT, které se používá k predikci rizika záchvatů po cévní mozkové příhodě, je významně vyšší u pacientů s únikem BBB, což naznačuje, že narušení BBB by mohlo být prediktivním faktorem pro vaskulární epilepsii. Přetrvávání dysfunkce BBB i po skončení akutní fáze naznačuje, že terapeutické strategie zaměřené na opravu nebo stabilizaci BBB by mohly být prospěšné při prevenci dalšího poškození neuronů a zlepšení dlouhodobých výsledků zotavení.

Závěrem lze říct, že výsledky této studie přispívají k hlubšímu pochopení dysfunkce BBB u ischemické cévní mozkové příhody a zdůrazňují její význam pro progresi cévní mozkové příhody a její potenciál jako terapeutického cíle. Použití pokročilých zobrazovacích technik v klinických podmínkách i na experimentálních modelech poskytlo zásadní vhled do časoprostorové dynamiky poškození BBB a zdůraznilo potřebu budoucího výzkumu zaměřeného na vývoj intervencí, které mohou řešit chronické následky cévní mozkové příhody, včetně cévní epilepsie a degenerace neuronů. Potenciální intervence by se tedy mohly zaměřit na modulaci propustnosti BBB, a to buď ochranou její integrity v akutní fázi, nebo podporou její opravy v subakutní fázi.

References

Abo-Ramadan, U., Durukan, A., Pitkonen, M., Marinkovic, I., Tatlisumak, E., Pedrono, E., Soinne, L., *et al.* (2009), "Post-ischemic leakiness of the blood-brain barrier: A quantitative and systematic assessment by Patlak plots", *Experimental Neurology*, Vol. 219 No. 1, pp. 328–333, doi: 10.1016/j.expneurol.2009.06.002.

Alfadeel, H.A. (2020), "Role of Diffusion Weighted Imaging in Enhancing MR Imaging in Recent Is-chemic Stroke Patients", *Al-Mukhtar Journal of Sciences*, Omar Al-Mukhtar University, Vol. 35 No. 2, pp. 104–115, doi: 10.54172/mjsc.v35i2.316.

Allen, L.M., Hasso, A.N., Handwerker, J. and Farid, H. (2012), "Sequence-specific MR imaging findings that are useful in dating ischemic stroke", *Radiographics*, Vol. 32 No. 5, pp. 1285–1297, doi: 10.1148/rg.325115760.

Alvi, A.M., Kury, L.T. Al, Ijaz, M.U., Shah, F.A., Khan, M.T., Sheikh, A.S., Nadeem, H., *et al.* (2020), "Post-treatment of synthetic polyphenolic 1,3,4 oxadiazole compound A3, attenuated ischemic stroke-induced neuroinflammation and neurodegeneration", *Biomolecules*, MDPI, Vol. 10 No. 6, doi: 10.3390/biom10060816.

Ansar, S., Chatzikonstantinou, E., Wistuba-Schier, A., Mirau-Weber, S., Fatar, M., Hennerici, M.G. and Meairs, S. (2014), "Characterization of a New Model of Thromboembolic Stroke in C57 black/6J mice", *Translational Stroke Research*, Springer US, Vol. 5 No. 4, pp. 526–533, doi: 10.1007/s12975-013-0315-9.

Balsara, R.D., Chapman, S.E., Sander, I.M., Donahue, D.L., Liepert, L., Castellino, F.J. and Matthew Leevy, W. (2014), "Non-invasive imaging and analysis of cerebral ischemia in living rats using positron emission tomography with 18F-FDG", *Journal of Visualized Experiments*, Journal of Visualized Experiments, No. 94, doi: 10.3791/51495.

Bardutzky, J., Shen, Q., Henninger, N., Bouley, J., Duong, T.Q. and Fisher, M. (2005), "Differences in ischemic lesion evolution in different rat strains using diffusion and perfusion imaging", *Stroke*, Vol. 36 No. 9, pp. 2000–2005, doi: 10.1161/01.STR.0000177486.85508.4d.

Barichello, T., Collodel, A., Hasbun, R. and Morales, R. (2019), "An Overview of the Blood-Brain Barrier", *Neuromethods*, Vol. 142, Humana Press Inc., pp. 1–8, doi: 10.1007/978-1-4939-8946-1_1.

Bernier, L.P., Brunner, C., Cottarelli, A. and Balbi, M. (2021), "Location Matters: Navigating Regional Heterogeneity of the Neurovascular Unit", *Frontiers in Cellular Neuroscience*, Frontiers Media S.A., 30 June, doi: 10.3389/fncel.2021.696540.

Berny-Lang, M.A., Hurst, S., Tucker, E.I., Pelc, L.A., Wang, R.K., Hurn, P.D., Di Cera, E., *et al.* (2011), "Thrombin mutant W215A/E217A treatment improves neurological outcome and reduces cerebral infarct size in a mouse model of ischemic stroke", *Stroke*, Vol. 42 No. 6, pp. 1736–1741, doi: 10.1161/STROKEAHA.110.603811.

Bertoglio, D., Verhaeghe, J., Santermans, E., Amhaoul, H., Jonckers, E., Wyffels, L., Van Der Linden, A., *et al.* (2017), "Non-invasive PET imaging of brain inflammation at disease onset predicts spontaneous recurrent seizures and reflects comorbidities", *Brain, Behavior, and Immunity*, Academic Press Inc., Vol. 61, pp. 69–79, doi: 10.1016/j.bbi.2016.12.015.

Boje, K.M.K., Jaworowicz, D. and Raybon, J.J. (2003), "Neuroinflammatory role of prostaglandins during experimental meningitis: Evidence suggestive of an in vivo relationship between nitric oxide and prostaglandins", *Journal of Pharmacology and Experimental Therapeutics*, Vol. 304 No. 1, pp. 319–325, doi: 10.1124/jpet.102.041533.

Bouley, J., Fisher, M. and Henninger, N. (2007), "Comparison between coated vs. uncoated suture middle cerebral artery occlusion in the rat as assessed by perfusion/diffusion weighted imaging", *Neuroscience Letters*, Vol. 412 No. 3, pp. 185–190, doi: 10.1016/j.neulet.2006.11.003.

Braeuninger, S. and Kleinschnitz, C. (2009), "Rodent models of focal cerebral ischemia: procedural pitfalls and translational problems", *Experimental & Translational Stroke Medicine*, Springer Nature, Vol. 1 No. 1, doi: 10.1186/2040-7378-1-8.

Brandl, S. and Reindl, M. (2023), "Blood–Brain Barrier Breakdown in Neuroinflammation: Current In Vitro Models", *International Journal of Molecular Sciences*, Multidisciplinary Digital Publishing Institute (MDPI), 1 August, doi: 10.3390/ijms241612699.

Brima, T., Mikulecká, A. and Otáhal, J. (2013), “Impacts of perinatal induced photothrombotic stroke on sensorimotor performance in adult rats”, *Physiological Research*, Vol. 62 No. 1, pp. 85–94, doi: 10.33549/physiolres.932447.

Brima, T., Otáhal, J. and Mareš, P. (2013), “Increased susceptibility to pentetrazol-induced seizures in developing rats after cortical photothrombotic ischemic stroke at P7”, *Brain Research*, Vol. 1507, pp. 146–153, doi: 10.1016/j.brainres.2013.02.037.

Brožíčková, C. and Otáhal, J. (2013), “Effect of an inhibitor of neuronal nitric oxide synthase 7-nitroindazole on cerebral hemodynamic response and brain excitability in urethane-anesthetized rats”, *Physiological Research*, Vol. 62 No. SUPPL 1, doi: 10.33549/physiolres.932564.

Brunner, N., Stein, L., Cornelius, V., Knittel, R., Fallier-Becker, P. and Amasheh, S. (2020), “Blood-Brain Barrier Protein Claudin-5 Expressed in Paired Xenopus laevis Oocytes Mediates Cell-Cell Interaction”, *Frontiers in Physiology*, Frontiers Media S.A., Vol. 11, doi: 10.3389/fphys.2020.00857.

Brunner, S.N., Bogert, N. V., Schnitzbauer, A.A., Juengel, E., Moritz, A., Werner, I., Kornberger, A., *et al.* (2017), “Levosimendan protects human hepatocytes from ischemia-reperfusion injury”, *PLoS ONE*, Public Library of Science, Vol. 12 No. 11, doi: 10.1371/journal.pone.0187839.

Campos, F., Qin, T., Castillo, J., Seo, J.H., Arai, K., Lo, E.H. and Waeber, C. (2013), “Fingolimod reduces hemorrhagic transformation associated with delayed tissue plasminogen activator treatment in a mouse thromboembolic model”, *Stroke*, Vol. 44 No. 2, pp. 505–511, doi: 10.1161/STROKEAHA.112.679043.

Canazza, A., Minati, L., Boffano, C., Parati, E. and Binks, S. (2014), “Experimental models of brain ischemia: A review of techniques, magnetic resonance imaging, and investigational cell-based therapies”, *Frontiers in Neurology*, Frontiers Media SA, doi: 10.3389/fneur.2014.00019.

Cao, Y., Yang, L. and Cheng, H. (2022), "Ginkgolide B Protects Against Ischemic Stroke via Targeting AMPK/PINK1", *Frontiers in Pharmacology*, Frontiers Media S.A., Vol. 13, doi: 10.3389/fphar.2022.941094.

Carmichael, S.T. (n.d.). *Rodent Models of Focal Stroke: Size, Mechanism, and Purpose*.

Castro Dias, M., Coisne, C., Baden, P., Enzmann, G., Garrett, L., Becker, L., Hölter, S.M., *et al.* (2019), "Claudin-12 is not required for blood-brain barrier tight junction function", *Fluids and Barriers of the CNS*, BioMed Central Ltd., Vol. 16 No. 1, doi: 10.1186/s12987-019-0150-9.

Cavaglia M, Dombrowski SM, Drazba J, Vasanji A, Bokesch PM and Janigro D. (2001), "Regional variation in brain capillary density and vascular response to ischemia.", *Brain Res*, No. 910, pp. 81–93.

Chassidim, Y., Veksler, R., Lublinsky, S., Pell, G.S., Friedman, A. and Shelef, I. (2013), *Quantitative Imaging Assessment of Blood-Brain Barrier Permeability in Humans FLUIDS AND BARRIERS OF THE CNS*.

Chen, C.C., Chang, M.W., Chang, C.P., Chan, S.C., Chang, W.Y., Yang, C.L. and Lin, M.T. (2014), "A forced running wheel system with a microcontroller that provides high-intensity exercise training in an animal ischemic stroke model", *Brazilian Journal of Medical and Biological Research*, Associacao Brasileira de Divulgacao Cientifica, Vol. 47 No. 10, pp. 858–868, doi: 10.1590/1414-431X20143754.

Chen, Z., Chopp, M., Zacharek, A., Li, W., Venkat, P., Wang, F., Landschoot-Ward, J., *et al.* (2019), "Brain-Derived Microparticles (BDMPs) Contribute to Neuroinflammation and Lactadherin Reduces BDMP Induced Neuroinflammation and Improves Outcome After Stroke", *Frontiers in Immunology*, Frontiers Media S.A., Vol. 10, doi: 10.3389/fimmu.2019.02747.

Cheng, T., Petraglia, A.L., Li, Z., Thiyagarajan, M., Zhong, Z., Wu, Z., Liu, D., *et al.* (2006), "Activated protein C inhibits tissue plasminogen activator-induced brain hemorrhage", *Nature Medicine*, Vol. 12 No. 11, pp. 1278–1285, doi: 10.1038/nm1498.

Chiang, C.W., Wang, Y., Sun, P., Lin, T.H., Trinkaus, K., Cross, A.H. and Song, S.K. (2014), "Quantifying white matter tract diffusion parameters in the presence of increased extra-fiber cellularity and vasogenic edema", *NeuroImage*, Academic Press Inc., Vol. 101, pp. 310–319, doi: 10.1016/j.neuroimage.2014.06.064.

Cho, A.H., Kim, H.R., Kim, W. and Yang, D.W. (2015), "White matter hyperintensity in ischemic stroke patients: It may regress over time", *Journal of Stroke*, Korean Stroke Society, Vol. 17 No. 1, pp. 60–66, doi: 10.5853/jos.2015.17.1.60.

Conforti, P., Mezey, S., Nath, S., Chu, Y.H., Malik, S.C., Martínez Santamaría, J.C., Deshpande, S.S., *et al.* (2022), "Fibrinogen regulates lesion border-forming reactive astrocyte properties after vascular damage", *GLIA*, John Wiley and Sons Inc, Vol. 70 No. 7, pp. 1251–1266, doi: 10.1002/glia.24166.

Coyle, P. and Jokelainen, P. (1982), "Dorsal Cerebral Arterial Collaterals of the Rat", *The Anatomical Record*, No. 203(3), pp. 397–404.

Curry, J.M., Hanke, M.L., Piper, M.G., Bailey, M.T., Bringardner, B.D., Sheridan, J.F. and Marsh, C.B. (2010), "Social disruption induces lung inflammation", *Brain, Behavior, and Immunity*, Vol. 24 No. 3, pp. 394–402, doi: 10.1016/j.bbi.2009.10.019.

David, H.N., Haelewyn, B., Risso, J.J., Colloc'H, N. and Abraini, J.H. (2010), "Xenon is an inhibitor of tissue-plasminogen activator: Adverse and beneficial effects in a rat model of thromboembolic stroke", *Journal of Cerebral Blood Flow and Metabolism*, Vol. 30 No. 4, pp. 718–728, doi: 10.1038/jcbfm.2009.275.

Denic, A., Macura, S.I., Mishra, P., Gamez, J.D., Rodriguez, M. and Pirko, I. (2011), "MRI in Rodent Models of Brain Disorders", *Neurotherapeutics*, January, doi: 10.1007/s13311-010-0002-4.

Di, Z., Wu, X., Xie, W. and Lin, X. (2021), "Effect of Pericytes on Cerebral Microvasculature at Different Time Points of Stroke", *BioMed Research International*, Hindawi Limited, doi: 10.1155/2021/5281182.

Dibble, M., Di Cio', S., Luo, P., Balkwill, F. and Gautrot, J.E. (2023), "The impact of pericytes on the stability of microvascular networks in response to nanoparticles", *Scientific Reports*, Nature Research, Vol. 13 No. 1, doi: 10.1038/s41598-023-31352-x.

DiNapoli, V.A., Rosen, C.L., Nagamine, T. and Crocco, T. (2006), “Selective MCA occlusion: A precise embolic stroke model”, *Journal of Neuroscience Methods*, Vol. 154 No. 1–2, pp. 233–238, doi: 10.1016/j.jneumeth.2005.12.026.

Dirnagl, U. (2012), “Pathobiology of injury after stroke: The neurovascular unit and beyond”, *Annals of the New York Academy of Sciences*, Blackwell Publishing Inc., Vol. 1268 No. 1, pp. 21–25, doi: 10.1111/j.1749-6632.2012.06691.x.

Dotson, A.L., Chen, Y., Zhu, W., Libal, N., Alkayed, N.J. and Offner, H. (2015), “Partial MHC Constructs Treat Thromboembolic Ischemic Stroke Characterized by Early Immune Expansion”, *Translational Stroke Research*, Springer US, Vol. 7 No. 1, pp. 70–78, doi: 10.1007/s12975-015-0436-4.

Eady, T.N., Khoutorova, L., Obenaus, A., Mohd-Yusof, A., Bazan, N.G. and Belayev, L. (2014), “Docosahexaenoic acid complexed to albumin provides neuroprotection after experimental stroke in aged rats”, *Neurobiology of Disease*, Academic Press Inc., Vol. 62, pp. 1–7, doi: 10.1016/j.nbd.2013.09.008.

Eidizadeh, A., Khajehalichalehshtari, M., Freyer, D. and Trendelenburg, G. (2015), “Assessment of the therapeutic potential of metallothionein-II application in focal cerebral ischemia in vitro and in vivo”, *PLoS ONE*, Public Library of Science, Vol. 10 No. 12, doi: 10.1371/journal.pone.0144035.

Engel, O., Kolodziej, S., Dirnagl, U. and Prinz, V. (2011), “Modeling stroke in mice - Middle cerebral artery occlusion with the filament model”, *Journal of Visualized Experiments*, Journal of Visualized Experiments, No. 47, doi: 10.3791/2423.

Engelhardt, B. and Sorokin, L. (2009), “The blood-brain and the blood-cerebrospinal fluid barriers: Function and dysfunction”, *Seminars in Immunopathology*, November, doi: 10.1007/s00281-009-0177-0.

Fanne, R.A., Nassar, T., Yarovoi, S., Rayan, A., Lamensdorf, I., Karakoveski, M., Vadim, P., *et al.* (2010), “Blood-brain barrier permeability and tPA-mediated neurotoxicity”, *Neuropharmacology*, Vol. 58 No. 7, pp. 972–980, doi: 10.1016/j.neuropharm.2009.12.017.

Faridová, A.T., HEŘMAN, H., DANAČÍKOVÁ, Š., SVOBODA, J. and OTÁHAL, J. (2023), "Serum Biomarkers Of Hypoxic-Ischemic Brain Injury", *Physiological Research*, Czech Academy of Sciences, Vol. 72, pp. S461–S474, doi: 10.33549/physiolres.935214.

Fiebig, T., Figueiredo, G., Boll, H., Kerl, H.U., Noelte, I.S., Forster, A., Groden, C., *et al.* (2013), "A Low Cost Metal-Free Vascular Access Mini-Port for Artifact Free Imaging and Repeated Injections in Mice", *PLoS ONE*, Vol. 8 No. 6, doi: 10.1371/journal.pone.0065939.

Fluri, F., Schuhmann, M.K. and Kleinschnitz, C. (2015), "Animal models of ischemic stroke and their application in clinical research", *Drug Design, Development and Therapy*, Dove Medical Press Ltd., Vol. 9, pp. 3445–3454, doi: 10.2147/DDDT.S56071.

FOUR-VESSEL OCCLUSION MODEL/Furlow. (n.d.). .

Frahm, J., Boretius, S., Watanabe, T. and Michaelis, T. (2006), "Magnetic Resonance Imaging of Animal Brain In Vivo", *ALTEX: Alternativen Zu Tierexperimenten*, Vol. 23, pp. 110–114.

Friedrich, J., Lindauer, U. and Höllig, A. (2022), "Procedural and Methodological Quality in Preclinical Stroke Research–A Cohort Analysis of the Rat MCAO Model Comparing Periods Before and After the Publication of STAIR/ARRIVE", *Frontiers in Neurology*, Frontiers Media S.A., Vol. 13, doi: 10.3389/fneur.2022.834003.

Fukumoto, M., Nakaizumi, A., Zhang, T., Lentz, S.I., Shibata, M., Puro, D.G. and Vulnerability, P.D. (2012), "Vulnerability of the retinal microvasculature to oxidative stress: ion channel-dependent mechanisms", *Am J Physiol Cell Physiol*, Vol. 302, pp. 1413–1420, doi: 10.1152/ajpcell.00426.2011.-Although.

Gaddamanugu, S., Shafaat, O., Sotoudeh, H., Sarrami, A.H., Rezaei, A., Saadatpour, Z. and Singhal, A. (2022), "Clinical applications of diffusion-weighted sequence in brain imaging: beyond stroke", *Neuroradiology*, Springer Science and Business Media Deutschland GmbH, 1 January, doi: 10.1007/s00234-021-02819-3.

Galovic, M., Döhler, N., Erdélyi-Canavese, B., Felbecker, A., Siebel, P., Conrad, J., Evers, S., *et al.* (2018), "Prediction of late seizures after ischaemic stroke with a novel prognostic model (the SeLECT score): a multivariable prediction model development and validation study", *The Lancet Neurology*, Lancet Publishing Group, Vol. 17 No. 2, p. 143, doi: 10.1016/S1474-4422(17)30404-0.

Gao, H.M., Zhou, H., Zhang, F., Wilson, B.C., Kam, W. and Hong, J.S. (2011), "HMGB1 acts on microglia Mac1 to mediate chronic neuroinflammation that drives progressive neurodegeneration", *Journal of Neuroscience*, Vol. 31 No. 3, pp. 1081–1092, doi: 10.1523/JNEUROSCI.3732-10.2011.

Gião, T., Teixeira, T., Almeida, M.R. and Cardoso, I. (2022), "Choroid Plexus in Alzheimer's Disease—The Current State of Knowledge", *Biomedicines*, MDPI, Vol. 10 No. 2, doi: 10.3390/biomedicines10020224.

Giraud, M., Cho, T.H., Nighoghossian, N., Maucort-Boulch, D., Deiana, G., Østergaard, L., Baron, J.C., *et al.* (2015), "Early Blood Brain Barrier Changes in Acute Ischemic Stroke: A Sequential MRI Study", *Journal of Neuroimaging*, Vol. 25 No. 6, pp. 959–963, doi: 10.1111/jon.12225.

Goldim, M.P. de S., Della Giustina, A. and Petronilho, F. (2019), "Using Evans Blue Dye to Determine Blood-Brain Barrier Integrity in Rodents", *Current Protocols in Immunology*, Blackwell Publishing Inc., Vol. 126 No. 1, doi: 10.1002/cpim.83.

González-Marrero, I., Castañeyra-Ruiz, L., M. González-Toledo, J., Castañeyra-Ruiz, A., de Paz-Carmona, H., Ruiz-Mayor, L., Castañeyra-Perdomo, A., *et al.* (2012), "High Blood Pressure Effects on the Brain Barriers and Choroid Plexus Secretion", *Neuroscience and Medicine*, Scientific Research Publishing, Inc, Vol. 03 No. 01, pp. 60–64, doi: 10.4236/nm.2012.31009.

Gouw, A.A., Seewann, A., Van Der Flier, W.M., Barkhof, F., Rozemuller, A.M., Scheltens, P. and Geurts, J.J.G. (2011), "Heterogeneity of small vessel disease: A systematic review of MRI and histopathology correlations", *Journal of Neurology, Neurosurgery and Psychiatry*, BMJ Publishing Group, doi: 10.1136/jnnp.2009.204685.

Gu, C., Liu, J., Li, Y., Zhang, Q., Lin, C., Huang, J., Duan, W., *et al.* (2023), "Comparison of ketamine/xylazine and isoflurane anesthesia on the establishment of mouse middle cerebral artery occlusion model", *Experimental Animals*, International Press Editing Centre Incorporation, Vol. 72 No. 2, pp. 209–217, doi: 10.1538/expanim.22-0131.

Guan, Y., Wang, Y., Yuan, F., Lu, H., Ren, Y., Xiao, T., Chen, K., *et al.* (2012), "Effect of suture properties on stability of middle cerebral artery occlusion evaluated by synchrotron radiation angiography", *Stroke*, Vol. 43 No. 3, pp. 888–891, doi: 10.1161/STROKEAHA.111.636456.

Gubskiy, I.L., Namestnikova, D.D., Cherkashova, E.A., Chekhonin, V.P., Baklaushev, V.P., Gubsky, L. V. and Yarygin, K.N. (2018), "MRI Guiding of the Middle Cerebral Artery Occlusion in Rats Aimed to Improve Stroke Modeling", *Translational Stroke Research*, Springer US, Vol. 9 No. 4, pp. 417–425, doi: 10.1007/s12975-017-0590-y.

Gursoy-Ozdemir, Y., Yemisci, M. and Dalkara, T. (2012), "Microvascular protection is essential for successful neuroprotection in stroke", *Journal of Neurochemistry*, Vol. 123, pp. 2–11, doi: 10.1111/j.1471-4159.2012.07938.x.

Hagmann, P., Jonasson, L., Maeder, P., Thiran, J.P., Wedeen, J. Van and Meuli, R. (2006), "Understanding diffusion MR imaging techniques: From scalar diffusion-weighted imaging to diffusion tensor imaging and beyond", *Radiographics*, Vol. 26 No. SPEC. ISS., doi: 10.1148/rg.26si065510.

Han, R.H., Johanns, T.M., Roberts, K.F., Tao, Y., Luo, J., Ye, Z., Sun, P., *et al.* (2023), "Diffusion basis spectrum imaging as an adjunct to conventional MRI leads to earlier diagnosis of high-grade glioma tumor progression versus treatment effect", *Neuro-Oncology Advances*, Oxford University Press, Vol. 5 No. 1, doi: 10.1093/noajnl/vdad050.

Hase, Y., Ding, R., Harrison, G., Hawthorne, E., King, A., Gettings, S., Platten, C., *et al.* (2019), "White matter capillaries in vascular and neurodegenerative dementias", *Acta Neuropathologica Communications*, NLM (Medline), Vol. 7 No. 1, p. 16, doi: 10.1186/s40478-019-0666-x.

Hawkins, B.T., Gu, Y.H., Izawa, Y. and Del Zoppo, G.J. (2013), "Disruption of dystroglycan-laminin interactions modulates water uptake by astrocytes", *Brain Research*, Vol. 1503, pp. 89–96, doi: 10.1016/j.brainres.2013.01.049.

Henriques, I.L., Gutiérrez-Fernández, M., Rodríguez-Frutos, B., Ramos-Cejudo, J., Otero-Ortega, L., Navarro Hernanz, T., Cerdán, S., *et al.* (2015), "Intralesional patterns of

MRI ADC maps predict outcome in experimental stroke", *Cerebrovascular Diseases*, S. Karger AG, Vol. 39 No. 5–6, pp. 293–301, doi: 10.1159/000381727.

Hill, S.A., Blaeser, A.S., Coley, A.A., Xie, Y., Shepard, K.A., Harwell, C.C., Gao, W.J., *et al.* (2019), "Sonic hedgehog signaling in astrocytes mediates cell type-specific synaptic organization", *ELife*, eLife Sciences Publications Ltd, Vol. 8, doi: 10.7554/eLife.45545.001.

Hossmann, K.A. (2012), "The two pathophysiologies of focal brain ischemia: Implications for translational stroke research", *Journal of Cerebral Blood Flow and Metabolism*, July, doi: 10.1038/jcbfm.2011.186.

Howells, D.W., Porritt, M.J., Rewell, S.S.J., O'Collins, V., Sena, E.S., Van Der Worp, H.B., Traystman, R.J., *et al.* (2010), "Different strokes for different folks: The rich diversity of animal models of focal cerebral ischemia", *Journal of Cerebral Blood Flow and Metabolism*, August, doi: 10.1038/jcbfm.2010.66.

Hoyer, C., Gass, N., Weber-Fahr, W. and Sartorius, A. (2014), "Advantages and challenges of small animal magnetic resonance imaging as a translational tool", *Neuropsychobiology*, S. Karger AG, doi: 10.1159/000360859.

Hrishikesh Bhagwat, Bronstein, S., Bhatt, A. and Nguyen, V. (2022), "Neurogenesis: Gene-Based Strategies for Treating Ischemic Stroke", *Berkeley Pharma Tech Journal of Medicine*, No. 2 (1), pp. 30–57, doi: https://doi.org/10.52243/bptjm.v1i2.22.

Hu, Y., Yang, Z.H., Yan, F., Huang, S.F., Wang, R.L., Han, Z.P., Fan, J.F., *et al.* (2023), "CCA repair or ECA ligation—Which middle cerebral artery occlusion is better in the reperfusion mouse model?", *Ibrain*, Wiley-VCH Verlag, Vol. 9 No. 3, pp. 258–269, doi: 10.1002/ibra.12128.

Hubert, V., Chauveau, F., Dumot, C., Ong, E., Berner, L.P., Canet-Soulas, E., Ghersi-Egea, J.F., *et al.* (2019), "Clinical imaging of choroid plexus in health and in brain disorders: A mini-review", *Frontiers in Molecular Neuroscience*, Frontiers Media S.A., 12 February, doi: 10.3389/fnmol.2019.00034.

Iadecola, C. and Nedergaard, M. (2007), "Glial regulation of the cerebral microvasculature", *Nature Neuroscience*, November, doi: 10.1038/nn2003.

Ihle-Hansen, H., Thommessen, B., Fagerland, M.W., Wyller, T.B., Engedal, K., Øksengård, A.R., Stenset, V., *et al.* (2012), "Impact of White Matter Lesions on Cognition in Stroke Patients Free from Pre-Stroke Cognitive Impairment: A One-Year Follow-Up Study", *Dementia and Geriatric Cognitive Disorders Extra*, S. Karger AG, Vol. 2 No. 1, pp. 38–47, doi: 10.1159/000336817.

Janský, P., Růžičková, T., Olšerová, A., Reichl, J., Vosko, M.S., Šťovíčková, L., Paulasová-Schwabová, J., *et al.* (2020), "Occurrence and risk factors of unprovoked epileptic seizures in ischaemic stroke patients", *Ceska a Slovenska Neurologie a Neurochirurgie*, Czech Medical Association J.E. Purkyne, Vol. 83 No. 3, pp. 278–284, doi: 10.14735/amcsnn2020278.

Jayakumar, A.R., Panickar, K.S., Curtis, K.M., Tong, X.Y., Moriyama, M. and Norenberg, M.D. (2011), "Na-K-Cl cotransporter-1 in the mechanism of cell swelling in cultured astrocytes after fluid percussion injury", *Journal of Neurochemistry*, Vol. 117 No. 3, pp. 437–448, doi: 10.1111/j.1471-4159.2011.07211.x.

Jia, J.M., Chowdary, P.D., Gao, X., Ci, B., Li, W., Mulgaonkar, A., Plautz, E.J., *et al.* (2016), "Control of cerebral ischemia with magnetic nanoparticles", *Nature Methods*, Nature Publishing Group, Vol. 14 No. 2, pp. 160–166, doi: 10.1038/nmeth.4105.

Jia, J.M., Peng, C., Wang, Y., Zheng, J. and Ge, W.P. (2018), "Control of occlusion of middle cerebral artery in perinatal and neonatal mice with magnetic force", *Molecular Brain*, BioMed Central Ltd., Vol. 11 No. 1, doi: 10.1186/s13041-018-0389-0.

Jiang, X., Andjelkovic, A. V., Zhu, L., Yang, T., Bennett, M.V.L., Chen, J., Keep, R.F., *et al.* (2018), "Blood-brain barrier dysfunction and recovery after ischemic stroke", *Progress in Neurobiology*, Elsevier Ltd, 1 April, doi: 10.1016/j.pneurobio.2017.10.001.

Jiang, Z., Li, C., Arrick, D.M., Yang, S., Baluna, A.E. and Sun, H. (2014), "Role of nitric oxide synthases in early blood-brain barrier disruption following transient focal cerebral ischemia", *PLoS ONE*, Public Library of Science, Vol. 9 No. 3, doi: 10.1371/journal.pone.0093134.

Jin, Z., Liang, J., Li, J. and Kolattukudy, P.E. (2018), "Novel Role of MCP-Induced Protein 1 in Ischemic Brain Damage in Animals of Transient Focal Ischemia", 11 December, doi: 10.20944/preprints201812.0128.v1.

Jolly, S., Bazargani, N., Quiroga, A.C., Pringle, N.P., Attwell, D., Richardson, W.D. and Li, H. (2018), “G protein-coupled receptor 37-like 1 modulates astrocyte glutamate transporters and neuronal NMDA receptors and is neuroprotective in ischemia”, *GLIA*, John Wiley and Sons Inc., Vol. 66 No. 1, pp. 47–61, doi: 10.1002/glia.23198.

Kadry, H., Noorani, B. and Cucullo, L. (2020), “A blood–brain barrier overview on structure, function, impairment, and biomarkers of integrity”, *Fluids and Barriers of the CNS*, BioMed Central Ltd, 1 December, doi: 10.1186/s12987-020-00230-3.

Kala, D. (2022), *Image Processing Pipelines for Analysis of Clinical Human MRI Doctoral Thesis*, Czech Technical University in Prague, October.

Kala, D., Svoboda, J., Litvinec, A., Pošusta, A., Lisý, J., Šulc, V., Tomek, A., *et al.* (2017), “/GD-Tracker/ A software for blood-brain barrier permeability assessment”, *Lekar a Technika*, Vol. 47 No. 2.

Karthikeyan, S., Jeffers, M.S., Carter, A. and Corbett, D. (2019), “Characterizing Spontaneous Motor Recovery Following Cortical and Subcortical Stroke in the Rat”, *Neurorehabilitation and Neural Repair*, SAGE Publications Inc., Vol. 33 No. 1, pp. 27–37, doi: 10.1177/1545968318817823.

Kim, B.J., Kang, H.G., Kim, H.-J., Ahn, S.-H., Kim, N.Y., Warach, S. and Kang, D.-W. (2014), “Magnetic Resonance Imaging in Acute Ischemic Stroke Treatment”, *Journal of Stroke*, Korean Stroke Society, Vol. 16 No. 3, p. 131, doi: 10.5853/jos.2014.16.3.131.

Kim, H., Urquhart, R., Pontarelli, F., Jover-Mengual, T., Ofengeim, D. and Hwang, J.Y. (2023), “Protocol for establishing a global ischemia model using a 4-vessel occlusion in rats”, *STAR Protocols*, Cell Press, Vol. 4 No. 4, doi: 10.1016/j.xpro.2023.102630.

Kim, J.H., Kim, S.Y., Kim, B., Lee, S.R., Cha, S.H., Lee, D.S. and Lee, H.J. (2021), “Prospects of therapeutic target and directions for ischemic stroke”, *Pharmaceuticals*, MDPI AG, Vol. 14 No. 4, doi: 10.3390/ph14040321.

Kincer, L.P., Schnell, G., Swanstrom, R., Miller, M.B., Spudich, S., Eron, J.J., Price, R.W., *et al.* (2022), “HIV-1 is Transported into the Central Nervous System by Trafficking Infected Cells”, *Pathogens and Immunity*, Case Western Reserve University, Vol. 7 No. 2, pp. 131–142, doi: 10.20411/pai.v7i2.524.

Knox, E.G., Lynch, C.M.K., Lee, Y.S., O'Driscoll, C.M., Clarke, G., Cryan, J.F. and Aburto, M.R. (2023), "The gut microbiota is important for the maintenance of blood–cerebrospinal fluid barrier integrity", *European Journal of Neuroscience*, John Wiley and Sons Inc, Vol. 57 No. 2, pp. 233–241, doi: 10.1111/ejn.15878.

Koch, S., Mueller, S., Foddis, M., Bienert, T., von Elverfeldt, D., Knab, F., Farr, T.D., *et al.* (2019), "Atlas registration for edema-corrected MRI lesion volume in mouse stroke models", *Journal of Cerebral Blood Flow and Metabolism*, SAGE Publications Ltd, Vol. 39 No. 2, pp. 313–323, doi: 10.1177/0271678X17726635.

Koto, T., Takubo, K., Ishida, S., Shinoda, H., Inoue, M., Tsubota, K., Okada, Y., *et al.* (2007), "Hypoxia disrupts the barrier function of neural blood vessels through changes in the expression of claudin-5 in endothelial cells", *American Journal of Pathology*, American Society for Investigative Pathology Inc., Vol. 170 No. 4, pp. 1389–1397, doi: 10.2353/ajpath.2007.060693.

Krey, L., Lühder, F., Kusch, K., Czech-Zechmeister, B., Könnecke, B., Outeiro, T.F. and Trendelenburg, G. (2015), "Knockout of silent information regulator 2 (SIRT2) preserves neurological function after experimental stroke in mice", *Journal of Cerebral Blood Flow and Metabolism*, Nature Publishing Group, Vol. 35 No. 12, pp. 2080–2088, doi: 10.1038/jcbfm.2015.178.

Krueger, M., Härtig, W., Reichenbach, A., Bechmann, I. and Michalski, D. (2013), "Blood-Brain Barrier Breakdown after Embolic Stroke in Rats Occurs without Ultrastructural Evidence for Disrupting Tight Junctions", *PLoS ONE*, Vol. 8 No. 2, doi: 10.1371/journal.pone.0056419.

Labat-gest, V. and Tomasi, S. (2013), "Photothrombotic ischemia: a minimally invasive and reproducible photochemical cortical lesion model for mouse stroke studies", *Journal of Visualized Experiments : JoVE*, No. 76, doi: 10.3791/50370.

Lansberg, M.G., Thijs, V.N., O'brien, M.W., Ali, J.O., De Crespigny, A.J., Tong, D.C., Moseley, M.E., *et al.* (2001), *Evolution of Apparent Diffusion Coefficient, Diffusion-Weighted, and T2-Weighted Signal Intensity of Acute Stroke*, *AJNR Am J Neuroradiol*, Vol. 22.

Lansberg, M.G., Wintermark, M., Kidwell, C.S., Warach, S. and Albers, G.W. (2015), "Magnetic Resonance Imaging of Cerebrovascular Diseases", *Stroke: Pathophysiology, Diagnosis, and Management*, Elsevier Inc., pp. 768–789, doi: 10.1016/B978-0-323-29544-4.00048-7.

Lanz, T. V., Becker, S., Osswald, M., Bittner, S., Schuhmann, M.K., Opitz, C.A., Gaikwad, S., *et al.* (2013), "Protein kinase Cβ as a therapeutic target stabilizing blood-brain barrier disruption in experimental autoimmune encephalomyelitis", *Proceedings of the National Academy of Sciences of the United States of America*, National Academy of Sciences, Vol. 110 No. 36, pp. 14735–14740, doi: 10.1073/pnas.1302569110.

Lapilover, E.G., Lippmann, K., Salar, S., Maslarova, A., Dreier, J.P., Heinemann, U. and Friedman, A. (2012), "Peri-infarct blood-brain barrier dysfunction facilitates induction of spreading depolarization associated with epileptiform discharges", *Neurobiology of Disease*, Vol. 48 No. 3, pp. 495–506, doi: 10.1016/j.nbd.2012.06.024.

Lee, I.H., Ha, S.K., Lim, D.J. and Choi, J. Il. (2024), "Risk Factors and Clinical Outcomes of Arterial Re-Occlusion After Successful Mechanical Thrombectomy for Emergent Intracranial Large Vessel Occlusion", *Journal of Clinical Medicine*, Multidisciplinary Digital Publishing Institute (MDPI), Vol. 13 No. 24, doi: 10.3390/jcm13247640.

Lee, I.J., Yang, Y.C., Hsu, J.W., Chang, W.T., Chuang, Y.J. and Liau, I. (2017), "Zebrafish model of photochemical thrombosis for translational research and thrombolytic screening in vivo", *Journal of Biophotonics*, Wiley-VCH Verlag, Vol. 10 No. 4, pp. 494–502, doi: 10.1002/jbio.201500287.

Lee, K.H., Jeong, E.H. and Joa, K.L. (2022), "Effects of Stroke Lesions and Timing of Rehabilitation on the Compensatory Movement Patterns During Stroke Recovery", *American Journal of Physical Medicine and Rehabilitation*, Lippincott Williams and Wilkins, Vol. 101 No. 11, pp. 1031–1037, doi: 10.1097/PHM.0000000000001968.

Lee, S., Hong, Y., Park, S., Lee, S.R., Chang, K.T. and Hong, Y. (2014), "Comparison of surgical methods of transient middle cerebral artery occlusion between rats and mice", *The Journal of Veterinary Medical Science / the Japanese Society of Veterinary Science*, Vol. 76 No. 12, pp. 1555–1561, doi: 10.1292/jvms.14-0258.

Lei, Z., Zhang, H., Liang, Y. and Xu, Z.C. (2016), “Reduced expression of IA channels is associated with post-ischemic seizures”, *Epilepsy Research*, Elsevier, Vol. 124, pp. 40–48, doi: 10.1016/j.eplepsyres.2016.05.008.

Li, C., Lan, C., Zhang, X., Yin, L., Hao, X., Tian, J., Lin, L., *et al.* (2019), “Evaluation of Diffusional Kurtosis Imaging in Sub-acute Ischemic Stroke: Comparison with Rehabilitation Treatment Effect”, *Cell Transplantation*, SAGE Publications Ltd, Vol. 28 No. 8, pp. 1053–1061, doi: 10.1177/0963689719837919.

Li, J., Ma, X., Yu, W., Lou, Z., Mu, D., Wang, Y., Shen, B., *et al.* (2012), “Reperfusion Promotes Mitochondrial Dysfunction following Focal Cerebral Ischemia in Rats”, *PLoS ONE*, Vol. 7 No. 9, doi: 10.1371/journal.pone.0046498.

Li, S., Wernersbach, I., Harms, G.S. and Schäfer, M.K.E. (2022), “Microglia subtypes show substrate- and time-dependent phagocytosis preferences and phenotype plasticity”, *Frontiers in Immunology*, Frontiers Media S.A., Vol. 13, doi: 10.3389/fimmu.2022.945485.

Li, W., Qu, Z., Prakash, R., Chung, C., Ma, H., Hoda, M.N., Fagan, S.C., *et al.* (2013), “Comparative analysis of the neurovascular injury and functional outcomes in experimental stroke models in diabetic Goto-Kakizaki rats”, *Brain Research*, Elsevier B.V., Vol. 1541, pp. 106–114, doi: 10.1016/j.brainres.2013.10.021.

Li, X., Lyu, J., Li, R., Jain, V., Shen, Y., del Águila, Á., Hoffmann, U., *et al.* (2022), “Single-cell transcriptomic analysis of the immune cell landscape in the aged mouse brain after ischemic stroke”, *Journal of Neuroinflammation*, BioMed Central Ltd, Vol. 19 No. 1, doi: 10.1186/s12974-022-02447-5.

Li, Y., Tan, L., Yang, C., He, L., Liu, L., Deng, B., Liu, S., *et al.* (2023), “Distinctions between the Koizumi and Zea Longa methods for middle cerebral artery occlusion (MCAO) model: a systematic review and meta-analysis of rodent data”, *Scientific Reports*, Nature Research, Vol. 13 No. 1, doi: 10.1038/s41598-023-37187-w.

Li, Y. and Zhang, J. (2021), “Animal models of stroke”, *Animal Models and Experimental Medicine*, John Wiley and Sons Inc, 1 September, doi: 10.1002/ame2.12179.

Liddle, L.J., Kalisvaart, A.C.J., Abrahart, A.H., Almekhlafi, M., Demchuk, A. and Colbourne, F. (2022), "Targeting focal ischemic and hemorrhagic stroke neuroprotection: Current prospects for local hypothermia", *Journal of Neurochemistry*, John Wiley and Sons Inc, 1 January, doi: 10.1111/jnc.15508.

Lin, M.P. and Liebeskind, D.S. (2016), *Imaging of Ischemic Stroke*, *Continuum (Minneap Minn)*, Vol. 22.

Lin, T.H., Zhan, J., Song, C., Wallendorf, M., Sun, P., Niu, X., Yang, R., *et al.* (2021), "Diffusion Basis Spectrum Imaging Detects Axonal Loss After Transient Dexamethasone Treatment in Optic Neuritis Mice", *Frontiers in Neuroscience*, Frontiers Media S.A., Vol. 14, doi: 10.3389/fnins.2020.592063.

Lin, T.Y., Huang, W.J., Wu, C.C., Lu, C.W. and Wang, S.J. (2014), "Acacetin inhibits glutamate release and prevents kainic acid-induced neurotoxicity in rats", *PLoS ONE*, Public Library of Science, Vol. 9 No. 2, doi: 10.1371/journal.pone.0088644.

Liszczak, T.M., Hedley-Whyte, E.T., Adams, J.F., Han, D.H., Kolluri, V.S., Vacanti, F.X., Heros, R.C., *et al.* (1984), "Limitations of tetrazolium salts in delineating infarcted brain", *Acta Neuropathologica*, Vol. 65 No. 2, pp. 150–157, doi: 10.1007/BF00690469.

Liu, H.S., Chung, H.W., Chou, M.C., Liou, M., Wang, C.Y., Kao, H.W., Chiang, S.W., *et al.* (2013), "Effects of microvascular permeability changes on contrast-enhanced t1 and pharmacokinetic mr imagings after ischemia", *Stroke*, Vol. 44 No. 7, pp. 1872–1877, doi: 10.1161/STROKEAHA.113.001558.

Liu, K.J., Liang, J., Qi, Z., Liu, W., Wang, P., Shi, W., Dong, W., *et al.* (2015), "Normobaric Hyperoxia Slows Blood-Brain Barrier Damage and Expands the Therapeutic Time Window for Tissue-Type Plasminogen Activator Treatment in Cerebral Ischemia", *Stroke*, Lippincott Williams and Wilkins, Vol. 46 No. 5, pp. 1344–1351, doi: 10.1161/STROKEAHA.114.008599.

Liu, Q., Li, Y., Lu, H. and Tong, S. (2014), "Real-time high resolution laser speckle imaging of cerebral vascular changes in a rodent photothrombosis model", *Biomedical Optics Express*, Optica Publishing Group, Vol. 5 No. 5, p. 1483, doi: 10.1364/boe.5.001483.

Liu, X., Su, P., Meng, S., Aschner, M., Cao, Y., Luo, W., Zheng, G., *et al.* (2017), “Role of matrix metalloproteinase-2/9 (MMP2/9) in lead-induced changes in an in vitro blood-brain barrier model”, *International Journal of Biological Sciences*, Ivyspring International Publisher, Vol. 13 No. 11, pp. 1351–1360, doi: 10.7150/ijbs.20670.

Longa, E.Z., Weinstein, P.R., Carlson, S. and Cummins, R. (1989), “Reversible Middle Cerebral Artery Occlusion Without Craniectomy in Rats”, *Stroke*, No. 20, pp. 84–97.

Loor, G., Kondapalli, J., Iwase, H., Chandel, N.S., Waypa, G.B., Guzy, R.D., Vanden Hoek, T.L., *et al.* (2011), “Mitochondrial oxidant stress triggers cell death in simulated ischemia-reperfusion”, *Biochimica et Biophysica Acta - Molecular Cell Research*, Vol. 1813 No. 7, pp. 1382–1394, doi: 10.1016/j.bbamcr.2010.12.008.

Lopez, M.S. and Vemuganti, R. (2018), “Modeling transient focal ischemic stroke in rodents by intraluminal filament method of middle cerebral artery occlusion”, *Methods in Molecular Biology*, Vol. 1717, Humana Press Inc., pp. 101–113, doi: 10.1007/978-1-4939-7526-6_9.

Löscher, W. and Friedman, A. (2020), “Structural, molecular, and functional alterations of the blood-brain barrier during epileptogenesis and epilepsy: A cause, consequence, or both?”, *International Journal of Molecular Sciences*, MDPI AG, 2 January, doi: 10.3390/ijms21020591.

Lu, D., Wu, Y., Qu, Y., Shi, F., Hu, J., Gao, B., Wang, B., *et al.* (2016), “A modified method to reduce variable outcomes in a rat model of four-vessel arterial occlusion”, *Neurological Research*, Taylor and Francis Ltd., Vol. 38 No. 12, pp. 1102–1110, doi: 10.1080/01616412.2016.1249996.

Ma, J., Ma, Y., Shuaib, A. and Winship, I.R. (2020), “Improved collateral flow and reduced damage after remote ischemic perconditioning during distal middle cerebral artery occlusion in aged rats”, *Scientific Reports*, Nature Research, Vol. 10 No. 1, doi: 10.1038/s41598-020-69122-8.

Madla, C.M., Qin, Y., Gavins, F.K.H., Liu, J., Dou, L., Orlu, M., Murdan, S., *et al.* (2022), “Sex Differences in Intestinal P-glycoprotein Expression in Wistar versus Sprague Dawley Rats”, *Pharmaceutics*, MDPI, Vol. 14 No. 5, doi: 10.3390/pharmaceutics14051030.

Mansour, T., Sileem, S., El-Barody, M. and Okasha, A. (2020), “Role Of Magnetic Resonance Imaging With Diffusion-Weighted Images In Assessment Of Patients with Pre-eclampsia In Pre And Postpartum Periods”, *Al-Azhar International Medical Journal*, Al-Azhar University, Vol. 0 No. 0, pp. 0–0, doi: 10.21608/aimj.2020.43406.1324.

Mao, Y., Huang, Y., Zhang, L. and Nan, G. (2017), “Spontaneous recanalization of atherosclerotic middle cerebral artery occlusion”, *Medicine (United States)*, Lippincott Williams and Wilkins, Vol. 96 No. 27, doi: 10.1097/MD.0000000000007372.

Matos Diaz, I., Liang, J.W., Ostojic, L.V. and Tansy, A.P. (2017), “Acute Stroke Multimodal Imaging: Present and Potential Applications toward Advancing Care”, *Seminars in Neurology*, Thieme Medical Publishers, Inc., Vol. 37 No. 5, pp. 558–565, doi: 10.1055/s-0037-1607355.

McBride, D.W., Wu, G., Nowrangi, D., Flores, J.J., Hui, L., Krafft, P.R. and Zhang, J.H. (2018), “Delayed Recanalization Promotes Functional Recovery in Rats Following Permanent Middle Cerebral Artery Occlusion”, *Translational Stroke Research*, Springer US, Vol. 9 No. 2, pp. 185–198, doi: 10.1007/s12975-018-0610-6.

Mcbride, D.W. and Zhang, J.H. (2017), *Precision Stroke Animal Models: The Permanent MCAO Model Should Be the Primary Model, Not Transient MCAO*.

McConnell, H.L., Kersch, C.N., Woltjer, R.L. and Neuwelt, E.A. (2017), “The translational significance of the neurovascular unit”, *Journal of Biological Chemistry*, American Society for Biochemistry and Molecular Biology Inc., 20 January, doi: 10.1074/jbc.R116.760215.

McCullough, L.D. and Liu, F. (2011), “Middle cerebral artery occlusion model in rodents: Methods and potential pitfalls”, *Journal of Biomedicine and Biotechnology*, doi: 10.1155/2011/464701.

McMillin, M.A., Frampton, G.A., Seiwell, A.P., Patel, N.S., Jacobs, A.N. and DeMorrow, S. (2015), “TGFβ1 exacerbates blood-brain barrier permeability in a mouse model of hepatic encephalopathy via upregulation of MMP9 and downregulation of claudin-5”, *Laboratory Investigation*, Nature Publishing Group, Vol. 95 No. 8, pp. 903–913, doi: 10.1038/labinvest.2015.70.

Mecca, A.P., Regenhardt, R.W., O'Connor, T.E., Joseph, J.P., Raizada, M.K., Katovich, M.J. and Sumners, C. (2011), "Cerebroprotection by angiotensin-(1-7) in endothelin-1-induced ischaemic stroke", *Experimental Physiology*, Blackwell Publishing Ltd, Vol. 96 No. 10, pp. 1084–1096, doi: 10.1113/expphysiol.2011.058578.

Mohr, C., Brady, J.D. and Rossi, D.J. (2010), "Young age and low temperature, but not female gender delay ATP loss and glutamate release, and protect Purkinje cells during simulated ischemia in cerebellar slices", *Neuropharmacology*, Vol. 58 No. 2, pp. 392–403, doi: 10.1016/j.neuropharm.2009.09.013.

Moisan, A., Favre, I.M., Rome, C., Grillon, E., Naegele, B., Barbieux, M., De Fraipont, F., *et al.* (2014), "Microvascular plasticity after experimental stroke: A molecular and MRI study", *Cerebrovascular Diseases*, S. Karger AG, Vol. 38 No. 5, pp. 344–353, doi: 10.1159/000368597.

Morris, M.E., Rodriguez-Cruz, V. and Felmlee, M.A. (2017), "SLC and ABC Transporters: Expression, Localization, and Species Differences at the Blood-Brain and the Blood-Cerebrospinal Fluid Barriers", *AAPS Journal*, Springer New York LLC, Vol. 19 No. 5, pp. 1317–1331, doi: 10.1208/s12248-017-0110-8.

Mukda, S., Tsai, C.Y., Leu, S., Yang, J.L. and Chan, S.H.H. (2019), "Pinin protects astrocytes from cell death after acute ischemic stroke via maintenance of mitochondrial anti-apoptotic and bioenergetics functions", *Journal of Biomedical Science*, BioMed Central Ltd., Vol. 26 No. 1, doi: 10.1186/s12929-019-0538-5.

Muoio, V., Persson, P.B. and Sendeski, M.M. (2014), "The neurovascular unit - concept review", *Acta Physiologica*, Blackwell Publishing Ltd, doi: 10.1111/apha.12250.

Murphy, R.K.J., Sun, P., Xu, J., Wang, Y., Sullivan, S., Gamble, P., Wagner, J., *et al.* (2016), "Magnetic resonance imaging biomarker of axon loss reflects cervical spondylotic myelopathy severity", *Spine*, Lippincott Williams and Wilkins, Vol. 41 No. 9, pp. 751–756, doi: 10.1097/BRS.0000000000001337.

Nahirney, P.C., Reeson, P. and Brown, C.E. (2016), "Ultrastructural analysis of blood-brain barrier breakdown in the peri-infarct zone in young adult and aged mice", *Journal of Cerebral Blood Flow and Metabolism*, Nature Publishing Group, Vol. 36 No. 2, pp. 413–425, doi: 10.1177/0271678X15608396.

Narushima, I., Kita, T., Kubo, K., Yonetani, Y., Momochi, C., Yoshikawa, I., Ohno, N., *et al.* (2003), "Highly enhanced permeability of blood-brain barrier induced by repeated administration of endothelin-1 in dogs and rats", *Pharmacology and Toxicology*, Vol. 92 No. 1, pp. 21–26, doi: 10.1034/j.1600-0773.2003.920104.x.

Neumann-Haefelin, T., Kastrup, ; A, De Crespigny, ; A, Yenari, ; M A, Ringer, ; T, Sun, ; G H and Moseley, ; M E. (2000), *Serial MRI After Transient Focal Cerebral Ischemia in Rats Dynamics of Tissue Injury, Blood-Brain Barrier Damage, and Edema Formation*.

Nie, B., Liu, H., Chen, K., Jiang, X. and Shan, B. (2014), "A statistical parametric mapping toolbox used for voxel-wise analysis of FDG-PET images of rat brain", *PLoS ONE*, Public Library of Science, Vol. 9 No. 9, doi: 10.1371/journal.pone.0108295.

Nitta, T., Hata, M., Gotoh, S., Seo, Y., Sasaki, H., Hashimoto, N., Furuse, M., *et al.* (2003), "Size-selective loosening of the blood-brain barrier in claudin-5-deficient mice", *Journal of Cell Biology*, Vol. 161 No. 3, pp. 653–660, doi: 10.1083/jcb.200302070.

Obenaus, A. and Badaut, J. (2022), "Role of the non-invasive imaging techniques in monitoring and understanding the evolution of brain edema", *Journal of Neuroscience Research*, John Wiley and Sons Inc, 1 May, doi: 10.1002/jnr.24837.

Oliff, H.S., Coyle, P. and Weber, E. (1997), *Journal of Cerebral Blood Flow and Metabolism Rat Strain and Vendor Differences In Collateral Anastomoses*.

Oluwasegun, D.O., Sunday, S.A. and Sunday, A.M. (2019), "Assessment of the effect of post-natal lead exposure on the hippocampus of developing Wistar rats", *African Journal of Cellular Pathology*, Academic Journals, Vol. 11 No. 4, pp. 23–32, doi: 10.5897/ajcpath2019.0021.

Ospel, J.M., Rex, N., Oueidat, K., McDonough, R., Rinkel, L., Baird, G., Collins, S., *et al.* (2024), "Infarcts Due to Large Vessel Occlusions Continue to Grow Despite Near-Complete Reperfusion After Endovascular Treatment", *Journal of Stroke*, Korean Stroke Society, Vol. 26 No. 2, pp. 260–268, doi: 10.5853/jos.2023.02621.

Ostrova, I. V., Kalabushev, S.N., Ryzhkov, I.A. and Tsokolaeva, Z.I. (2021), “A novel thromboplastin-based rat model of ischemic stroke”, *Brain Sciences*, MDPI, Vol. 11 No. 11, doi: 10.3390/brainsci11111475.

Pang, J., Zhang, J.H. and Jiang, Y. (2019), “Delayed recanalization in acute ischemic stroke patients: Late is better than never?”, *Journal of Cerebral Blood Flow and Metabolism*, SAGE Publications Ltd, 1 December, doi: 10.1177/0271678X19881449.

Perkins, C.J., Kahya, E., Roque, C.T., Roche, P.E. and Newman, G.C. (2001), *Fluid-Attenuated Inversion Recovery and Diffusion-and Perfusion-Weighted MRI Abnormalities in 117 Consecutive Patients With Stroke Symptoms*.

Pfeiffer, F., Schäfer, J., Lyck, R., Makrides, V., Brunner, S., Schaeren-Wiemers, N., Deutsch, U., *et al.* (2011), “Claudin-1 induced sealing of blood-brain barrier tight junctions ameliorates chronic experimental autoimmune encephalomyelitis”, *Acta Neuropathologica*, Vol. 122 No. 5, pp. 601–614, doi: 10.1007/s00401-011-0883-2.

Pirko, I., Fricke, S.T., Johnson, A.J., Rodriguez, M. and Macura, S.I. (2005), “Magnetic Resonance Imaging, Microscopy, and Spectroscopy of the Central Nervous System in Experimental Animals”, *NeuroRx: The Journal of the American Society for Experimental NeuroTherapeutics*, Vol. 2, pp. 250–264.

Pirzad Jahromi, G., Seidi, S., Sadr, S.S., Shabanzadeh, A.P., Keshavarz, M., Kaka, G.R., Hosseini, S.K., *et al.* (2012), “Therapeutic Effects of a Combinatorial Treatment of Simvastatin and Bone Marrow Stromal Cells on Experimental Embolic Stroke”, *Basic and Clinical Pharmacology and Toxicology*, Vol. 110 No. 6, pp. 487–493, doi: 10.1111/j.1742-7843.2011.00848.x.

Powers, W.J., Rabinstein, A.A., Ackerson, T., Adeoye, O.M., Bambakidis, N.C., Becker, K., Biller, J., *et al.* (2019), “Guidelines for the early management of patients with acute ischemic stroke: 2019 update to the 2018 guidelines for the early management of acute ischemic stroke a guideline for healthcare professionals from the American Heart Association/American Stroke Association”, *Stroke*, Lippincott Williams and Wilkins, 1 December, doi: 10.1161/STR.0000000000000211.

Prabhakaran, S., Ruff, I. and Bernstein, R.A. (2015), “Acute stroke intervention: A systematic review”, *JAMA - Journal of the American Medical Association*, American Medical Association, 14 April, doi: 10.1001/jama.2015.3058.

Ragoschke-Schumm, A. and Walter, S. (2018), “DAWN and DEFUSE-3 trials: is time still important?”, *Radiologe*, Springer Verlag, 1 November, doi: 10.1007/s00117-018-0406-4.

Ren, M., Lin, Z.J., Qian, H., Choudhury, G.R., Liu, R., Liu, H. and Yang, S.H. (2012), “Embolic middle cerebral artery occlusion model using thrombin and fibrinogen composed clots in rat”, *Journal of Neuroscience Methods*, Vol. 211 No. 2, pp. 296–304, doi: 10.1016/j.jneumeth.2012.09.006.

Resenberg, G. and Yang, Y. (2007), “Vasogenic edema due to tight junction disruption by matrix metalloproteinases in cerebral ischemia”, *Neurosurg. Focus*, No. 22 (5), p. 1.

Ruiz, A., Alberdi, E. and Matute, C. (2014), “CGP37157, an inhibitor of the mitochondrial Na+/Ca2+ exchanger, protects neurons from excitotoxicity by blocking voltage-gated Ca2+ channels”, *Cell Death and Disease*, Nature Publishing Group, Vol. 5 No. 4, doi: 10.1038/cddis.2014.134.

Rustenhoven, J., Smyth, L.C., Jansson, D., Schweder, P., Aalderink, M., Scotter, E.L., Mee, E.W., *et al.* (2018), “Modelling physiological and pathological conditions to study pericyte biology in brain function and dysfunction”, *BMC Neuroscience*, BioMed Central Ltd., Vol. 19 No. 1, doi: 10.1186/s12868-018-0405-4.

Rutkowsky, J.M., Wallace, B.K., Wise, P.M., O’donnell, M.E. and O’donnell, M.E. (2011), “Effects of estradiol on ischemic factor-induced astrocyte swelling and AQP4 protein abundance”, *Am J Physiol Cell Physiol*, Vol. 301, pp. 204–212, doi: 10.1152/ajpcell.00399.2010.-In.

Ryu, H.W., Lim, W., Jo, D., Kim, S., Park, J.T., Min, J.J., Hyun, H., *et al.* (2018), “Low-dose evans blue dye for near-infrared fluorescence imaging in photothrombotic stroke model”, *International Journal of Medical Sciences*, Ivyspring International Publisher, Vol. 15 No. 7, pp. 696–702, doi: 10.7150/ijms.24257.

Sadowska, G.B., Ahmedli, N., Chen, X. and Stonestreet, B.S. (2015), “Ontogeny of tight junction protein expression in the ovine cerebral cortex during development”, *Neuroscience*, Elsevier Ltd, Vol. 310, pp. 422–429, doi: 10.1016/j.neuroscience.2015.09.062.

Salas-Perdomo, A., Miró-Mur, F., Gallizioli, M., Brait, V.H., Justicia, C., Meissner, A., Urra, X., *et al.* (2019), “Role of the S1P pathway and inhibition by fingolimod in preventing hemorrhagic transformation after stroke”, *Scientific Reports*, Nature Publishing Group, Vol. 9 No. 1, doi: 10.1038/s41598-019-44845-5.

Sanderson, T.H. and Wider, J.M. (2013), “2-vessel occlusion/hypotension: a rat model of global brain ischemia.”, *Journal of Visualized Experiments : JoVE*, No. 76, doi: 10.3791/50173.

Sá-Pereira, I., Brites, D. and Brito, M.A. (2012), “Neurovascular unit: A focus on pericytes”, *Molecular Neurobiology*, Humana Press Inc., doi: 10.1007/s12035-012-8244-2.

Sarvari, S., Moakedi, F., Hone, E., Simpkins, J.W. and Ren, X. (2020), “Mechanisms in blood-brain barrier opening and metabolism-challenged cerebrovascular ischemia with emphasis on ischemic stroke”, *Metabolic Brain Disease*, Springer, 1 August, doi: 10.1007/s11011-020-00573-8.

Saunders, N.R., Dziegielewska, K.M., Møllgård, K. and Habgood, M.D. (2015), “Markers for blood-brain barrier integrity: How appropriate is Evans blue in the twenty-first century and what are the alternatives?”, *Frontiers in Neuroscience*, Frontiers Media S.A., doi: 10.3389/fnins.2015.00385.

Schiffer, W.K., Mirrione, M.M., Biegon, A., Alexoff, D.L., Patel, V. and Dewey, S.L. (2006), “Serial microPET measures of the metabolic reaction to a microdialysis probe implant”, *Journal of Neuroscience Methods*, Vol. 155 No. 2, pp. 272–284, doi: 10.1016/j.jneumeth.2006.01.027.

Secor, D., Li, F., Ellis, C.G., Sharpe, M.D., Gross, P.L., Wilson, J.X. and Tyml, K. (2010), “Impaired microvascular perfusion in sepsis requires activated coagulation and P-selectin-mediated platelet adhesion in capillaries”, *Intensive Care Medicine*, Vol. 36 No. 11, pp. 1928–1934, doi: 10.1007/s00134-010-1969-3.

Sekiya, T., Viberg, A., Kojima, K., Sakamoto, T., Nakagawa, T., Ito, J. and Canlon, B. (2012), “Trauma-specific insults to the cochlear nucleus in the rat”, *Journal of Neuroscience Research*, Vol. 90 No. 10, pp. 1924–1931, doi: 10.1002/jnr.23093.

Selvamani, A. and Sohrabji, F. (2010), “Reproductive age modulates the impact of focal ischemia on the forebrain as well as the effects of estrogen treatment in female rats”, *Neurobiology of Aging*, Elsevier Inc., Vol. 31 No. 9, pp. 1618–1628, doi: 10.1016/j.neurobiolaging.2008.08.014.

Serlin, Y., Shelef, I., Knyazer, B. and Friedman, A. (2015), “Anatomy and physiology of the blood-brain barrier”, *Seminars in Cell and Developmental Biology*, Academic Press, 1 February, doi: 10.1016/j.semcdb.2015.01.002.

Seul, K., Kyung, C. and Seong Yun Kim. (2008), “White Matter Damage and Hippocampal Neurodegeneration Induced by Permanent Bilateral Occlusion of Common Carotid Artery in the Rat: Comparison between Wistar and Sprague-Dawley Strain”, *Korean J Physiol Pharmacol*, No. 12(3), pp. 89–94.

Shimizu, F., Sano, Y., Saito, K., Abe, M.A., Maeda, T., Haruki, H. and Kanda, T. (2012), “Pericyte-derived glial cell line-derived neurotrophic factor increase the expression of claudin-5 in the blood-brain barrier and the blood-nerve barrier”, *Neurochemical Research*, Vol. 37 No. 2, pp. 401–409, doi: 10.1007/s11064-011-0626-8.

Singh Badhan, R.K., Chenel, M. and Penny, J.I. (2014), “Development of a physiologically-based pharmacokinetic model of the rat central nervous system”, *Pharmaceutics*, MDPI AG, Vol. 6 No. 1, pp. 97–136, doi: 10.3390/pharmaceutics6010097.

Smith, E.J., Stroemer, R.P., Gorenkova, N., Nakajima, M., Crum, W.R., Tang, E., Stevanato, L., *et al.* (2012), “Implantation site and lesion topology determine efficacy of a human neural stem cell line in a rat model of chronic stroke”, *Stem Cells*, Vol. 30 No. 4, pp. 785–796, doi: 10.1002/stem.1024.

Solár, P., Zamani, A., Kubíčková, L., Dubový, P. and Joukal, M. (2020), “Choroid plexus and the blood-cerebrospinal fluid barrier in disease”, *Fluids and Barriers of the CNS*, BioMed Central Ltd., 6 May, doi: 10.1186/s12987-020-00196-2.

Sommer, C.J. (2017), “Ischemic stroke: experimental models and reality”, *Acta Neuropathologica*, Springer Verlag, 1 February, doi: 10.1007/s00401-017-1667-0.

Srinivasan, A., Goyal, M., Al Azri, F. and Lum, C. (2006), “State-of-the-art imaging of acute stroke”, *Radiographics*, October, doi: 10.1148/rg.26si065501.

Strbian, D., Durukan, A., Pitkonen, M., Marinkovic, I., Tatlisumak, E., Pedrono, E., Abo-Ramadan, U., *et al.* (2008), “The blood-brain barrier is continuously open for several weeks following transient focal cerebral ischemia”, *Neuroscience*, Vol. 153 No. 1, pp. 175–181, doi: 10.1016/j.neuroscience.2008.02.012.

Ström, J.O., Theodorsson, A. and Theodorsson, E. (2013), *Method Parameters’ Impact on Mortality and Variability in Rat Stroke Experiments: A Meta-Analysis*.

Su, X., Tang, W., Luan, Z., Yang, Y., Wang, Z., Zhang, Y., Wang, Q., *et al.* (2018), “Protective effect of miconazole on rat myelin sheaths following premature infant cerebral white matter injury”, *Experimental and Therapeutic Medicine*, Spandidos Publications, Vol. 15 No. 3, pp. 2443–2449, doi: 10.3892/etm.2018.5717.

Su, Z., Ye, Y., Shen, C., Qiu, S., Sun, Y., Hu, S., Xiong, X., *et al.* (2022), “Pathophysiology of Ischemic Stroke: Noncoding RNA Role in Oxidative Stress”, *Oxidative Medicine and Cellular Longevity*, Hindawi Limited, doi: 10.1155/2022/5815843.

Sun, L., Zhou, W., Mueller, C., Sommer, C., Heiland, S., Bauer, A.T., Marti, H.H., *et al.* (2010), “Oxygen therapy reduces secondary hemorrhage after thrombolysis in thromboembolic cerebral ischemia”, *Journal of Cerebral Blood Flow and Metabolism*, Vol. 30 No. 9, pp. 1651–1660, doi: 10.1038/jcbfm.2010.50.

Svoboda, J., Litvinec, A., Kala, D., Pošusta, A., Vávrová, L., Jiruška, P. and Otáhal, J. (2019), “Strain differences in intraluminal thread model of middle cerebral artery occlusion in rats”, *Physiological Research*, Czech Academy of Sciences, Vol. 68 No. 1, pp. 37–48, doi: 10.33549/physiolres.933958.

Sweeney, M.D., Zhao, Z., Montagne, A., Nelson, A.R. and Zlokovic, B. V. (2019), “Blood-brain barrier: From physiology to disease and back”, *Physiological Reviews*, Vol. 99 No. 1, pp. 21–78, doi: 10.1152/physrev.00050.2017.

Symms, M., Jäger, H.R., Schmierer, K. and Yousry, T.A. (2004), “A review of structural magnetic resonance neuroimaging”, *Journal of Neurology, Neurosurgery and Psychiatry*, BMJ Publishing Group, doi: 10.1136/jnnp.2003.032714.

Tajes, M., Ramos-Fernández, E., Weng-Jiang, X., Bosch-Morató, M., Guivernau, B., Eraso-Pichot, A., Salvador, B., *et al.* (2014), “The blood-brain barrier: Structure, function and therapeutic approaches to cross it”, *Molecular Membrane Biology*, Informa Healthcare, doi: 10.3109/09687688.2014.937468.

Tamura, A. and Teasdale, tG M. (1981), *Focal Cerebral Ischaemia in the Rat: 1. Description of Technique and Early Neuropathological Consequences Following Middle Cerebral Artery Occlusion*, *Journal ’!F Cerehral Blood Flow and Metaholism*, Vol. 1.

Taninishi, H., Jung, J.Y., Izutsu, M., Wang, Z., Sheng, H. and Warner, D.S. (2015), “A blinded randomized assessment of laser Doppler flowmetry efficacy in standardizing outcome from intraluminal filament MCAO in the rat”, *Journal of Neuroscience Methods*, Elsevier, Vol. 241, pp. 111–120, doi: 10.1016/j.jneumeth.2014.12.006.

Tate, W.J., Polding, L.C., Kemp, S., Mlynash, M., Heit, J.J., Marks, M.P., Albers, G.W., *et al.* (2019), “Thrombectomy Results in Reduced Hospital Stay, More Home-Time, and More Favorable Living Situations in DEFUSE 3”, *Stroke*, Lippincott Williams and Wilkins, Vol. 50 No. 9, pp. 2578–2581, doi: 10.1161/STROKEAHA.119.025165.

Tedyanto, E.H., Tini, K. and Pramana, N.A.K. (2022), “Magnetic Resonance Imaging in Acute Ischemic Stroke”, *Cureus*, Springer Science and Business Media LLC, doi: 10.7759/cureus.27224.

Thrane, A.S., Rappold, P.M., Fujita, T., Torres, A., Bekar, L.K., Takano, T., Peng, W., *et al.* (2011), “Critical role of aquaporin-4 (AQP4) in astrocytic Ca2+ signaling events elicited by cerebral edema”, *Proceedings of the National Academy of Sciences of the United States of America*, Vol. 108 No. 2, pp. 846–851, doi: 10.1073/pnas.1015217108.

Thrippleton, M.J. (2019), “MRI measurement of blood–brain barrier leakage: minding the gaps”, *Journal of Physiology*, Blackwell Publishing Ltd, 1 February, doi: 10.1113/JP277425.

Thrippleton, M.J., Backes, W.H., Sourbron, S., Ingrisch, M., van Osch, M.J.P., Dichgans, M., Fazekas, F., *et al.* (2019), “Quantifying blood-brain barrier leakage in small vessel disease: Review and consensus recommendations”, *Alzheimer’s and Dementia*, Elsevier Inc., 1 June, doi: 10.1016/j.jalz.2019.01.013.

Thurgur, H. and Pinteaux, E. (2019), “Microglia in the Neurovascular Unit: Blood–Brain Barrier–microglia Interactions After Central Nervous System Disorders”, *Neuroscience*, Elsevier Ltd, 1 May, doi: 10.1016/j.neuroscience.2018.06.046.

Trotman-Lucas, M., Kelly, M.E., Janus, J. and Gibson, C.L. (2019), “Middle cerebral artery occlusion allowing reperfusion via common carotid artery repair in mice”, *Journal of Visualized Experiments*, Journal of Visualized Experiments, Vol. 2019 No. 143, doi: 10.3791/58191.

Trueman, R.C., Diaz, C., Farr, T.D., Harrison, D.J., Fuller, A., Tokarczuk, P.F., Stewart, A.J., *et al.* (2017), “Systematic and detailed analysis of behavioural tests in the rat middle cerebral artery occlusion model of stroke: Tests for long-term assessment”, *Journal of Cerebral Blood Flow and Metabolism*, SAGE Publications Ltd, Vol. 37 No. 4, pp. 1349–1361, doi: 10.1177/0271678X16654921.

Tuo, Q. zhang, Zhang, S. ting and Lei, P. (2022), “Mechanisms of neuronal cell death in ischemic stroke and their therapeutic implications”, *Medicinal Research Reviews*, John Wiley and Sons Inc, 1 January, doi: 10.1002/med.21817.

Unekawa, M., Tsukada, N., Takizawa, T., Tomita, Y., Nakahara, J. and Izawa, Y. (2024), “Striatal Blood Flow Changes by Middle Cerebral Artery Occlusion and Its Effect on Neurological Deficits in Mice”, *Microcirculation*, John Wiley and Sons Inc, Vol. 31 No. 6, doi: 10.1111/micc.12861.

Valentová, Z. (2020), *Evaluation of a new model of miniature focal cortical ischemia*, Master’s thesis, Charles University Faculty of Physical Education and Sport, Prague, July.

Veksler, R., Vazana, U., Serlin, Y., Prager, O., Ofer, J., Shemen, N., Fisher, A.M., *et al.* (2020), “Slow blood-to-brain transport underlies enduring barrier dysfunction in American football players”, *Brain*, Oxford University Press, Vol. 143 No. 6, pp. 1826–1842, doi: 10.1093/brain/awaa140.

Wang, H., Zhu, L., Li, G., Zuo, M., Ma, X. and Wang, J. (2020), “Perfusion parameters of intravoxel incoherent motion based on tumor edge region of interest in cervical cancer: evaluation of differentiation and correlation with dynamic contrast-enhanced MRI”, *Acta Radiologica*, SAGE Publications Inc., Vol. 61 No. 8, pp. 1087–1095, doi: 10.1177/0284185119890086.

Wang, H.L. and Lai, T.W. (2014), “Optimization of Evans blue quantitation in limited rat tissue samples”, *Scientific Reports*, Nature Publishing Group, Vol. 4, doi: 10.1038/srep06588.

Wang, Q., Wang, Y., Liu, J., Sutphen, C.L., Cruchaga, C., Blazey, T., Gordon, B.A., *et al.* (2019), “Quantification of white matter cellularity and damage in preclinical and early symptomatic Alzheimer’s disease”, *NeuroImage: Clinical*, Elsevier Inc., Vol. 22, doi: 10.1016/j.nicl.2019.101767.

Wilhelm, I., Nyúl-Tóth, Á., Suciu, M., Hermenean, A. and Krizbai, I.A. (2016), “Heterogeneity of the blood-brain barrier”, *Tissue Barriers*, Taylor and Francis Inc., 2 January, doi: 10.1080/21688370.2016.1143544.

Wintermark, M., Albers, G.W., Alexandrov, A. V., Alger, J.R., Bammer, R., Baron, J.C., Davis, S., *et al.* (2008), “Acute stroke imaging research roadmap”, *American Journal of Neuroradiology*, Vol. 29, doi: 10.1161/STROKEAHA.107.512319.

Woitzik, J. and Schilling, L. (2002), “Control of completeness and immediate detection of bleeding by a single laser-Doppler flow probe during intravascular middle cerebral artery occlusion in rats”, *Journal of Neuroscience Methods*, Vol. 122 No. 1, pp. 75–78.

Wu, D., Chen, Q., Chen, X., Han, F., Chen, Z. and Wang, Y. (2023), “The blood–brain barrier: structure, regulation, and drug delivery”, *Signal Transduction and Targeted Therapy*, Springer Nature, 1 December, doi: 10.1038/s41392-023-01481-w.

Wu, L., Chen, C., Li, Y., Guo, C., Fan, Y., Yu, D., Zhang, T., *et al.* (2020), “UPLC-Q-TOF/MS-Based Serum Metabolomics Reveals the Anti-Ischemic Stroke Mechanism of Nuciferine in MCAO Rats”, *ACS Omega*, American Chemical Society, Vol. 5 No. 51, pp. 33433–33444, doi: 10.1021/acsomega.0c05388.

Xie, Y., Li, J., Fan, G., Qi, S. and Li, B. (2014), “Reperfusion promotes mitochondrial biogenesis following focal cerebral ischemia in rats”, *PLoS ONE*, Public Library of Science, Vol. 9 No. 3, doi: 10.1371/journal.pone.0092443.

Xue, Q., Pei, H., Liu, Q., Zhao, M., Sun, J., Gao, E., Ma, X., *et al.* (2017), “MICU1 protects against myocardial ischemia/reperfusion injury and its control by the importer receptor Tom70”, *Cell Death and Disease*, Springer Nature, Vol. 8 No. 7, doi: 10.1038/CDDIS.2017.280.

Ye, Y., Li, Q., Pan, C.S., Yan, L., Sun, K., Wang, X.Y., Yao, S.Q., *et al.* (2022), “QiShenYiQi Inhibits Tissue Plasminogen Activator–Induced Brain Edema and Hemorrhage after Ischemic Stroke in Mice”, *Frontiers in Pharmacology*, Frontiers Media S.A., Vol. 12, doi: 10.3389/fphar.2021.759027.

Ye, Z., Price, R.L., Liu, X., Lin, J., Yang, Q., Sun, P., Wu, A.T., *et al.* (n.d.). *Title: Diffusion Histology Imaging Combining Diffusion Basis Spectrum Imaging (DBSI) and Machine Learning Improves Detection and Classification of Glioblastoma Pathology Running Title: Detection and Classification of Glioblastoma Pathology*.

Yoshimura, S., Dorok, M., Mamrak, U., Wehn, A., Krestel, E., Khalin, I. and Plesnila, N. (2024), “Minimizing variability in the filament middle cerebral artery occlusion model in C57BL/6 mice by surgical optimization - the PURE-MCAo Model”, 24 January, doi: 10.1101/2024.01.22.576769.

Zbesko, J.C., Nguyen, T.V. V., Yang, T., Frye, J.B., Hussain, O., Hayes, M., Chung, A., *et al.* (2018), “Glial scars are permeable to the neurotoxic environment of chronic stroke infarcts”, *Neurobiology of Disease*, Academic Press Inc., Vol. 112, pp. 63–78, doi: 10.1016/j.nbd.2018.01.007.

Zeng, L., Hu, S., Zeng, L., Chen, R., Li, H., Yu, J. and Yang, H. (2023), “Animal Models of Ischemic Stroke with Different Forms of Middle Cerebral Artery Occlusion”, *Brain Sciences*, Multidisciplinary Digital Publishing Institute (MDPI), 1 July, doi: 10.3390/brainsci13071007.

Zeng, X.N., Xie, L.L., Liang, R., Sun, X.L., Fan, Y. and Hu, G. (2012), “AQP4 Knockout Aggravates Ischemia/Reperfusion Injury in Mice”, *CNS Neuroscience and Therapeutics*, Vol. 18 No. 5, pp. 388–394, doi: 10.1111/j.1755-5949.2012.00308.x.

Zhai, Z. and Feng, J. (2018), “Left-right asymmetry influenced the infarct volume and neurological dysfunction following focal middle cerebral artery occlusion in rats”, *Brain and Behavior*, John Wiley and Sons Ltd, Vol. 8 No. 12, doi: 10.1002/brb3.1166.

Zhang, J.K., Sun, P., Jayasekera, D., Greenberg, J.K., Javeed, S., Dibble, C.F., Blum, J., *et al.* (2022), “Utility of Diffusion Basis Spectrum Imaging in Quantifying Baseline Disease Severity and Prognosis of Cervical Spondylotic Myelopathy”, *Spine*, Wolters Kluwer Health, Vol. 47 No. 24, pp. 1687–1693, doi: 10.1097/BRS.0000000000004456.

Zhang, L., Zhang, R.L., Jiang, Q., Ding, G., Chopp, M. and Zhang, Z.G. (2015), “Focal embolic cerebral ischemia in the rat”, *Nature Protocols*, Nature Publishing Group, Vol. 10 No. 4, pp. 539–547, doi: 10.1038/nprot.2015.036.

Zhang, W., Zhu, L., An, C., Wang, R., Yang, L., Yu, W., Li, P., *et al.* (2020), “The blood brain barrier in cerebral ischemic injury – Disruption and repair”, *Brain Hemorrhages*, KeAi Communications Co., 1 March, doi: 10.1016/j.hest.2019.12.004.

Zhang, X., Gu, Y., Li, P., Jiang, A., Sheng, X., Jin, X., Shi, Y., *et al.* (2019), “Matrix metalloproteases-mediated cleavage on β-dystroglycan may play a key role in the blood–brain barrier after intracerebral hemorrhage in rats”, *Medical Science Monitor*, International Scientific Information, Inc., Vol. 25, pp. 794–800, doi: 10.12659/MSM.908500.

Zhang, Z., Zhang, L., Yepes, M., Jiang, Q., Li, Q., Arniego, P., Coleman, T.A., *et al.* (2002), “Adjuvant treatment with neuroserpin increases the therapeutic window for tissue-type plasminogen activator administration in a rat model of embolic stroke”, *Circulation*, Vol. 106 No. 6, pp. 740–745, doi: 10.1161/01.CIR.0000023942.10849.41.

Zhu, W., Libal, N.L., Casper, A., Bodhankar, S., Offner, H. and Alkayed, N.J. (2014), “Recombinant T Cell Receptor Ligand Treatment Improves Neurological Outcome in the Presence of Tissue Plasminogen Activator in Experimental Ischemic Stroke”, *Translational Stroke Research*, Springer US, Vol. 5 No. 5, pp. 612–617, doi: 10.1007/s12975-014-0348-8.

Zlokovic, B. V. (2008), “The Blood-Brain Barrier in Health and Chronic Neurodegenerative Disorders”, *Neuron*, 24 January, doi: 10.1016/j.neuron.2008.01.003.

List of figures and tables

Overview of Author’s publications

Publications related to thesis topic

Svoboda, J., Litvinec, A., Kala, D., Pošusta, A., Vávrová, L., Jiruška, P. and Otáhal, J. (2019), “Strain differences in intraluminal thread model of middle cerebral artery occlusion in rats”, *Physiological Research*, Czech Academy of Sciences, Vol. 68 No. 1, pp. 37–48, doi: 10.33549/physiolres.933958.

IF:1.9

Kala, D., Šulc, V., Olšerová, A., Svoboda, J., Prysiazhniuk, Y., Pošusta, A., Kynčl, M., *et al.* (2022), “Evaluation of Blood-Brain Barrier Integrity by the Analysis of Dynamic Contrast-Enhanced MRI – a Comparison of Quantitative and Semi-Quantitative Methods”, *Physiological Research*, Czech Academy of Sciences, Vol. 71, pp. S259–S275, doi: 10.33549/physiolres.934998.

IF:1.9

Kala, D., Svoboda, J., Litvinec, A., Pošusta, A., Lisý, J., Šulc, V., Tomek, A., *et al.* (2017), “/GD-Tracker/ A software for blood-brain barrier permeability assessment”, *Lekar a Technika*, Vol. 47 No. 2.

Svoboda, J., Kala, D., Litvinec, A., Jiruška, P., Otáhal, J. (2017) Mozek – svět za bariérou. *Vesmír*, Vol. 96, 564 - 565

Publications under peer-review

Michal, L., Kala, D., Olšerová, A., Šulc V., Prysiazniuk Y., Svoboda, J., Šanda, J., Kynčl, M., Otáhal, J., Tomek, A. Spatio-Temporal Dynamics of MRI Diffusion Metrics in Ischemic Brain Regions in Stroke Patients with Hemorrhagic Transformation Following Endovascular Therapy. *European Stroke Journal*

Kala, D., Prysiazhniuk, Y., Jánský, P., Olšerová, A., Šrámková, T., Benešová, K., Magerová, H., Šulc, V., Schwabová, P., Holubová, Z., Svoboda, J., Michal, L., Kynčl, M., Šanda, J., Marusič, P., Otáhal, J., Tomek, A. Postischemic Cavity Development: A Potential Predictor of Clinical Outcomes? *PlosOne*

Publications not directly related to thesis topic

Daněk, J., Danačíková, Š., Kala, D., Svoboda, J., Kapoor, S., Pošusta, A., Folbergrová, J., *et al.* (2022), "Sulforaphane Ameliorates Metabolic Changes Associated With Status Epilepticus in Immature Rats", *Frontiers in Cellular Neuroscience*, Frontiers Media S.A., Vol. 16, doi: 10.3389/fncel.2022.855161.

IF:4.2

Faridová, A.T., Heřman, H., Danačíková, Š., Svoboda, J. and Otáhal, J. (2023), "Serum Biomarkers Of Hypoxic-Ischemic Brain Injury", *Physiological Research*, Czech Academy of Sciences, Vol. 72, pp. S461–S474, doi: 10.33549/physiolres.935214.

IF:1.9

Kapoor, S., Kala, D., Svoboda, J., Daněk, J., Faridová, A., Brnoliaková, Z., Mikulecká, A., *et al.* (2022), "The Effect of Sulforaphane on Perinatal Hypoxic-Ischemic Brain Injury in Rats", *Physiological Research*, Czech Academy of Sciences, Vol. 71 No. 3, pp. 401–411, doi: 10.33549/physiolres.934878.

IF:1.9

Curriculum Vitae

Personal data

Name: Jan Svoboda, Mgr. Date of birth: 18. srpen 1989

Phone: (+420) 607100141

E-mail: jan.svoboda@lfmotol.cuni.cz

Education

Graduated:

- Specialization in Health Care, Physiotherapy, master's degree, Faculty of Physical Education and Sport, Charles University in Prague (2013-2015)
- Specialization in Health Care, Physiotherapy, Faculty of Physical Education and Sport, Charles University in Prague (2009-2013)
- Gymnasium Přípotoční (2005- 2009, matriculation exam - Čj, B, Che, Aj)

Current study:

- Doctoral study program Biomechanics, Faculty of Physical Education and Sport, Charles University in Prague and Institute of Physiology, Academy of Sciences of the Czech Republic (from 2015 to present)

Courses taken outside the scope of study

- Massage course - sports, relaxation and reconditioning massage UK FTVS
- Dynamic neuromuscular stabilization, part A, B
- Training course for obtaining qualification and professional competence in the field of experimental animals according to §15d (3) of Act No. 246/1992 Coll. - design of experiments and experimental projects

Work experience

- masseur at Aeditus (from 2012 to 2013)
- physiotherapist at CKP Roseta s.r.o. (from 2013 to 2015)
- physiotherapist VO2MAX (from 2015 to 2016)
- PhD student, Department of Developmental Epileptology, Academy of Sciences of the Czech Republic (2015 to present)
- Academic staff member of the Department of Anatomy and Biomechanics, Faculty of Physical Education, Charles University (2015-2021)
- Researcher, Department of Pathological Physiology, 2nd Faculty of Medicine, Charles University (2022 to present)